HDL-CR-78-089-1

LEVEL II

RADIATION EFFECTS IN SATELLITE CABLES

April 1978

Prepared by
Jason M. Wilkenfeld, Roland E. Leadon and Charles E. Malion
IRT Corporation

Under contract
DAAG39-76-C-0089

U.S. Army Electronics Research and Development Command
Harry Diamond Laboratories
Adelphi, MD 20783

The findings of this report are not to be construed as an official Department of the Army position unless so designated by other authorized documents.

Citation of manufacturers' or trade names does not constitute an official indorsement or approval of the use thereof.

Destroy this report when it is no longer needed. Do not return it to the originator.

UNCLASSIFIED

SECURITY CLASSIFICATION OF THIS PAGE (When Data Entered)

REPORT DOCUMENTATION PAGE	READ INSTRUCTIONS BEFORE COMPLETING FORM
1. REPORT NUMBER: HDL-CR-78-089-1	2. GOVT ACCESSION NO. / 3. RECIPIENT'S CATALOG NUMBER
4. TITLE (and Subtitle): Radiation Effects In Satellite Cables	5. TYPE OF REPORT & PERIOD COVERED: Final 4/1/77-3/31/78
	6. PERFORMING ORG. REPORT NUMBER: IRT-8148-021
7. AUTHOR(s): Jason M. Wilkenfeld, Roland E. Leadon, and Charles E. Mallon	8. CONTRACT OR GRANT NUMBER(s): DAAG39-76-C-0089
9. PERFORMING ORGANIZATION NAME AND ADDRESS: IRT Corporation, P. O. Box 80817, San Diego, California 92138	10. PROGRAM ELEMENT, PROJECT, TASK AREA & WORK UNIT NUMBERS: 99QAXTA007-64
11. CONTROLLING OFFICE NAME AND ADDRESS: Harry Diamond Laboratories, 2800 Powder Mill Road, Adelphi, Maryland 20783	12. REPORT DATE: April 1978 / 13. NUMBER OF PAGES: 191
14. MONITORING AGENCY NAME & ADDRESS (if different from Controlling Office)	15. SECURITY CLASS. (of this report): Unclassified / 15a. DECLASSIFICATION/DOWNGRADING SCHEDULE

16. DISTRIBUTION STATEMENT (of this Report)

Approved for public release; distribution unlimited

17. DISTRIBUTION STATEMENT (of the abstract entered in Block 20, if different from Report)

18. SUPPLEMENTARY NOTES

19. KEY WORDS (Continue on reverse side if necessary and identify by block number)

Cable	Stored charge
Shielded Wire	Trapped charge
Polymer	Satellites
X-rays	Space radiation

20. ABSTRACT (Continue on reverse side if necessary and identify by block number)

A combined experimental and analytical study was made of the mechanisms which determine the response of satellite cables to x-rays. Parameters investigated include gaps, with and without trapped air, polymer type, stored charge effects introduced by manufacturing or handling, trapping of space electrons in the dielectric, radiation conductivity, sample-to-sample and manufacturer-to-manufacturer variations, and dose effects. It was found that the principal mechanism enhancing response was the presence of gaps between

DD FORM 1 JAN 73 1473 EDITION OF 1 NOV 65 IS OBSOLETE

20. ABSTRACT (Continued)

conductors and dielectrics which are naturally present in braided shield cables and can be introduced by bending in semirigids. The presence of stored charge was less significiant. An equilibrium distribution of trapped electrons will be built up in a period of about one-half hour for the artificial trapped environment and in about 20 days in the natural space environment, which will obliterate any previously stored charge. The so-called first pulse anomaly will occur only when one has a cable containing air filled gaps. In this case, the first shot rather than the n^{th} shot response will be most typical of cable behavior.

ACKNOWLEDGEMENTS

We gratefully acknowledge the assistance, encouragement, and helpful discussions with many individuals and organizations: Captain Mike Bell and Lt. Col. Ted Hawranick of the Defense Nuclear Agency; Dave Clement, Bob Lowell of the Electromagnetic Hardness Department, TRW; Fred Nunez, Len Mullich and the other members of the Satellite Cable Group of TRW; Don McMorrow of MRC; Tom Mattingley of Ford Aerospace; Albert Martin, Bruce Michels, and John Ronchetto of Raychem; Terry Flanagan and Ray Denson of JAYCOR; and Andy Weiman of IRT Corporation.

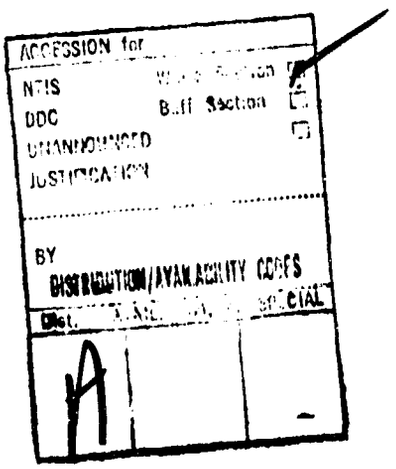

EXECUTIVE SUMMARY

A combined experimental and analytical investigation has been performed to study the so-called anomalous first-pulse responses to x-rays in five representative satellite coaxial and single-conductor braided-shield cables. This response pattern is characterized by first-pulse responses which are much larger than expected, which are often of opposite sign than predicted, and which decrease significantly with accumulated dose. These anomalies have, at various times, been attributed to gaps, stored charge in the dielectric due to manufacturing and handling, trapped charge due to previous radiation history, either from space radiation or a previous irradiation, and ionization of air trapped in gaps. This program was undertaken to investigate in a systematic way the relative contributions of geometry, environment, and radiation factors to the net cable response, to bound the magnitude of the stored and trapped charge effects, to minimize or at least identify the manner in which the experimental techniques used for measurements in a simulator affect responses, and to develop some statistics on response variations between cables of the same nominal type.

For each set of experiments, cable responses were measured simultaneously for three supposedly-identical samples (same manufacturer and pretreatment) to obtain some inefficient statistics. Beam fluence, dose, and dose rate were mapped on every shot. The test variables included the same cable types from different manufacturers, different mechanical working of the cables (bending or flexing) to simulate handling effects, thermal annealing to see if persistent stored charge/polarization could be relaxed, and looking at response as a function of dose and irradiation time history. Portions of representative cable samples of each type were sectioned and photomicrographed to obtain estimates of the size and location of the cable gaps which were identified as an important factor in determing cable responses. All of the tests were performed in vacuum in an attempt to simulate conditions under which satellites would be exposed in a real environment. The tests were performed on the SPIRE Pulse 6000 machine. The incident fluence per pulse varied between 0.15 and 0.35 mcal/cm^2, corresponding to an external dose of about 20 rads(Si). Each set of cables was exposed to anywhere from 5 to 30 pulses, depending on the observed response.

For unbent, as-received, semirigid cables, the measured and predicted responses (assuming no gaps) agreed in sign (positive) and in magnitude within a factor of two. (A positive response means a net flow of charge from the center conductor through an external load resistor to the outer shield. In other words, the net motion of electrons inside the cable is from the center conductor toward the shield.) For these tests, there was only minor shot-to-shot variation in the responses. Bending the semirigid cables usually caused a large (positive) increase in the first-pulse response. For a few samples, the net response after bending was negative and comparable in magnitude to the response for unbent cables. These changes can be explained by assuming that the bending creates gaps on the order of 20 to 200 μm between the conductors and the dielectrics. Gaps near the center conductor produce an enhanced positive response and those near the shield produce negative responses. The initially large positive responses decreased from shot to shot by factors of 3 to 5 for accumulated doses of less than 1 krads(Si).

Although it is difficult to obtain accurate estimates of gap sizes by sectioning the cables because of the irregularity of cable cross sections, calculations using gaps sizes estimated in this manner gave agreement within a factor of about 5 compared to measured first-pulse responses for all sets of the three braided-shield cables. In several cases, the agreement was considerably better. The Spec 44 cable showed little shot-to-shot variation in response while the maximum change for one of the RG-178B/U cables was a decrease of about 3.5 with accumulated dose. The largest changes with accumulated dose occurred with the Spec 88B cables. Factors of 10 decrease were common and, for one cable, the response changed from unipolar negative to bipolar (negative to positive) and then unipolar positive. Annealing and flexing these cables sometimes affected the responses.

Based on an analysis of these results and other information in the literature, the following conclusions have been drawn:

1. For as-received flexible and unbent semirigid cables, the spread in the first pulse response data for a group of three samples from the same manufacturer was within a factor of 3 and within a factor of 4 for all samples of the same cable type (different manufacturers). For semirigid cables, bending increased the first pulse responses by as much as a factor of 40 and sometimes caused considerable scatter in response and even reversal of signs

compared to the responses for as-received cables. Some annealed flexible cables had spreads in the first-pulse responses of factors of 8 for the same manufacturer.

2. Of the identified factors that affect cable responses, gaps between conductors and dielectrics are probably the most important factor in determining the magnitude and the sign of the responses evoked by x-rays. While these gaps are large enough to significantly alter radiation responses, they produce little detectable change in the normal electrical behavior of cables.

3. Very large gaps can be introduced in semirigid cables by bending according to accepted fabrication practices. These gaps greatly increase the cable responses.

4. Handling and thermal annealing of braided cables can somewhat alter their responses but not by orders of magnitude since the initial gap effects are usually quite large and predominant.

5. There is little evidence that stored-charge significantly affects the X-ray response of cables in vacuum.

6. In a space electron environment, any charge stored in a satellite cable prior to launch will be replaced, in times on the order of 20 days, with the equilibrium distribution created by space electrons. In a post-explosion environment, equilibrium is reached in about 1/2 hour.

7. The shot-to-shot decrease in responses with accumulated dose is not an annealing, but a radiation-polarization, effect. Since this polarization could enhance the response for a photon pulse arriving from a different direction, "radiation-annealing" is not a useful procedure to reduce or control subsequent radiation responses, nor is it a means of preconditioning a cable to obtain a "true" cable response.

8. Thermally annealing cables at temperatures which are within recommended cable operating temperatures has no significant effect on responses. This is not surprising in view of observation No. 5 above.

9. It is postulated that the decrease in cable responses on successive pulses is due to the buildup of electric fields across the gaps whose source is the

emitted charge trapped in the dielectric which drives a reverse current across the gap through the ionized air trapped in the gap. This reverse current opposes the effect of the photo-driven current and reduces the response of the cable as measured in an external circuit. Cables which show little shot-to-shot variation apparently are more easily outgassed than the cables that showed large variations. Such cables can still show an enhanced response over the ideal case because of the presence of gaps.

10. Based on the postulated model in (9), one would not expect to see the shot-to-shot decrease in response, at low doses, for well - outgassed cables such as one would expect in a satellite environment. However, a cable may have gaps that are not easily outgassed because they are not connected to the cable exterior. Air could be trapped in such gaps for long periods of time and thus affect the response of cables in the hard vacuum of space.

11. A noticeable decrease in response with accumulated dose for cables without trapped air would occur only after considerably larger fluences when charge buildup in the dielectric becomes large enough to produce significant return currents through the dielectric itself. However, the departure from linear behavior with fluence will probably occur at a higher fluence than in the ideal gap-free case if gaps are present between the conductor and the dielectrics. The fluence at which this decrease will become significant is inversely proportional to the radiation-conductivity coefficient for the polymer dielectric.

12. The model in (9) implies that the first-pulse responses, as measured with a low-dose pulse, are more representative of the "true" response of a satellite cable than the asymptotic responses at large accumulated doses.

13. Laboratory experiments on cables to be used in satellite environments should be performed on well-outgassed samples. The pulse-to-pulse variations for a few low-dose pulses should be observed and the initial pulse used to obtain the magnitude of the normalized response.

14. A minimum of three samples of each cable type and treatment should be tested to provide some indication of the spread in the data for supposedly identical samples. Tests should also be made to determine the outgassing

properties of each cable type as well as representative gap sizes not only for as-received cables but also after representative handling and bending.

15. The recommended procedure for extrapolating test data from laboratory doses and spectra to threat conditions is to use a combination of analysis and experiment. The experimental results should be compared to calculations for the laboratory situation and any discrepancies between experiment and prediction should be interpreted in terms of cable gaps and possibly trapped air. The response for that cable when exposed to the threat dose and spectrum can then be calculated based on the structural model developed during testing.

TABLE OF CONTENTS

LIST OF FIGURES

LIST OF TABLES

1. INTRODUCTION

In order to produce a satisfactory radiation-hard spacecraft, one of the major vulnerability mechanisms that must be considered is the response of electrical cables to direct excitation by incident x-ray and gamma photons. Therefore, it is important to be able to predict with reasonable accuracy the response of system cables to the threat environment in order to determine system survivability and needed levels of circuit protection. In practice, this means using analytic or computer based techniques, which are validated by simulator testing, to calculate the response at fluences and spectra of interest.

For this discussion, a cable is defined as either (a) two or more equal-length, insulated conductors, solid or stranded, twisted or molded together without a common covering, or (b) one insulated conductor with a metallic covering shield or outer conductor.[1] Thus, this definition includes such species as coaxial cables, both flexible and semi-rigid, shielded wires, and shielded pairs, all of which may be used in a missile or spacecraft, usually as part of a cable harness consisting of several cables in a common assembly.

Throughout the history of radiation-effects studies, system designers and analysts have been plagued with the problem of how to obtain realistic (even order of magnitude) estimates of cable responses to their threat photon pulses. The calculation of cable responses from first principles is complicated by uncertainties in the cable geometry, material properties, and the interaction processes between the photons and electrons and the cable material. Also, there is a cancellation effect between the contributions to the cable responses from the different cable conductors such that the net response is often a relatively small difference between two large numbers. The experimental situation is perhaps even more clouded. The responses of supposedly identical types of cables tested under similar conditions often differ by orders of magnitude, and sometimes even in sign. Moreover, the response of the same piece of cable often changes drastically for successive pulses of photons. In many tests it has been observed that the

[1] MIL-W-83575, Military Specification, Wiring Harness, Space Vehicle, Design and Testing, 1 March 1973.

response of a cable to the first pulse is larger than the subsequent responses. This phenomenon of a larger first-pulse response has often been called the "first-pulse anomaly."

Over the years, numerous analytic and experimental studies have been undertaken in an attempt to identify the factors which affect cable responses to incident photon pulses and the causes of the anomalous responses. It is now felt that all of the contributing mechanisms have been identified and it is indeed possible to understand cable response to radiation. The major factors that have been identified are discussed below.

1.1 RADIATION GENERATED PHOTOCURRENTS

The incident photons interact with the electrons in the cable conductors and dielectrics and produce photocurrents inside and between the materials. The resulting charge displacement produces electric fields and voltages between the various cable conductors which, in turn, cause replacement currents to flow from one conductor to another through the attached external circuits. Under threat conditions, these replacement currents can cause equipment upset and/or burnout unless adequate hardening procedures are used in the system design.

1.2 GAPS BETWEEN CABLE CONDUCTORS AND DIELECTRICS

Because the range of the secondary electrons that are emitted from the conductors into the dielectrics by the incident x-rays is relatively short ($\approx$10 μm), the presence of small gaps, comparable in size to the electron ranges, can significantly increase the effective range of the emitted electrons and enhance the resultant replacement current. This effect has been discussed extensively in References 2 through 7. The size of the gaps,

[2] J. M. Wilkenfeld and R. E. Leadon, Research on the Physics of Transient Radiation Effects in Coaxial Cables, Monthly Progress Reports for Harry Diamond Laboratories Contract DAAG39-77-C-0089, IRT Documents 8148-011 and 8148-015, March 1977, May 1977.

[3] D. M. Clement, L. C. Nielsen, T. J. Sheppard, and C. E. Wuller, Stored Charge Release in Cables in Low Fluence X-Ray Environments, Topical report prepared on DNA Contract DNA001-77-C-0084, 9 April 1977.

[4] D. M. Clement and C. E. Wuller, Cable Parameter and Photon Source Parameter Sensitivity in Low Fluence X-Ray Environments, Topical report on Contract DNA001-77-C-0084, 8 April 1977.

[5] R. L. Fitzwilson, M. J. Bernstein, and T. E. Alston, Radiation-Induced Currents in Subminiature Coaxial Cables, IEEE Trans. Nucl. Sci., NS-20, 58 (1973).

[6] F. Hai, P. A. Beemer, C. E. Wuller, and D. M. Clement, "Measured and Predicted Radiation-Induced Currents in Semi-Rigid Coaxial Cables," IEEE Trans. Nucl. Sci., NS-24, (1977).

[7] W. Chadsey, B. L. Beers, V. W. Pine, and C. W. Wilson, "Radiation-Induced Signals in Cables," IEEE Trans. Nucl. Sci., NS-23, 1933 (1976).

at least in semirigid cables, can be increased by bending. The presence of gaps in braided-shield cables is a major factor in determining their response.

1.3 AIR CONDUCTIVITY

Air trapped in gaps between conductors and dielectrics will be ionized by incident radiation. The photocurrent generated by the radiation will also set up a polarization field due to trapping of electrons emitted from conductors into the dielectric. The resultant field will generate a current flow in the gap which opposes the photocurrent. The net replacement current in the external circuit will be diminished or, in some cases, even change sign. It has been convincingly argued that the presence of air in gaps is a prerequisite for observing anomolous effects in cable responses exposed to simulator irradiation.[3]

1.4 INTERFACE ENHANCEMENT

Because the atomic number of conductors, especially those with coatings, is much higher than that of dielectrics, the net secondary emission current generated by the x-ray exposure is much larger from the conductor to the dielectric than from the dielectric to the conductor. Moreover, it can be an order of magnitude or more larger than the primary photocurrent in the dielectric.[7] This net current across the interface is the main driving function for the external replacement current. In addition, there is a dose-enhanced photoconductivity in the insulator near the conductor-dielectric interface. The stopping of the emitted secondary electrons also produces a space-charge polarization field between the dielectric and the conductor. This electric field, coupled with the radiation-induced conductivity, causes a conduction current to flow which opposes the primary photocurrent. Since the polarization field is dose dependent, so is the conduction current. This produces a nonlinear response which leads to a saturation of the cable signal at high fluences. The enhanced dielectric photoconductivity in the bulk of the dielectric also causes the radiation-induced signal to be attenuated as it propagates along the cable.

1.5 STORED CHARGE

It has been shown that manufacturing, conditioning, or handling processes can introduce trapped space or polarization charge into polymer dielectrics.[2,8] The

[8] J. Wilkenfeld and V. Junkkarinen, Thermal and Radiation Depolarization of Persistent Charge Stored in Polymer Dielectrics, IRT Document INTEL-RT 8124-005, August 1976.

presence of stored charge in cable dielectrics has been proposed as one of the prerequisites for observing anomalous cable response in a simulator test.[3] Postulated processes for the introduction of stored charge include: (a) the electro-kinetic charging of the dielectric during extrusion; (b) heterocharging as a consequence of polymerization or fabrication processes; (c) radiation cross-linking of the dielectric by energetic electrons to improve dielectric properties.[2]

1.6 TRAPPED CHARGE

Previous irradiation will generate photocurrents which result in the trapping of charge in cable dielectrics. Such radiation-induced charging can be brought about by (a) prior exposure in a simulator, (b) a multipulse threat environment, or (c) exoatmospheric trapped electron belts.[9]

1.7 EFFECT OF BIAS OR OTHER EXTERNAL LOAD ON RESPONSE

Under simulator environments it has been observed that the cable responses change with the magnitude of the external bias voltage.

The original intent of the present investigation was to (1) investigate the relation, if any, between the first-pulse anomalies and the charge stored in cable dielectrics by manufacturing and handling processes, (2) determine test techniques to remove stored charge from cables, (3) assess the importance of stored charge for satellite systems, (4) determine analytically the effect of trapped charge on the response of cables to x-radiation, (5) recommend procedures for testing cables in laboratories, and (6) for extrapolating test data to threat levels and photon spectra. However, during the program, evidence began to accumulate that stored charge was probably not as important for cable responses in satellite situations as had first been believed. Consequently, the emphasis was changed to try to determine the causes of the often-observed shot-to-shot decreases in the cable responses and to develop a model for these results. Because the program now focused on the phenomenology which determined cable behavior, and not on development of codes for prediction of cable response in arbitrary cables geometries, it was agreed with the Contracting Officer's Representative to limit the investigaton to typical coaxial cables, both flexible and semirigid, that are used in satellites.

---

[9] R. Leadon, Effect of Trapped Space Electrons on Cable Responses, Topical report prepared for Computer Sciences Corporation under Contract F29601-76-C-0014, IRT Document 0031-067, 26 May 1977.

The remainder of this report is organized as follows. Section 2 begins with an outline of a typical life history of a satellite cable to identify the processes, such as extrusion, handling, bending, or flexing, which might introduce stored charge into its dielectrics and influence its response to a photon pulse. The several processes which are known to produce stored charge in dielectrics are discussed. Based on the published literature, estimates are made of the probable amounts of stored charge for each process. Section 3 describes the theory of cable responses to photon pulses, in particular for coaxial cables. The theory is given first for an ideal coaxial cable without gaps or stored charge and for a low dose rate per pulse so that radiation-induced electrical conductivity can be ignored. The discussion is then extended successively to cable gaps in vacuum, high-fluence effects including radiation-induced conductivity, stored and trapped charge, and ionization of air trapped in the cable gaps. Many of the detailed calculations and derivations are deferred to Appendices A through D. Section 4 describes the experimental techniques used to measure the response of a group of representative satellite cables to x-rays. Also described are sample characterization, preiradiation cable treatments, test setup and data recording, and machine characterization and dosimetry methods. The results of the experiments are summarized in a series of tables and analyzed in Section 5. The detailed shot-to-shot normalized amplitudes versus accumulated fluence and dose are given in Appendix E. Section 6 contains an assessment of our results, cable response mechanisms, and testing procedures in general.

2. CHARGE STORAGE AND HANDLING PROCESSES AFFECTING CABLE RESPONSE

2.1 INTRODUCTION

In this section some of the factors which can alter cable responses are identified. This discussion is based on a hypothetical satellite life history, from fabrication of components to orbit, presented in Section 2.2. This life history has been used as a basis for identifying processes which alter cable responses. It can be seen that there are three mechanisms which can significantly alter the response of cables from that of the ideal, gap-free cable. These mechanisms, which are discussed in Sections 2.3, are:

1. The introduction of persistent bulk or surface stored charge into the cable during manufacture, during extrusion of the molten polymer through a metal die to form the inner dielectric, by the friction produced by rubbing the finished polymer against another material, and during irradiation cross linking of the polymer to improve its thermal and mechanical properties.

2. The introduction of gaps between cable conductors and dielectric either during manufacture when, for example, braid shielding is put over the dielectric, or during subsequent fabrication of the cable harness, or, for example, when semirigid cables are bent. As will be discussed in Section 3 of this report, the effect of a gap on cable response may be altered if air remains trapped in the gap during photon exposure.

3. Exposure to the natural and artificial trapped space-electron environment where charge will be built up in the interior of cable dielectrics. For satellites in orbit, this process is more important than process (1) because the space electron flux will wash out any previous stored charge distribution in times ~1/2 hour for the artificial trapped environment and ~20 days for the natural trapped electron flux.

The manner in which each of these mechanisms alter the response of the cable to cause the "anomalous" response is discussed in subsequent sections.

2.2 SATELLITE CABLE LIFE HISTORY

To identify correlations between processes known to alter cable response and the manufacturing, handling, testing, and launch procedures to which satellite cables are subjected, as well as their subsequent exposure to the space radiation environment, a representative cable life history has been assembled. Satellite cables are taken from a subset of the aerospace military types and are qualified according to the relevant Mil Specs. Additional requirements may be placed on the performance of these cables because of the special environment in which they operate, such as low outgassing of jacket or primary dielectrics as given in particular satellite specs. In assembling this information, we have used a variety of sources. These have included the relevant Mil Specs for coaxial cables and shielded, insulated wire:

1. MIL-C-17E: Cables, Radio Frequency, Flexible and Semi-Rigid, General Specification for, 12 July 1974.
2. MIL-C-27500D: Cable, Electrical, Shielded and Unshielded, Aerospace, 13 August 1976.
3. MIL-W-81381A: Wire, Electric, Polyimide-Insulated, Copper-Copper Alloy, 4 October 1976.
4. MIL-W-81044B: Wire, Electric, Cross-Linked Polyalkene, Cross-Linked Alkene-Imide Polymer, or Polyarylene Insulated, Copper or Copper Alloy, 23 February 1976.
5. MIL-W-22759D: Wire, Electric, Fluoropolymer-Insulated, Copper or Copper Alloy, 29 June 1973.
6. MIL-C-45224C: Cable and Harness Assemblies, Electrical, Missile System, General Specification for, 8 February 1971.
7. MIL-W-83575 (USAF): Wire Harness, Space Vehicle, Design and Testing, 1 March 1973.

These specs control the assembly and testing of missile and spacecraft wiring harnesses and the following govern testing of spacecraft.

8. MIL-STD-1540A Test Requirements for Space Vehicles, 15 May 1974. (USAF).

9. MIL-STD-810A: Military Standard Environmental Test Methods for Aerospace and Ground Equipment, 23 June 1964, and Test Documents for several spacecraft systems.

The information from the Mil Specs has been supplemented by discussions with cable and satellite manufacturers, and examination of the specifications for particular spacecraft cable and cable harnesses and of the relevant acceptance test documents which provide specific information on test and space environments.

The life history of a typical spacecraft can be broken into seven phases. These are graphically illustrated in the flow chart of Figure 1. In the flow chart, processes which may introduce stored or trapped charge or alter cable response by gap formation are marked with an asterisk. These phases are:

1. Manufacture of the cable components. This task includes polymerization of the dielectric and its formation into powder, pellets, or tape, and the drawing of the cable conductors and any post-treatment such as annealing, plating, or stranding to produce desired mechanical, electrical, or geometric characteristics. We have identified the polymerization process as possibly creating persistent internal polarization.

2. Manufacture of a finished cable. The assembly process can be logically broken down into several steps: placing the primary dielectric coating on the inner conductor; processing and testing the partially formed cable; adding the outer conductor and jacket; and final processing. Possible charge storage processes in this phase include: (1) extrusion; (2) spooling of the cable after the primary dielectric is applied (friction); and (3) radiation cross linking of either the primary dielectric or jacket. A much more significant effect is the creation of gaps between cable conductors and dielectrics. For example, the braid shielding enclosing the dielectrics of a single cable or those of a multiple-conductor single-shield bundle invariably contain gaps $\sim$10-40 μm whose presence enhances the response of a cable by an order of

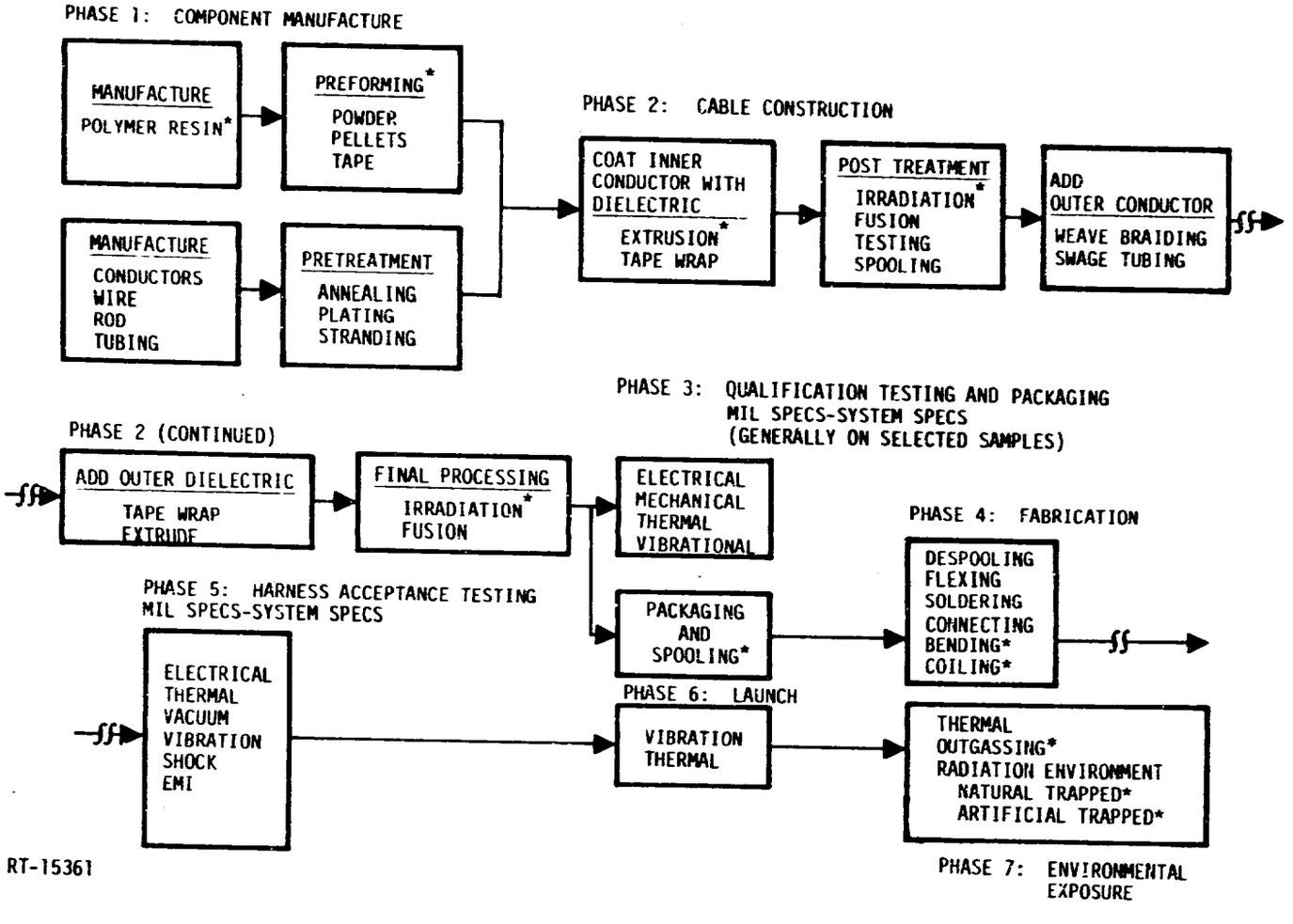

Figure 1. Typical spacecraft cable life history

magnitude. This effect has been discussed many times in the past but cannot usually be quantified. Good discussions are given in References 7 and 10.

3. Qualification testing of the cable to determine whether it meets the relevant military and systems specifications. Most of the tests are performed on selected samples, which are subsequently discarded; therefore, such tests have no effect on cable which is used to manufacture cable harnesses. However, there are two exceptions. First, 100 percent of the primary dielectric and jacket materials are tested for breakdown. This is typically an a.c. test (60 Hz), and probably does not significantly polarize the dielectrics as the orientation times for heterocharging at ~300°K are typically much longer (i.e., they are lower frequency processes). The second exception is a test for conductor continuity. Such a test should have no significant affect on the cable dielectric. After testing, the cable is spooled. While the spooling restrictions are cable specific, a typical requirement is that the cable spool i.d. be ≥20 times the o.d. of the cable. Thus, a significant increase in gap is not expected to be introduced except possibly in semirigid cables.

4. Fabrication of a cable harness. This includes tasks such as despooling, flexing, soldering, forming connectors, and bendings and coilings to form a cable hardness. Bending and coiling of cables to follow structure or provide stress relief, especially of semirigid cable, can significantly alter cable response. Test data discussed in Sections 4 and 5 demonstrate that bends of semirigid cable can introduce gaps which can significantly alter their radiation response but have a negligible effect on electrical properties. On the other hand, flexing of shielded wire has little effect on response as the predominant factor is the presence of gaps between the dielectric and the outer braid.

5. Testing of the completed cable harness. The specific electrical, thermal, and mechanical tests performed are governed by MIL-C-45224C and MIL-W-83575 (USAF), as modified by particular system specifications. Cables

[10] D. M. Clement and C. E. Wuller, Assessment of Cable Response Sensitivity to Cable and Source Parameters in Low Fluence X-ray Environments, DNA Topical Report 4407T, 8 April 1977.

which are part of assembled spacecraft or missile harnesses are 100 percent acceptance tested. Therefore, if any of the test procedures are likely to create persistent charge in a dielectric, it will occur during this phase rather than during Phase 3. None of the thermal vibrational or electrical tests are likely to alter cable response except as they increase the gap size between conductors and dielectrics.

6. Satellite launch. After a satellite is manufactured and tested, it is launched. During the launch period it is subject to thermal and vibrational stresses which are probably in excess of those generated by motion of the satellite while in orbit.

7. Environment exposure. The ambient radiation environment to which a satellite is exposed in orbit will inject significant trapped charge into cable dielectrics. The most important components of this environment are the natural and artificial trapped electron fluxes. The former consists of electrons with energies of $\simeq$0.05 to 4 MeV ($<E>\simeq$0.1 MeV) at current densities of $\leq 5 \times 10^{-12}$ amp/cm^2. The latter consists of electrons with energies of $\sim$0.1 to 5 MeV ($<E>\simeq$1 MeV), at current densities of $\simeq 10^{-10}$ amp/cm^2.[11] As we discuss in Chapter 3 and Appendix D, the space electron environment will wipe out any stored charge effects while creating a new trapped charge distribution in the cable with times $\sim$1/2 hours for a typical fission electron spectrum and about 20 days for some natural environments. In addition, any trapped air remaining in the cable gaps may slowly outgas in the vacuum of space. The removal of air will alter cable response in a manner which depends on fluence and pressure. This effect is discussed in Chapter 3 and Reference 12.

2.3 MANUFACTURE OF CABLES - INTRODUCTION OF STORED CHARGE

In this section, we focus on the processes by which stored charge can be introduced into a cable. The other two significant factors, gaps and trapped charge, are discussed in Section 3 and the Appendices.

[11] J. Singley and J. J. Vettie, A Model Environment for Outer Space Electrons, NCSDS Report 72-13, Dec 1972.

[12] C. E. Wuller, L. Carlisle Nielsen, D. M. Clement, Definition of the Linear Response Region of X-ray Induced Cable Response, DNA Topical Report 4405T, 13 May 1977.

2.3.1 Polymer Processing

There is evidence that the steps employed to manufacture commercial polymers may leave persistent internal fields present in them or introduce dissociable impurities which may be polarized. Many polymers are manufactured from monomers which have orientable molecular dipoles. Chemicals are often added to the monomer to control the polymerization process or to produce a final material possessing desirable properties, such as resistance to oxidation. Such additives may dissociate under heat and bias to produce a persistent internal polarization. Such polarization of internal charge or dipoles is known as heterocharging.[13] Evidence of such behavior is implicit in the observation that the initial measurements of the conductivities of virgin polymers are often much higher than that determined for thoroughly annealed samples. This happens because the initial heating relaxes internal space-charge fields due to stored charge which causes an extra component of replacement current to flow in an external circuit in addition to the normal conductivity current. After annealing, one observes only the conductivity current.

In polar polymers (i.e., those containing orientable molecular dipoles), persistent internal fields can be created not only by burn-in, but also as a consequence of random local stresses introduced in the manufacture of the polymer.[14] For example, in films made from Mylar A (polyethylene terepthalate) the thermal relaxation of such dipoles releases an amount of charge ~100 pC/cm^2 if the polymer is heated to above 100°C. The appearance of peaks at 73.5°C and 105.3°C in the thermally stimulated current released when a sample is heated at a constant rate of temperature increase corresponds to the relaxation of dipoles as the glass transition is reached and as dissociable impurity space charge at the higher temperature becomes mobile and recombines.[13]

Similar persistent fields may also be present in other polar polymers which are used in aerospace cable dielectrics. Such polymers include polyimide (Kapton), poly-(vinylidene fluoride), otherwise known as PVF_2 or Kynar, polyarylene (Stylan), and polyalkene, as identified in the relevant Mil Specs[15] and the tabulations from other

---

[13] J. Van Turnhout, Thermally Stimulated Discharge of Polymer Electrets, Elsevier, Amsterdam 1975, Chapter 10.

[14] E. Sacher, J. Macromol Sci-Phys B6, 151 (1972).

[15] MIL-C-27500D (USAF), Cable, Electrical, Shielded and Unshielded, Aerospace.

cable programs.[3,16] No specific data has been found for the magnitude of the depolarization charge released from virgin samples of such polymers. Previous work[17] has identified such polarization to be a bulk phenomenon. The ultimate polarization due to the alignment of molecular dipoles is porportional to the difference between the static and high-frequency dielectric constants which is a measure of the nonelectronic polarizability of these materials. This difference can be roughly approximated by $\kappa - n^2$, where κ is the low-frequency dielectric constant and n is the optical index of refraction. There may also be an additional contribution from the relaxation of polarized dissociable impurities whose magnitude depends on the concentration of such impurities. Based on values for these parameters (q.v. Figure 25 of Reference 17), one estimates that the possibility for polarization in Kapton and polyarylene should be comparable to that in Mylar. PVF_2 may show a much greater effect because of its large low-frequency dielectric constant. In fact, the actual degree of polarization will depend on the strength of the local orienting field, the degree of mobility of molecular dipoles and/or space charges (which depends on the formation temperature), and finally on the concentration of polarizable or dissociable molecules. One can create such persistent polarization only if there is simultaneously present a sufficiently high temperature such that the molecular dipoles are free to rotate or that the space charges may dissociate and become mobile, as well as a means of separating the space charge and/or aligning the molecular dipoles such as an applied field or a uniaxial stress. This requires temperatures to be above the polymer's glass transition. Since polymer processing requires that the material have a relatively low viscosity, this condition is usually met at some point. The conditions to create polarization are clearly present when capacitors are put through the quality assurance procedure known as burn-in, and probably in the manufacture of polymer films which are often uniaxially or biaxially oriented to improve their mechanical properties. While polymer dielectrics used in cables are often raised to sufficiently high temperatures which make polarizable species mobile, it is not clear that a forming field or stress is present during their manufacture analogous to burn-in or the orientation applied to capacitor films. Therefore charging probably occurs by another method.

---

[16] F. Hai, Summary of Cable Response Experiments, SAMSO-TR-77-151 15 July 1977.

[17] J. Wilkenfeld, Radiation Effects in Insulator Materials, Final Report HDL-CR-77-089-1, IRT Report INTEL-RT 8148-011, Feb 1977.

In the absence of specific data on the depolarization response of virgin samples of any of the commonly used cable dielectrics, other than Mylar and Teflon TFE (polytetrafluoroethylene), one may estimate an upper bound for the net charge per unit outer dielectric area, q_{max}, released to an external circuit as a consequence of the depolarization of persistent internal fields. This bound is

$$q_{max} = \frac{(\kappa - n^2)}{\kappa} \frac{CV}{\pi d} \tag{1}$$

for a cable of capacitance per unit length C, containing a dielectric whose o.d. is d, possessing a dielectric constant κ and an index of refraction n. In Table I, we have calculated q_{max} for some of the dielectrics employed in aerospace cables based on information taken from References 15, 16 and 3 for a representative cable whose outer diameter is equal to that of an 0.218 cm (0.086 inch) semirigid cable (denoted as SR086), i.e., with an inner dielectric diameter of 0.051 cm and an outer dielectric diameter of 0.168 cm. This has been done for comparison with the model calculations for the radiation-induced replacement current. It is to be stressed that the data of Table I represent an upper bound to charge release possible either by thermal stimulation or radiation relaxation due to this one effect, i.e., bulk stored heterocharge, not taking into account other components of the net replacement current, such as the driven charge. Listed in Table I are two polymers (polyalkene and polyarylene) which have been used in spacecraft cable dielectrics for which we have no data on κ or n. It is unlikely that $\kappa > 3.5$ for these dielectrics which means that $q_{max} < 1$ nC/cm^2. While we have provided data for commonly used aerospace cables, nearly all of those used in spacecraft have Teflon TFE, polyalkene/PVF_2, or Kapton/FEP dielectrics. GPS uses cables with a Stylan dielectric (Spec 88). Therefore the cables chosen for testing were selected accordingly.

It is to be noted that the values of $\kappa - n^2$ for the fluorocarbons are rather high for these nonpolar polymers. It is our experience, based on measurements of films made from Teflon TFE configured in capacitors, that the net charge released in a thermal or radiation-induced discharge corresponds to a $\kappa - n^2 \leq 0.01$ or ≤ 100 pC/cm^2 for capacitors which were thermally annealed and consequently burned in. For annealed samples, the net charge release could be a factor of 10 or so higher, dependent on previous history. It can be seen that poly(vinylidene fluoride) may be especially problematic because its dielectric constant and, hence polarizability, is high. One of the

TABLE I. UPPER BOUND ON STORED CHARGE PER UNIT DIELECTRIC AREA FOR HETEROCHARGED POLYMERS

Polymer	κ (10^3 H_3)	κ-n^2	q_{max}[a] (nC/cm^2)
Polytetrafluoroethylene (Teflon TFE)	2.1	0.28	0.37
Polytetrafluoroethylene-Polyhexefluoropropylene copolymer (Teflon FEP)	2.1	0.30	0.40
Polyethylene	2.3	0.01	0.013
Polyalkene	2.85?		<1?
PE-PTFE copolymer (Tefzel)	2.6	0.65	0.86
Polyarylene (Stylan)	<3.5		<1?
Poly(ethylene terepthalate) (Mylar)	3.25	0.52	0.68
Polyimide (Kapton)	3.5	0.33	0.44
Poly(vinylidene fluoride) (Kynar)	8.1	6.0	8.0

[a] *For an SR086 cable*

sample cables, the Spec 44 has a dielectric composed of two layers, the outermost of which is PVF_2 (see Table II).

In principle, one can relax the persistent internal fields created by heterocharging by heating the cable to a sufficiently high temperature (above the glass transition temperature of the polymer dielectric) under short circuit. In practice, such a procedure may damage the cable by causing separation of the dielectric and conductor. The gaps introduced by such a procedure may significantly alter the radiation response of a cable so treated (q.v. Section 3.2). The reason for this is clear. Significant molecular motion and release of stored charge will occur above the glass transition temperature. Above this temperature, the viscosity of the polymer decreases markedly, so that it flows more readily, especially if the dielectric is under stress because of bending. In addition the unequal thermal expansion can also create gaps. Therefore, for test cables, it is not possible, as a practical matter, to relax persistent internal stress charge by annealing at temperatures above that for the glass transition.

2.3.2 Extrusion

The second procedure by which persistent stored charge may be introduced into a cable is extrusion. In the formation of a cable dielectric, the center conductor is pulled through a metal die. Also forced through the die is molten polymer under a pressure of several kpsi. This dielectric subsequently hardens on cooling to form the primary insulation. Such a process is known to store persistent charge in polymers. Taylor and coworkers have demonstrated that, when a molten polymer flows through a metal capillary, a dipole layer is formed along the interface.[18,19] As the polymer passes out of the capillary, this dipole layer is sheared, leaving the dielectric charged. As the dielectric is cooled, this charge may be frozen in or trapped. The amount of charge trapped for the polymers studied is 10^{-11} to 10^{-9} C/cm^3. It is believed that such charge lies within 10 μm or so of the surface, such that the equivalent effective surface charge is 5×10^{-11} to 5×10^{-9} C/cm^2 of extruded surface. The magnitude and sign of the charge trapped in the polymer depends on the properties of the particular polymer, any impurities present, the die material, the temperature of the polymer during extrusion,

[18] D. M. Taylor, T. J. Lewis, and T. P. T. Williams, J. Phys. D: Appl. Phys. 7, 1756 (1974).

[19] D. M. Taylor and T. J. Lewis, Proceedings 2nd International Conference on Static Electricity, Frankfurt, DFR (1973); Dechema Monograph, Vol. 72 (1974).

and on its mean flow velocity. As with other charge injected into polymers, it may persist for periods of several months or more at temperatures of ~300°K, residing in deep traps.

The authors of References 18 and 19 present data for the electrokinetic charging of polyethylene from which it is possible to make an estimate of the extrusion charging for this polymer under typical cable formation conditions. During our visit to Raychem Industries, manufacturers of space cable for satellites such as DSP, FLTSATCOM, GPS, and NATO 3, we learned that typical extrusion rates for polyethylene are 25 to 140 feet/minute corresponding to 0.13 to 0.71 m/sec. The temperature at which cross-linked polyolefin (a variety of polyethylene) dielectric was extruded was typically 400°F ≃204°C. The particular temperature and extrusion rates employed depend on the melt-flow viscosity of the polymer, and on the diameter of the dielectric to be formed. Data are given in References 18 and 19 for low- and high-density polyethylene extruded at temperatures of up to 190°C through a tungsten carbide capillary. Based on these data one finds that the net surface charge introduced into these polymers is approximately 50 to 250 pC/cm^2 for the low-density material, and ~500 pC/cm^2 for the high-density specimen. The sign of the charge stored is positive. These data assume laminar flow of the molten polymer. In Reference 19 it is shown that, if the flow of the polymer changes from laminar to plug (turbulent), then the stored charge can increase by a factor of 10 or more. The velocity at which plug flow occurs is temperature dependent. One may reasonably assume that the extrusion conditions are such that the polymer flows through the die in laminar flow to insure uniform filling of the dielectric volume without the formation of bubbles. However, the upper range of forming velocities at 400°F lies near that where the polymer flow becomes plug. The above estimates are probably not good to more than a factor of 2 or 3, as the net stored charge depends on both the capillary material, the additives present in the polymer, and temperature and flow velocity.

The limited data available for other polymers indicate that the charge stored in them as a consequence of extrusion may be a factor of 10 or so larger. Presumably, the stored charge can be relaxed by heating the cables to a sufficiently high temperature, well above the glass transition where the ohmic conductivity rises rapidly. Alternately, the relaxation of such charge can be promoted by making a thin outer layer of the dielectric a semiconductor so that the relaxation time is shortened. The effect of such treatment on dielectric attenuation is probably not significant for short lengths of

cable. However, this depends on the bandwidth of the signals propagated. Such a procedure will also diminish the effects of frictional charging.

2.3.3 Friction

When the surface of a polymer is rubbed against that of another material, frictional charging (triboelectricity) occurs rather readily. Such electrostatic charging can lead to significant problems in the processing of polymers where large uncontacted surface areas are involved, such as in making films. Where the change in properties can be tolerated, additives are incorporated in the polymers to enhance the relaxation of this frictional charge by increasing the material's conductivity. Where the charged surface is uncontacted (i.e., where there are no significant leakage paths, including those created by ambient moisture), such charge can persist for long periods of time. If surface dissipation does not occur, and the charge is not preferentially trapped near the surface because of a relatively large concentration of deep trapping sites created as a consequence of the charging process, then the injected charge will diffuse into the bulk polymer.[20]

A current model for the surface charging of polymers by friction is that of Davies.[21] This theory holds that the net surface charge per unit area σ injected into a polymer is porportional to the difference in work functions of the two contacting materials,

$$\sigma(\mathrm{C/cm^2}) = 1.77 \times 10^{-13}\, \kappa\, \frac{(\phi_m - \phi_d)}{\lambda} \qquad (2)$$

for a polymer with dielectric constant κ and work function ϕ_d, charged by a metal with a work function ϕ_m, both expressed in eV. In Davies' model, the charge is assumed to be uniformly injected up to a depth λ. The values of σ obtained correspond to maximum surface charge densities of ± 100 nC/cm^2 for materials charged in vacuum, a depth of penetration of the order of 0.05 μm, and dielectric work functions of 4 to 5 eV.

The values calculated from Equation 2 must represent an upper bound on the amount of charge stored on a polymer surface as a consequence of friction. This charge

---

[20] A. Wintle, J. Appl. Phys. 43, 2927 (1972).

[21] D. K. Davies, J. Phys. D: Appl. Phys. 2, 1533 (1969).

must relax in real cables in a variety of ways. First, the polymer surface may be contaminated as a result of manufacturing processes. A film of moisture may be present if air is trapped between the dielectric and outer conductor. These effects raise the surface conductivity of the polymer, and will thus enhance charge leakage, as will the presence of a metallic shield or outer conductor. Measurements made by Ong and van Turnhout[22] indicate that the level of charge induced by friction in high-density polyethylene in air is about 2 to 3 nC/cm^2. As the relative contact potential difference between the polymer and charging materials was not determined, it cannot be specified whether this value is a function of that difference or represents a practical limit after dissipation of loosely bound surface charge.

2.3.4 Radiation Cross Linking

One of the most interesting facts learned on a visit to Raychem Industries is that many of the cable dielectrics produced by this manufacturer are cross linked by exposure to fully penetrating electron irradiation after the cable is formed. Cross linking is carried out to improve the thermal and mechanical properties of the polymer by raising its maximum operating temperature and toughening it. Raychem is a major supplier of cable for the aerospace industry in general, and satellite manufacturers in particular (Spec 44/ and Spec 88/ cables are from Raychem). Many of the cables for the Defense Support Program (DSP), FLTSATCOM (FSC), Global Positioning System (GPS), and NATO 3 satellites have been supplied by this manufacturer.

In the manufacture of a typical cable with cross-linked polymers, the primary dielectric is extruded on the center conductor. Primary cross-linked dielectrics employed in Raychem cables include a modified polyethylene (polyolefin), combinations of polyalkene/poly(vinylidene fluoride), and polyarylene (stylan). After extrusion the dielectrics are irradiated. Specific dose and electron energy information is proprietary and was not available. However, it has been reported[23] that to cross link polyethylene, a dose of ~10 Mrads(C) is required. Based on a limited literature survey, this dose may vary by a factor of 10 either way for other polymers. After irradiation, the outer shield

---

[22] P. Ong and J. van Turnhout, Proceedings of the Second International Conference on Static Electricity, Dechema Monograph, Vol. 72 (1974).

[23] R. O. Bolt and J. G. Carroll, Radiation Effects on Organic Materials, Academic Press, New York (1963), p. 545.

or conductor is then added. Most spacecraft cables have an outer jacket which is also cross linked by radiation. Outer jackets are typically made from cross-linked, modified polyethylene, poly(vinylidene fluoride), and modified polyimide. After the outer jacket is extruded onto the polymer, it is cross linked. As we understand Raychem's manufacturing process, the irradiation is done with electrons whose energy is sufficient to penetrate the jacket but not the entire cable.

Clearly the cross-linking process will deposit some charge in the cable dielectric because of the stopping of the high-energy secondary electron component.

3. THEORY OF CABLE RESPONSE

3.1 INTRODUCTION

The response of a cable, that is, the net motion of charge between the inner and outer conductors, to a radiation pulse is dependent on several mechanisms whose net effect depends on the conditions of irradiation. These include the properties of the incident radiation, its fluence, flux and spectrum; properties of the cable materials which influence the generation and transport of photoelectrons, such as the atomic number of the constituent conductors and dielectrics, the dielectric constant, radiation-induced electrical conductivity coefficient, electron ranges; details of cable construction and structure, such as the relative atomic number of the conductor and dielectric which determines the degree to which dose and charge enhancement occurs at interfaces, the presence of gaps which, for x-ray-generated photoelectrons, can lead to significant range and response enhancement; and exposure conditions, i.e., whether testing is carried out in air or vacuum, and whether charge has been deposited in the cable because of prior exposure to radiation either in a simulator or in the space environment. Air-ionization effects in gaps can be significant in modifying the response of cable in simulators even when tests are carried out in vacuum. Our data shows that the relatively short pumpdown times (~18 mins. to hours) may not be sufficient to adequately evacuate trapped air for all cables although, in many cases, such times are sufficient. Outgassing times are very much cable dependent, i.e., on the cable structure and whether gaps are sealed. It must be stated that while it seems likely that the cables of orbiting satellites will be sufficiently outgassed to minimize trapped air effects, there may be cases where this is not the case. Trapped air effects are discussed in Section 3.6 using a model developed by David Clement et al of TRW[3]. In all cases, detailed calculations have been relegated to the appendices where numerical examples are given for representative situations.

In making analytical predictions of cable responses as functions of the above parameters, various approaches can be used with different degrees of sophistication and computer-aided automation. However, the physical model on which the calculations are

based is essentially the same regardless of the computational method used. In the following sections, the methods used in this program for predicting cable responses are sequentially described for models which become more sophisticated and more realistic as more of the above factors are incorporated. The simplest model describes the response to a low-fluence pulse of an ideal coaxial cable, that is, one without gaps, precharge, or previous radiation history. Then, in subsequent sections, modifications are described to predict the response to high-fluence pulses, which means accounting for the effect of radiation-induced conductivity on charge motion, and for real coaxial cables which may contain gaps, precharge, and whose response may change during exposure to repeated radiation pulses.

The quantity that is calculated as a measure of the cable response is the charge transfer per unit length of the cable, ΔQ. This quantity is obtained by first calculating the voltage ΔV_{OC} that would be developed in open circuit by the charge transfer in the cable and then multiplying by the cable capacitance per unit length. For a system assessment, the charge transfer ΔQ would be converted into a current source per unit length of the cable. The actual response of the circuit will depend on the length of the cable, its termination impedance, and the frequency content of the pulse. If the signal propagation time down the cable is short compared to the width of the pulse, and if the termination impedance is small, the time history of the circuit response will essentially follow the pulse. On the other hand, if the cable is short but the RC time constant of the system is longer than the applied pulse, the voltage in the circuit will rise approximately to the radiation-induced open-circuit value and then will decay away with the RC time constant. Finally, when the cable is long compared to the pulse width, the response will be dominated by the transmission line characteristics of the cable. Since these effects are system-dependent, they will not be discussed further in this report and we will only consider the driving functions per unit length of the cable.

3.2 RESPONSES OF IDEAL COAXIAL CABLES

The response of an ideal coaxial cable to x-ray radiation can be separated into the contribution from four effects, (1) the charge that is emitted inward from the outer conducting shield and is captured in the layer of the dielectric adjacent to the shield, (2) the charge that is emitted outward from the center conductor and is captured by the dielectric near that conductor, (3) the charge driven outward and inward from the dielectric into the shield and center conductor respectively, and (4) the charge that is

built up in the bulk of the dielectric because of attenuation of the photon beam. By charge conservation, the charge accumulated in the bulk of the dielectric is equal to the algebraic sum of effects (1), (2), and (3). Effect (1) produces a negative contribution to cable response, which is defined as electrons being driven out of the center conductor into the external termination, while effect (2) produces a positive contribution. The net effect of the inward and outward emission from the dielectric (effect 3) and charge accumulation in the dielectric (effect 4) will usually produce a negative contribution. Although effect (4) due to attenuation of the photon beam through the dielectric is always present, it is negligible for the small cables and relatively hard spectra considered in this program.

The net response of the cable is the algebraic sum of the four components. There is a partial concellation between the four contributions, which is fortunate since it reduces the net cable responses. However, it complicates the accurate prediction of cable signals because the net response is sometimes a small difference between relatively large numbers and a relatively small discrepancy in calculating any one of the components will have a disproportionately large effect on the net response. The following is the method that has been used to estimate these four contributions to the cable response.

The photons that are incident on the cable travel on essentially straight paths through the cylindrical cross section of the cables. Those photons which enter the cable near its line of symmetry (θ = 0, Figure 2) will pass through the sheath, dielectric, and center conductor. On the other hand, those that strike the outer conductor at positions such as paths 3 and 4 in Figure 2 will miss the center conductor. Moreover, the thicknesses of material which the photons traverse on various paths through the cable and the angles of incidence of the photon paths to the material surfaces are different. Therefore, a number of different paths through the cross section of the cable are selected to give a reasonable coverage of the circumference of the shield and center conductor. The number of such paths chosen is a compromise between a desire to keep the amount of computation to reasonable levels and the accuracy of the result desired. For the present calculations, four paths were used, two going through the center conductor and the other two missing the center conductor.

For each path through the cable, a multiple-plate version of the QUICKE2 computer code[24,25] was used to calculate the forward and reverse x-ray induced emission currents from the conductors and the dielectrics at their interfaces and the electron currents in the bulk of the dielectric. This code starts from an arbitrary incident

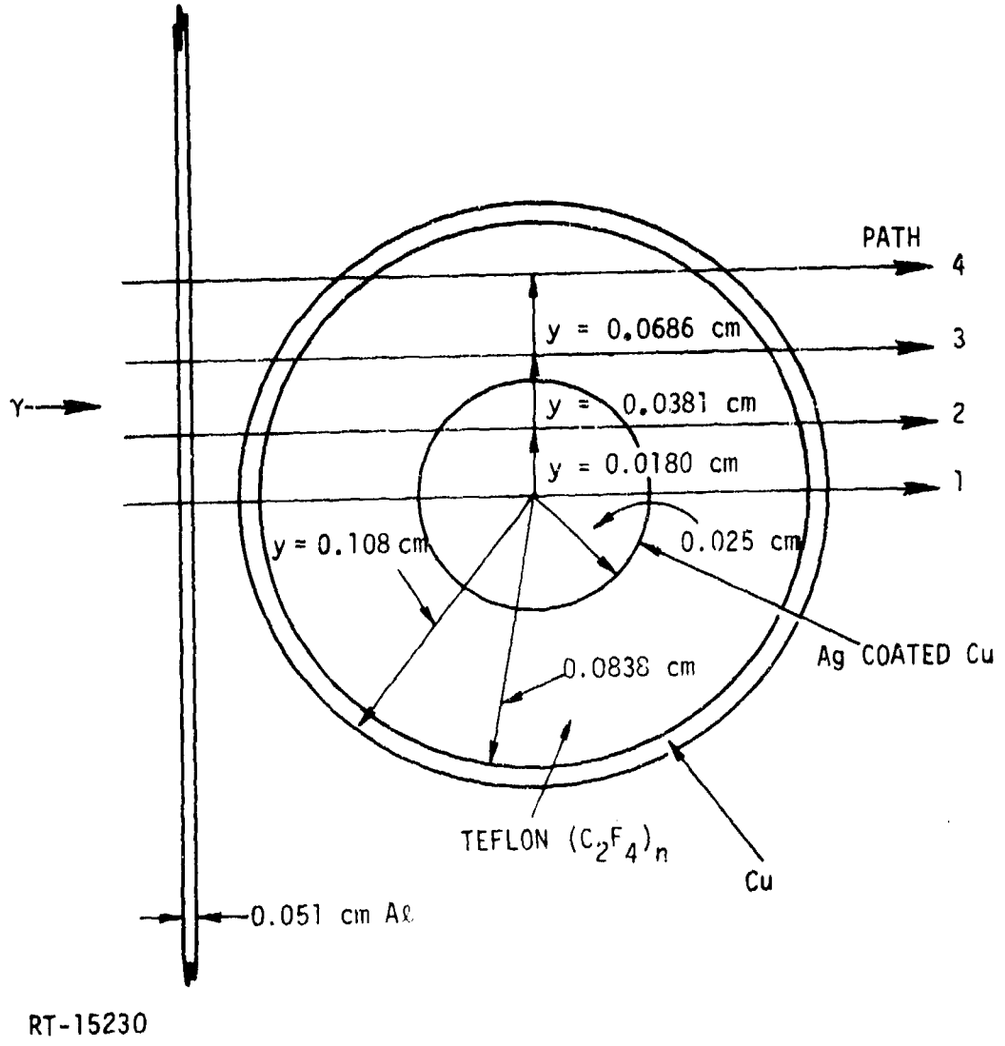

Figure 2. Illustration of a typical cable geometry (SR086) and photon paths used in the response calculations in Appendix A (not to scale). The 20 mils of Aℓ represents the walls of a satellite.

photon spectrum, attenuates the differential photon fluences according to the wavelength-dependent mass absorption coefficients while transporting the photon fluence through the specified thicknesses of the various materials, calculates the electron currents due to each component, and sums all currents over the photon spectrum. It also provides the equilibrium doses in the various materials and the average range (the first moment) of the electrons that are emitted from the conductors and captured in the adjoining dielectrics. Unfortunately, QUICKE2 does not rigorously calculate the enhanced dose and charge in the interface regions including multiple electron scatterings across the interface. Another code, QUICKE4, has been developed by the authors of QUICKE2 to calculate these interface enhancements.[26] However, it has not been documented or released as yet. In its absence, one can use Monte Carlo codes such as SANDYL[27] or POEM[28] or the algorithm method of Burke and Garth[29] to estimate the interface enhancements.

The contributions to the open-circuit voltage due to the charge emitted from the shield and the center conductor are obtained by plotting the respective first moments (emitted charge per unit area times its average range in the cable dielectric = QX/A) versus circumferential angle and averaging around the circumference. Typical sets of curves for the center conductor and sheath are shown in Figure 3 for incident 5 and 15 keV blackbody spectra. The resulting open-circuit voltage is

$$\Delta V_{OC} = \left(\frac{Q}{A}\bar{X}\right)_{AVE} \kappa\epsilon_0 \qquad (3)$$

---

[24] T. A. Dellin and C. J. MacCallum, IEEE Trans. Nucl. Sci. NS-20, 91 (1973).

[25] S. H. Rogers and A. J. Woods, Multiple-Plate Modification of QUICKE2 Analytical Electron Emission Code, IRT Report INTEL-RT-8141-026, 15 June 1976, prepared for Defense Nuclear Agency under Contract DNA001-76-C-0068.

[26] T. A. Dellin and C. J. MacCallum, IEEE Trans. Nucl. Sci., NS-23, 1844, (1976).

[27] H. H. Colbert, SANDYL, Sandia Laboratories Report, SLL-74-0012, May 1972.

[28] W. L. Chadsey, POEM, AFCRL Report TR-75-0324 (1975).

[29] E. A. Burke and J. C. Garth, IEEE Trans. Nucl. Sci., NS-23, 1838, (1976).

where ϵ_0 is the dielectric constant of free space and κ is the relative dielectric constant of the cable dielectric. The procedure defined by Equation 3 is rigorously correct for a coaxial cable.

Along each path through the dielectric (Figure 2), the QUICKE2 code gives the electron charge emitted inward and outward from the dielectric into the adjacent conductors and the forward and reverse electron currents "in the bulk" of the dielectric near each interface, that is, just far enough into the dielectric to be out of the interface depletion-enhancement regions. The difference between these bulk currents at the near and far edges of the dielectric gives the charge that is accumulated in the bulk of the dielectric. It is usually adequate to assume that this bulk charge density is uniformly distributed across the dielectric along the particular photon path although a more accurate distribution can be obtained by asking the QUICKE2 code for the bulk currents at other positions inside the dielectric.

The average first moment of this bulk charge around the circumference of the cable can be obtained by plotting the first moment versus angle, as in Figure 3, and integrating around the circumference. Equation 3 is then used to obtain the contribution of the bulk charge to ΔV_{OC}. Although this bulk charge density should always be checked, its effect for the present cables was very small and was ignored because the cable dielectrics are relatively thin. As a rule of thumb, this bulk charge becomes significant when the thickness of the dielectric is comparable to the average photon attenuation length in the dielectric.

Assuming that there is negligible accumulation of charge in the bulk of the dielectric, the electron current in the dielectric is just a uniform translation of charge (Figure 4). The charge that is emitted from one side of the dielectric is compensated for by a thin positive charge layer left behind at the opposite face of the dielectric. Only the portion of this charge that is captured by the center conductor ($= \Sigma_{em} d_i$, where Σ_{em} is the emission charge density and d_i is the diameter of the center conductor) will contribute to ΔV_{OC} (Figure 4). Its contribution is

$$\Delta V_{OC} = (\Sigma_{em} d_i)/C \qquad (4)$$

where C is the capacitance per unit length between the center conductor and the shield. The current in the dielectric that misses the center conductor (Figure 4) has a negligible effect on ΔV_{OC} because the emitted current is captured by the sheath and then flows back around the sheath to neutralize the positive layer left behind on the opposite edge of the dielectric.

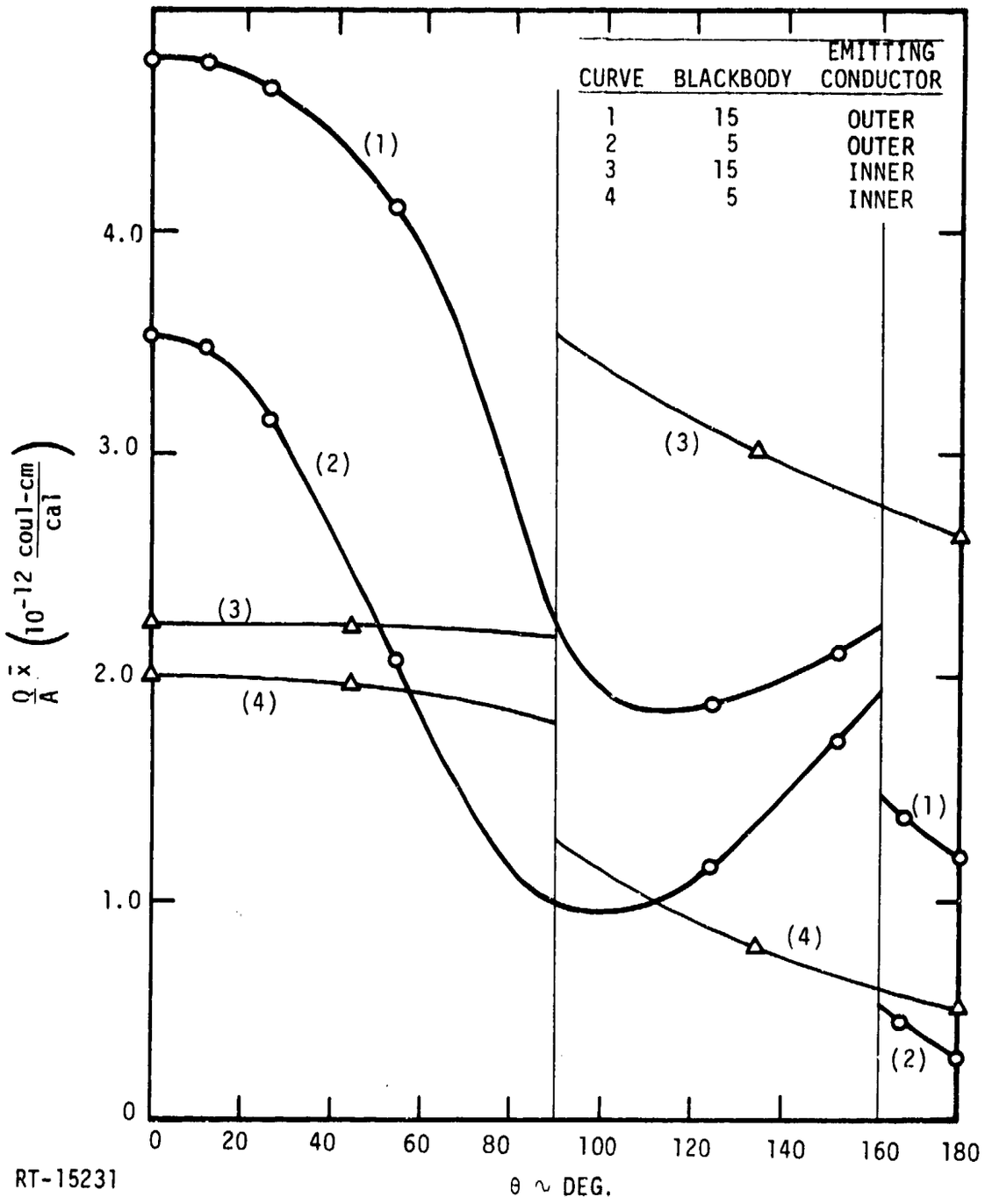

Figure 3. **Typical angular distributions of first moment of charge emitted from copper conductors and stopped in dielectric for an SR086 cable. For simplicity, the curves for the outer conductor are shown with a discontinuity at 162° corresponding to the start of shadowing by the center conductor and the curves for the inner conductor have a discontinuity at 90° where the emission goes from reverse to forward emission. With more paths through the cable, smooth transitions could be defined at these points but the discrepancy is not serious.**

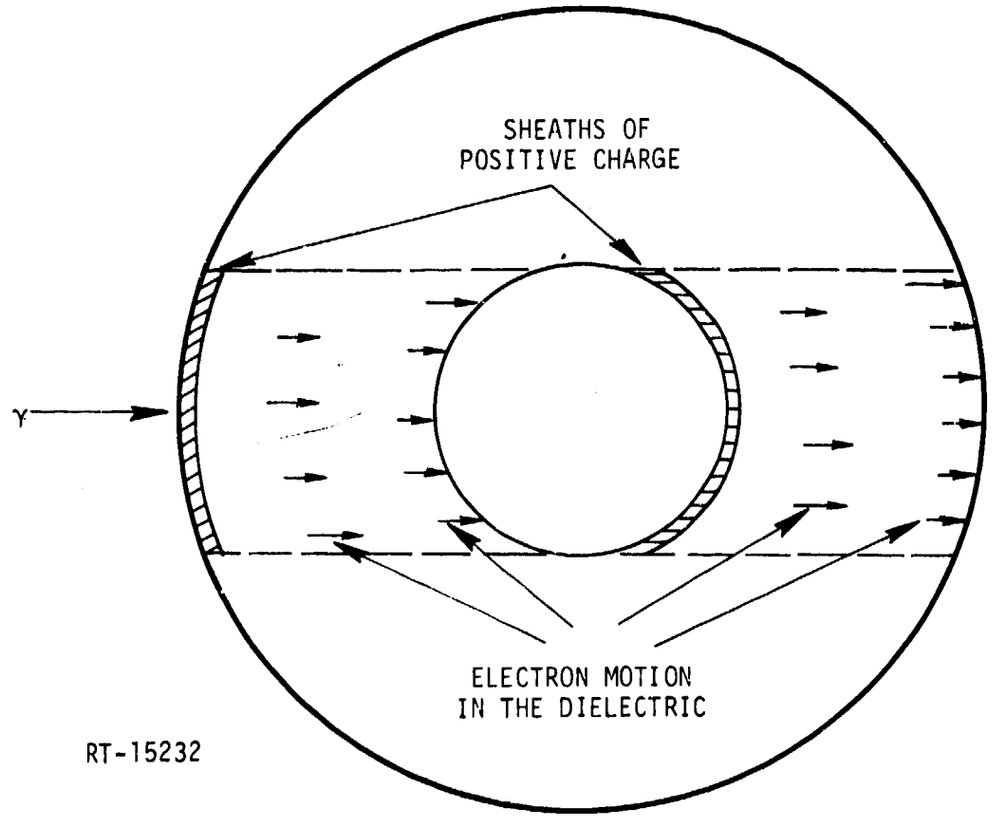

Figure 4. **Illustration of charge motion from dielectric to conductors which contributes to the voltage. It is assumed that no net charge accumulates in the bulk of the dielectric. Charge motion above and below the horizontal lines tangent to the inner conductor has negligible effect since the charge driven forward into the outer conductor in this region exactly cancels the positive sheath left behind near the outer conductor.**

In Appendix A, detailed calculations are given for the response of the ideal cable illustrated in Figure 2 for photon pulses of unit incident fluence (1 cal/cm^2) with 5, 8, and 15 keV blackbody spectra. The results of similar calculations for the 5 cables tested at SPIRE by IRT (using the spectra shown in Figure 8) are given in Appendix B, but not in as much detail as in Appendix A.

3.3 CABLE GAPS IN VACUUM

The major effects of gaps on cable responses in vacuum is an increase in the effective electron range $\bar{X}$. It is not necessary that the gap be uniform around the circumference of the cable. The important quantity is the average gap width. Assuming that there is negligible range shortening due to opposing electric fields across the gap, the gap width adds directly to the average electron range in the dielectric. Thus, Equation 3 can be used to calculate the effect of the gaps by replacing $\bar{X}$ by the gap width. The relative importance of gaps can be seen by noting that the average electron range in dielectrics for typical emitted electrons is about 10 μm. Typical gaps observed in braided-shield cables are $\geq$10 μm. Therefore their effect should dominate the responses for such cables.

If the gap is between the shield and the dielectric, the sign of the response due to the gap effect is negative, that is, electrons are driven out of the center conductor. If the gap is between the center conductor and the dielectric, the sign of the resulting response is positive.

The cable response for a 2.5 μm gap is also given in Appendix A. For a low fluence in a vacuum, the gap effect is linear in the gap width. It is to be noted that a gap width of ~25-50 μm, which would drastically alter a cable response, would have a negligible effect in its electrical properties.

3.4 HIGH-FLUENCE EFFECTS

For a high-fluence pulse, the electric fields that are built up in the interface dose-enhancement region because of trapped charge during the beginning of the pulse are sufficient to affect the total response of the cable. This effect comes about due to the radiation-induced electrical conductivity in the dose-enhancement region. The combination of the electrical field in the enhancement region and the radiation-induced conductivity produces an electrical current that opposes the emission current. For very large fluences, an equilibrium situation is reached during the pulse where the return

current exactly balances the emission current and there is no further increase in the cable response at larger fluences.

Chadsey et al.[7] has presented a mathematical model for the above effect in a planar geometry. Given the spatial distribution near the metal-dielectric interface of the enhanced dose and current ratios ($R_D(x)$ and $R_C(x)$ respectively) and the coefficient of radiation-induced conductivity in the dielectric (K_p), one can calculate the total net charge transfer (ΔQ) as a function of dose.

$$\Delta Q = \frac{dQ_0}{d\gamma} \frac{1}{\bar{x}} \int_0^{r_e} \frac{R_C(x)}{K_p R_D(x)} \left[1 - \exp(-\gamma_T K_p R_D(x))\right] dx \qquad (5)$$

where r_e is the maximum range of the secondary electrons in the dielectric, $\bar{x}$ is the mean electron range, γ_T is the total incident dose, and $dQ_0/d\gamma$ is the slope of the charge transfer versus dose at low doses where the radiation-induced conductivity can be ignored. In the general case, $R_C(x)$ and $R_D(x)$ will not be integrable analytic functions and Equation 5 has to be integrated numerically. In addition, $R_C(x)$ and $R_D(x)$ will undoubtedly be different for emission from the sheath and the center conductor and may vary around the circumference of the coaxial cable. Therefore, Equation 5 will have to be evaluated near the sheath and the outer conductor at various positions around the circumference and the average effect obtained. Because the electron range is usually much smaller than the radius of the cable, the planar equation (Equation 5) can be applied to each local point around the cable circumference and then averaged.

A more complete mathematical description of Chadsey's model and an illustration of the effect of dose on a typical cable for 5, 8, and 15 keV incident blackbody spectra are given in Appendix C. In the IRT cable experiments at SPIRE, the dose per pulse and total accumulated dose were small enough so that this enhancement effect could be ignored in analyzing the data. As shown in Figure C-1 of Appendix C, this effect does not start to become important until doses of around 0.02 cal/cm^2 for the largest value of K_p. This dose is about 10 times larger than the maximum dose accumulated on the cables in the SPIRE experiments.

3.5 STORED CHARGE

As discussed in Section 2 of this report, stored charge is a persistent surface or bulk charge introduced into the polymer dielectric as a consequence of manufacturing

or handling processes. The charge may be introduced into the bulk polymer during the polyemerization process, on the surface of the dielectric during its extrusion onto the center conductor, in the bulk through radiation cross linking, and on the surface through friction concurrent with placing the outer shielding on the dielectric or in bending and flexing shielded wires.

Estimates of upper bounds of the amount of charge stored for polymers of interest during each one of these processes have been given in Section 2. Unfortunately, except in the case of extrusion, little quantitative data is available for polymers of interest. Reference 18 indicates that the stored surface charge created as a consequence of extrusion is of the order of 5×10^{-11} to 5×10^{-9} C/cm^2 and it resides on the outer 10 μm of the dielectric surface. The polarity is a function both of the extruding conditions and the polymer.

There is additional evidence[17] that Teflon cables like SR-086 may have surface charges of $\sim 5 \times 10^{-11}$ C/cm^2 on their outer surfaces as a consequence of normal manufacturing or handling processes. This value is not inconsistent with model calculations for cable response based on the hypothesis that stored charge is present and affects cable response.[3] Thus, for the modeling calculation in this report, stored charge will be considered near the surface of the dielectric and, in the absence of specific data, the amount of this charge is treated as an adjustable parameter.

Once the stored charge is introduced into the dielectric, its effect on cable response due to an x-ray pulse is qualitatively similar to that of any other charge present in the cable. This charge creates electric fields which combine with the radiation-induced electrical conductivity to produce electrical currents which either enhance or degrade the effect of driven charges depending on the region and location of the stored charge.

3.6 TRAPPED CHARGE

When cable are exposed to an electron radiation source, either in the laboratory or in a space environment, some of the incident electrons are trapped in the cable dielectric and produce an electric field distribution between the conducting shield and the center conductor. If these fields increased indefinitely with exposure time, they would eventually exceed the electric breakdown strength of the dielectric and an arc discharge would occur. However, as the fields increase, they combine with the radiation-induced electrical conductivity in the dielectric to produce internal electrical currents that bleed off part of the incident charge that is trapped as discussed in

Section 3.4. If the electrical fields do not exceed the dielectric breakdown strength, the internal electric fields will approach a steady state condition where the bleed-off currents exactly balance the incident photocurrents. The detailed field distribution in the dielectric depends on the geometry and materials of the cable, the energy spectrum of the incident electrons, and the magnitude of the radiation-induced electrical conductivity per unit deposited dose. However, they are independent of the incident dose rate when the applied bias between the cable shield and the center conductor is zero (or negligibly small). In a real cable, it is not obvious a priori whether the steady state fields will be less or greater than the dielectric breakdown strength, and thus whether or not arc breakdowns are apt to occur.

Even if an arc discharge does not occur, the internal fields can have a potentially detrimental effect. Data from Phase V Skynet tests indicates that the presence of trapped charge can possibly enhance the response of the cable to a subsequent pulse of photons.

In order to estimate whether or not breakdowns in cables due to trapped space electrons are apt to occur and, if not, how much the built-in fields enhance the cable photon responses, calculations are reported in Appendix D for a typical satellite cable (SR 086) exposed to space electrons. The equilibrium field distribution depends on the cable geometry, electron energy spectrum, and the value of K_σ, the coefficient for radiation-induced conductivity. It is shown in Appendix D that the equilibrium field buildup is proportional to K_σ^{-1}. For a relatively large value of K_σ corresponding to Teflon, dielectric breakdown is unlikely to occur. However, for some polymer dielectrics, K_σ can be two orders of magnitude smaller than the value for Teflon. In that case, the steady state electric fields become comparable to the dielectric breakdown strengths and arc discharges are a distinct possibility.

For the cable used in the calculations in Appendix D, the enhanced response due to the trapped charge was comparable to the response of the cable without trapped charge or gaps.

For Teflon, the steady state fields are reached in about 1/2 hour in a fission-electron environment and in about 20 days for some fluences typical of some natural space environments. However, these times to steady state also increase inversely proportional to K_σ.

An additional important conclusion from this study is that any stored charge that is present in the satellite cable at launch will be washed out and replaced by the trapped

electrons on a time scale comparable to the time to approach the steady state distribution due to the natural space environment.

Details of these calculations and bases for the conclusions are given in Appendix D.

3.7 AIR IONIZATION

If there is air present in the gaps of the cable when the photon pulse occurs, the air will become ionized and provide a relatively high conductivity path across the gap from the metal to the dielectric. If there is no stored charge in the dielectric before the pulse, the cable response due to the gap will usually be monotonic, at least during the major part of the pulse. However, the air ionization will limit the magnitude of the cable response for large pulses because the conductivity of the gas will allow a reverse current to flow across the gap, opposing the emission current from the shield. After the incident pulse has ceased, there can be a small response of opposite sign to the normal cable signal because the reverse current across the gap will continue to flow as long as there is significant air conductivity in the gap and electric field across it.

If there is negative stored charge in the dielectric before the pulse, it is possible for the response to a photon pulse to be bipolar, with the initial signal in the opposite direction from the normal response with a gap. A model was proposed to explain this effect.[3] According to this model, the initial positive signal is due to the electrical current across the gap due to the air in the gap that is quickly ionized by the pulse and to the field created by stored charge. If the pulse is sufficiently large, all of the stored charge will be neutralized before the end of the pulse. When this occurs, the sign of the signal should reverse itself, again corresponding to the normal response due to a gap. Numerical predictions using this model agree reasonably well with the available cable data when a value of stored charge equal to 2×10^{-11} C/cm^2 is used. This value for the stored charge is on the low end of the range reported in Reference 18, but not inconsistent with measurements reported in Reference 17. The conclusion from Reference 3 was that there was little evidence of the release of stored charge except in cables with gaps and air.

4. EXPERIMENTAL TECHNIQUES

4.1 INTRODUCTION

This section describes the rationale behind and the manner in which cable testing at the SPIRE Pulse 6000 was carried out. Basically our aim was to provide well-characterized data from which the response of representative satellite cables in an x-ray simulator environment can be estimated. Section 4.2 describes the criteria by which the cables were chosen. As our primary interest was to search for stored charge effects, samples with a variety of dielectrics were examined. Section 4.3 describes the pretreatments applied to simulate bending and handling prior to irradiation. Annealing was carried out for some samples to see whether stored charge, if present, would be relaxed at temperatures within the operating range of each sample. Section 4.4 describes the exposure conditions. Multiple samples were examined to obtain inefficient statistics on samples (1) of the same type, manufacturer and preconditioning; (2) of the same type and manufacturer but with different prior treatments, and (3) of the same type but from different manufacturers. All of this was done in an attempt to bound the response of cables of a given type with a representative variety of prior conditioning. All irradiations were carried out in vacuum to be representative of the environment to which spacecraft cables might be exposed and to minimize trapped air effects. Careful dosimetry was taken during each shot to obtain a map of both fluence and flux over the test section, as described in Section 5.

4.2 CABLE SPECIFICATION

The list of cables examined during this program are given in Table II. Also included in the table are the general construction, an identification of manufacturer and type, an identification of representative military satellites which use this type of cable, and associated spacecraft-manufacturers' and Mil-Specs. The spacecraft-manufacturers' specs are based on the relevant cable manufacturers' and Mil-specs usually containing the most accurate information on the structure of each cable type and the acceptance and qualification tests which each undergoes.

TABLE II. CABLE TYPES STUDIED

	Type	Center Conductor	Primary Dielectric	Shield/Outer Conductor	Jacket	Manufacturer/ Catalog Number	Satellite Spec/Mil spec
1.	600 V space wire (Spec 44/)	22 AWG SPC[a]	Polyalkene/PVF_2[d]	TPC flat braid	PVF_2	Raychem 44/2412-22-9-9	NATO 3 A04-P12108 777 PT 3-33N-22 MIL-W-81044/2
2.	600 V general purpose wire, lightweight (Spec 83B)	20 AWG TPC[b]	Polyarylene	TPC flat braid	Polyarylene	Raychem 88B2111-20-9-9	GPS MIL-W-81044/25
3.	RG-178B/U 50 ohm coax	SPCW[c]	Extruded TFE[e]	SPC round braid	Extruded FEP[f]	Times, Belden	NATO 3 04-P12327 MIL-C-17/130 (Similar)
4.	0.141-inch semi-rigid 50 ohm coax	SPC	Extruded TFE	SPC tube		Uniform tubes UT-141C-SP Precision tubes BC-50141 Cablewave CT-141-50 (810004)	NATO 3 04-P12103 777 3A024-002V MIL-C-17/130(Similar)
5.	0.086 inch semi-rigid 50 ohm coax	SPC	Extruded TFE	SPC tube		Uniform tube UT-085C-SP Cablewave/CT-086-50	777 3A024-007 (Similar)
		SPCW	Extruded TFE	Cu tube		Precision tube AA-50085	777 3A024-001 MIL-C-17/133A

a. SPC = silver-plated copper
b. TPC = tinned-plated copper
c. SPCW = silver-plated copper covered steel
d. PVF_2 = radiation crosslinked poly(vinylidene fluoride)
e. TFE = tetrafluoroethylene (Teflon TFE)
f. FEP = fluorinated ethylene-propylene copolymer (Teflon FEP)

The cables were selected according to the following criteria:

1. They are commonly employed in satellites.

2. They cover the range of commonly employed dielectrics. While it was originally intended to look at cable samples representing all types of dielectrics employed in satellites, the large number of possible combinations of types and pretreatments and the limited testing time did not permit using all possible combinations. The dielectric types not examined included shielded wire cables made with Kapton/FEP tape insulation and coaxial cables made with polyethylene dielectrics. However, samples of these types were studied by TRW (types 3A002-006, PT3-59-93P).[3]

3. The cable has been subject to processes postulated in Section 2 to store persistent charge in dielectrics.

4. They have a simple structure - either single-conductor shielded-wire or coaxial cable. Since our principal intent was to look for changes in the radiation response due to stored charge or handling, we wanted to minimize the effects due to the complicated geometry of multiconductor shielded wires. Where possible, the composition of the inner and outer conductor, including the type of plating was chosen to be identical to minimize the effect of the imbalanced emission from different combinations of interfaces.

5. Samples from different manufacturers are available. Where available, samples of the same cable type and pretreatment, but from different manufacturers, were examined in order to obtain an estimate on the variation in response for the same cable type due to variations in manufacturing procedures.

6. Radiation test data is available on the same cable type under different irradiation conditions, i.e., spectrum and fluence. Predicting the response of cables in environments of system interest invariably depends on the extrapolation of data taken at fluences and spectra typical of simulators. It is important to determine whether a cable code correctly accounts for the role that each of these two parameters plays in determining the signal output from an irradiated cable.

The measured cable dimensions for each of the cable samples examined are given in Table III. The nominal values are taken from relevant specifications. Because it is known that gaps play an important role in determining cable response, especially in the case of braided-shield cables, an attempt was made to measure gap sizes. Samples of each type of cable were cross-sectioned, potted in epoxy and end-polished. Photomicrographs of each sample were taken from which the dimensional measurements given in the table were derived. Representative photographs were reproduced in Figure 5. The estimated gap widths are listed in Tables VI to X where response data is summarized. These gap widths were calculated by estimating the total gap area between dielectric and the shield or the center conductor and averaging around the circumference at an average gap radius.

4.3 PRE-IRRADIATION CABLE TREATMENTS

Before irradiation, the cables were subjected to a variety of treatments to simulate conditions that might occur in an actual system. Time did not permit testing all cable types with all treatments. However, as the sample exposure matrix (Table IV) indicates, enough different combinations were exposed to provide a reasonably complete coverage of various effects. In each case, some samples were exposed in an as-received state. For semirigid cables, this meant cutting pieces from straight sections that presumably had never been bent. For the flexible coaxial cables and shielded wires, samples were cut from the spool and subjected to the minimum amount of handling required to mount them for irradiation as straight segments.

For each cable type, at least one group of samples was examined after thermal annealing. Annealing was carried out for two reasons: first, to measure the x-ray response of the cable brought to a standard state after manufacture; second, to see if annealing could relax persistent stored charge. The annealing temperatures were chosen on the basis of the TSC spectra for the given dielectric and by the manufacturer's recommended maximum operating temperature. In some cases involving those cables with Teflon dielectrics (RG-178B/U, SR141, SR086), the recommended maximum operating temperatures (approximately 150°C) were below those at which the TSC spectra show their maximum.[30] For the cables with Teflon or Stylon, the

[30] R. E. Leadon, D. P. Snowden, and J. M. Wilkenfeld, Radiation Effects in Semiconductor and Insulator Materials, HDL-CR-76-152-1, IRT Report INTEL-RT 8124-004, 1 April 1976.

TABLE III. AVERAGE CABLE DIMENSIONS (IN μm)

Cable Type	Center Conductor		Dielectric			Outer Conductor			Jacket		
	Structure	O.D.	Structure	O.D.	Thickness	Structure	O.D.	Thickness	Structure	O.D.	Thickness
SR086											
Nominal	SPC[a]	510	PTFE[b]	1676	583	Cu[c]	2197	261			
Cableware		515		1666	576 ±90		2182 ±30	258			
Precision	SPCS[j]	424 (St) 545 (Cu)		1666	560		2166	250 ±22			
Uniform	SPC	515		1666	576 ±50		2182	258			
SP141											
Nominal	SPC	912	PTFE	3010	1049	Cu	3581	286			
Precision		933		3000	1034		3630 ±30	315			
Cableware		933		3000	1034		3600	300 ±34			
Uniform		933		3000	1034		3600	300			
RG-178B/U											
Nominal	SCCS	305	PTFE	864	280	SPCB[d]	1372	234	FEP[e]	<1905	<267
Times		363		848 ±30	243		1440 ±75	296		1804 ±76	227
Belden		363		894 ±15	265		1440 ±15	273		1834 ±45	197
SPEC 44/2414 22 AWG Shielded Wire											
Nominal	19/34 AWG SPC	838	PAK[f]	1016	76	TPFCB[h]	1321	153	PVF_2[g]	<1829	<254
			PVF_2	1168	76.5						
Measured		818		1030	106		1454 ±30	121 ±15		1849 ±60	198
				1212	91						
SPEC 88B2111 20 AWG Shielded Wire											
Nominal	19/32 AWG SPC	1016	PAR[i]	1295	140	TPFCB	1448	76.5	PAR	1930	241
Measured		1000		1273	137		1485	106		1970	243

a. SPC = Silver Plated Cu, plating <1 μm thick.
b. PTFE = Polytetrafluoroethylene
c. Cu = Copper
d. SPCB = Silver plated copper braid
e. FEP = 89% Polytetrafluoroethylene - 11% Hexafluoropropylene copolymer
f. PAK = Cross linked polyalkene
g. PVF_2 = Cross linked polyvinylidene fluoride
h. TPFCB = Tin plated flat Cu braid, plating <6 μm thick
i. PAR = Polyarylene
j. SPCS = Silver plated copper covered steel

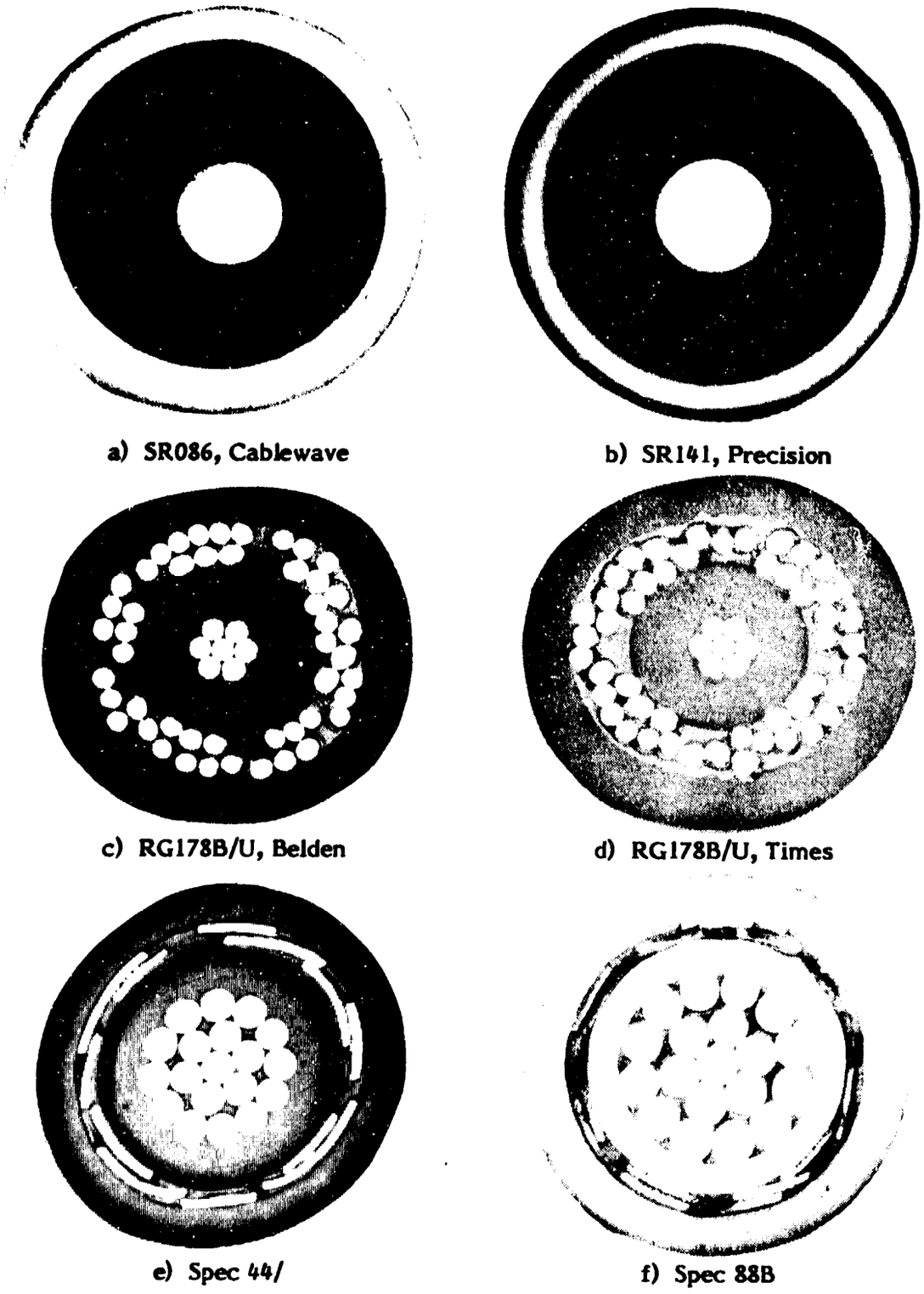

a) SR086, Cablewave

b) SR141, Precision

c) RG178B/U, Belden

d) RG178B/U, Times

e) Spec 44/

f) Spec 88B

Figure 5. Typical photomicrographs of sectioned cables

TABLE IV. SAMPLE EXPOSURE MATRIX

Type	Conditioning						
	As Received	Annealed	Annealed and Flexed	Annealed and Bent	Bent and Annealed	Second Irradiation
Polyalkene shielded wire (Spec 44/)	X	X				
Polyarylene shielded wire (Spec 88B)	X	X	X			X
RG-178 B/U						
Times	X	X	X			X
Belden	X					
SR141						
Uniform	X					
Cablewave	X	X				
Precision	X			X	X	X
SR086						
Uniform	X	X				
Precision	X			X	X	
Cablewave	X					

maximum operating temperature is 150°C, while for the Spec 44 it is 125°C. Annealing times were 12 hours. Thus it is possible that any persistent stored charge distributions that might be present in this dielectric would not be completely relaxed during the annealing. However, it has been our experience that heating such cables to temperatures significantly above their operating maximum for long periods of time can lead to cable damage. It is not likely that operational cables would be operated above the specified temperature limits (as opposed to what is done in qualification testing of particular cable types). Therefore, the annealing temperatures were kept to the recommended maximum operating temperature to avoid damage to the cable structure, which might alter its response unintentionally.

An effort was made to simulate in a realistic manner the worst case handling that satellite cables undergo between manufacture and incorporation into a cable harness. For flexible cables, this was approximated by giving each sample 10 180-degree flexures at different points along the sample. The semirigid cables were given a series of approximately 11 2.5 cm diameter U-shaped bends with a tool supplied by the manufacturer. Thus, each of these semirigid cables so treated was bent in a manner that preserved its electrical specifications. Some of the flexed and bent samples were annealed before bending. This was done in an attempt to remove stored charge introduced prior to this simulation of handling in an attempt to see whether this treatment introduced stored charge through friction. As a check to see whether stored charge affected the response of bent or flexed cables, several sets of samples so treated were given a subsequent annealing. One might expect that weakly bound frictional charge could be relaxed in a subsequent anneal.

It has been claimed that one can radiation anneal cables which have stored charges to obtain the "real" response of the cable. In an attempt to investigate this claim, several sets of samples were irradiated until a nearly uniform response per pulse was achieved and then allowed to set in vacuum for periods of 12 to 40 hours and reirradiated to see if the n plus first pulse was like the nth pulse. Our data, described in Section 5.4, indicates that what one in fact is observing is a reduction in response due to a buildup of electric fields whose source is the charge deposited by each shot. It is evident that the relaxation rate for different polymers is significantly different. This, of course, is a function of both the prompt and delayed components of the radiation conductivity.

Finally, in an attempt to bound the cable response for samples of a given type, three samples with the same pretreatment and from the same manufacturer were

examined during each shot to develop a set of inefficient statistics. In addition, cables of the same nominal type and from different manufacturers were also examined.

4.4 TEST SETUP

The cable irradiations were performed with the Simulation Physics (SPIRE) Pulse 6000 flash x-ray. (SPIRE was formerly known as Simulation Physics, Inc. (SPI)).

The irradiation conditions at the Pulse 6000 facility were chosen to satisfy the following criteria. The irradiation area was to be as large as possible for fluences of interest. This was done to permit the irradiation of several cable samples simultaneously and to look at reasonably long cable segments without having to introduce coiling except when, and in the manner, desired. To this end, two cathodes were employed. One is a linear cathode that is about 2.5 cm wide and 23 cm long. With this cathode, 3 miniature satellite cables could be irradiated at one time with a relatively uniform fluence. The length of cable exposed in this cathode was 22.9 cm. This cathode was employed for all cable irradiations except those of bent semirigid samples. With 300-kV charging, the observed fluence along the central horizontal axis was about 0.25-0.35 mcal/cm^2. The bent semirigid cable samples (47 cm long) were irradiated with the bremsstrahlung from a 30.5 cm diameter circular cathode. Measured fluences were about 0.08-0.17 mcal/cm^2 for 300 kV charging. In order to keep the fluence uniform to better than ±10 percent over the exposure area, the samples were placed inside a circle of 20 cm diameter. For the most part, the fluence variations over the exposure area of both cathodes fell within the desired limits. These spectra are somewhat hotter than those of an approximately 15-keV blackbody, which characterizes the spectrum under which other cable tests have been run at this facility. However, in planning these tests, it was felt to be more desirable to produce a sufficiently high fluence (greater than 0.1 mcal/cm^2) over the desired irradiation volumes in order to get sufficiently large cable signals than to match a particular spectrum. In addition the effect of spectral variation could be studied by comparing our data with that of TRW on similar cables taken with a 6.4 cm cathode and a 200 kV charge.

Because the cable samples were placed close to each cathode (less than 2 cm) and because the irradiation area was a considerable fraction of each cathode area, multipoint dosimetry was employed to obtain dose and pulse shape information over the exposure area. This data was recorded for each shot. Two 0.51 mm thick (approximately 1 g/cm^2) gold foil calorimeters provided by SPIRE recorded the fluence. Two PIN diodes were employed to provide the dose per pulse as well as the x-ray pulse shape.

The four dosimeters were arranged along the centerline of the linear cathode, as shown in Figure 6, which is a photograph of our exposure cassette. The calorimeter centers were each displaced 2.25 inches from the center of the cathode along the same axis. When the circular cathode was employed, the calorimeters were placed on a vertical axis on a 20 cm diameter circle, while the PIN diodes were left as shown.

The cable irradiations were all carried out in a vacuum of less than, or equal to, 2×10^{-4} torr. While interesting effects have been observed in connection with the presence of air in gaps,[3] vacuum irradiations were chosen in an attempt to approach the conditions relevant to satellite cables. However, we have not addressed the problem of outgassing in detail. The data of TRW[3] indicates that flexible cables outgas in times comparable to the pumpdown time at the SPIRE facility (approximately 15 minutes). Trapped air in semirigid cables outgasses more slowly and may be problematic. Outgassing times for representative cables should be examined in more detail but time did not permit a detailed study of this effect under the present program.

Both the pulse shape and the total emitted charge were recorded for each of the three cable samples examined during each exposure sequence. The net charge released per pulse was, for the most part, obtained by integration of the signal after amplification with an RC combination consisting of a 3K resistor and a 300 pf capacitor. The integrated data agreed reasonably well (±10 percent) with that obtained by numerically integrating the response waveform. In order to increase the size of the observed signals for convenient examination with the Tektronix 7000 series scopes employed, the cable signals were usually amplified with HP 8447 D providing a gain of ~26 dB or HP 462A RF (20 or 40 dB gain) amplifiers. Such amplification was mandatory in order to accurately determine the response of many of the semirigid cable samples whose peak unamplified signal was at the order of 1 to 3 mV.

Typical data is shown in Figure 7(a). This figure shows the response of the two samples into a 50 ohm load resistor. In every case, the other end of each cable was open-circuited, albeit shielded with a copper cup placed over it in contact with the outer conductor. In many cases, the observed cable signal comprised two parts. The initial part of the pulse, which represented most of the charge output as a consequence of irradiation, more or less followed the photon pulse. In many cases the observed cable response waveforms also had either a tail that was long compared to the pulse width or was bipolar. Such waveshapes have been observed by other investigators using this facility. It was found, when background shots were taken with the cable samples covered with a 3.20 mm thick sheet of lead, that in every case but one (for the Spec 88B

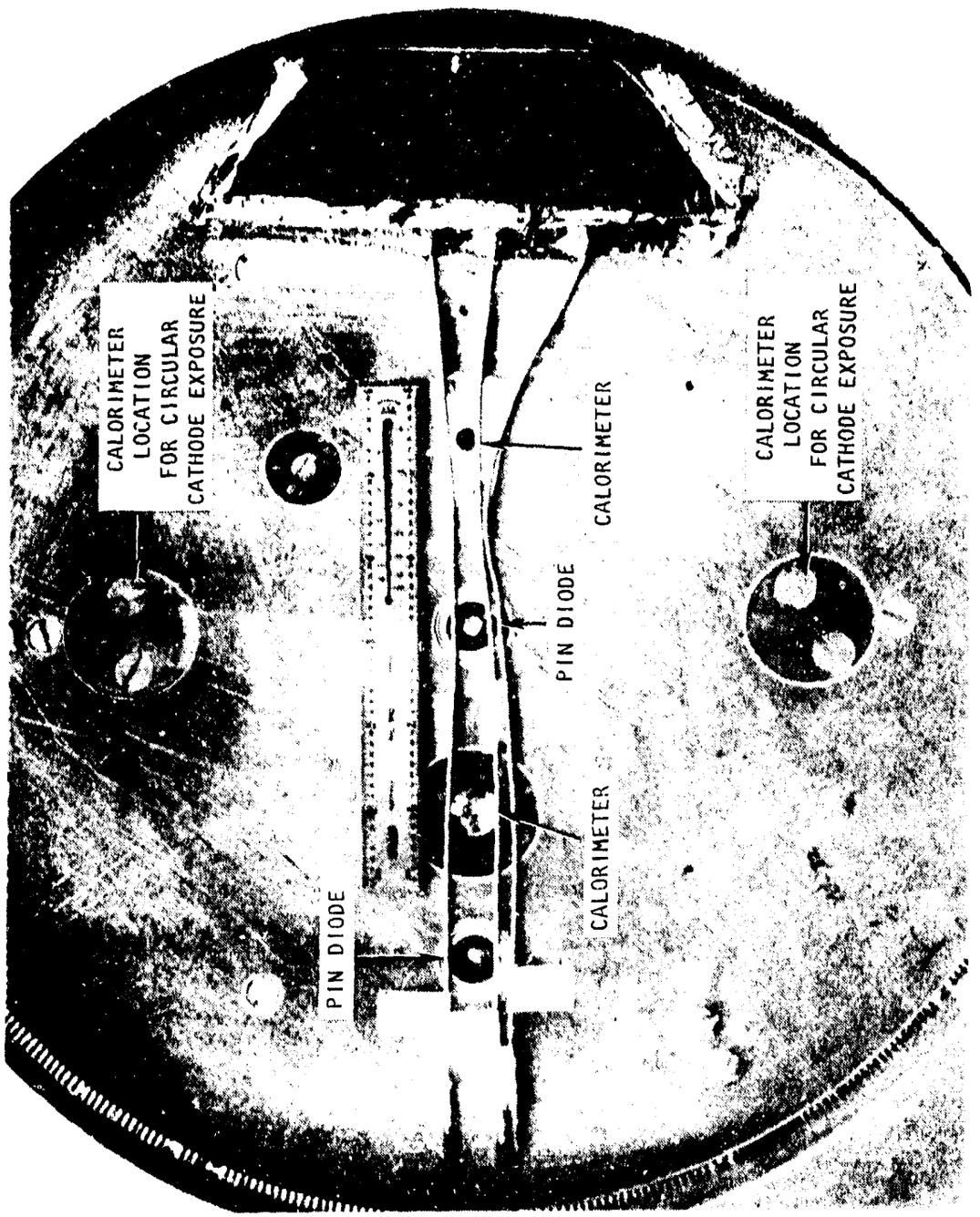

Figure 6. Experimental arrangement for cable exposures, during exposure by the 2.5 cm x 23 cm linear cathode. In practice, the bottom cable was aligned more in a straight line with the bend near the shielding covering in the feedthroughs and out of the high fluence region of the target area.

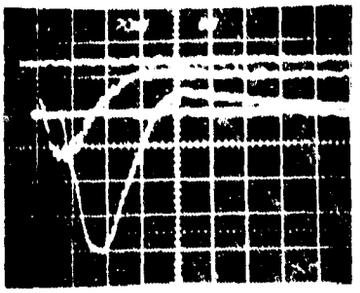

Figure 7(a). Third shot response of two samples of Cablewave System SR086 cable. The dose per pulse is ~20 rads(Si). The horizontal scale is 50 nsec/div. Upper vertical scale is 430 μV/div. Lower scale is 402 μV/div.

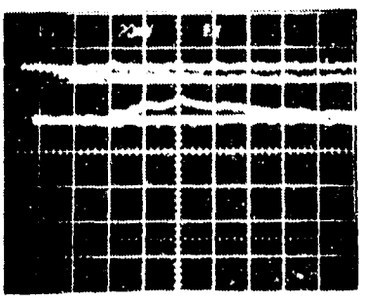

Figure 7(b). Tenth shot response of the same cables. The cables are covered with about 1/8 inch of lead. The delivered dose is about 0.1 rads(Si). Scope settings are the same.

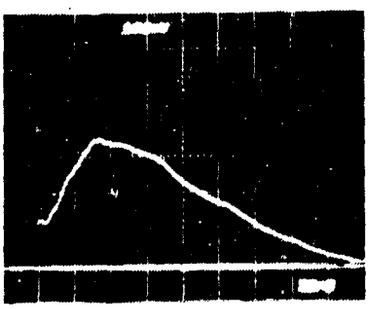

Figure 7(c). The SPIRE Pulse 6000 pulse shape as recorded by a PIN diode. The vertical scale represents 10V (0.2 amps)/div. The horizontal scale is 20 nsec/div.

cables) these tails persisted as shown in Figure 7(b). As the lead sheet attenuates the fluence by a factor of 100 or more, it is evident that the presence of the tails is due to machine generated RF noise which couples into the measurement system. A confirming argument that the response tails are due to RF coupling and not connected with the cable responses is that their sign and shape was channel dependent, i.e., the nature of the tails depended on the measurement channel rather than the cable, as the same tail persisted on a given channel for several different kinds of cables.

The exact location of the entrance of RF into the measurement system has not been determined. About one quarter way through the measurements, an attempt was made to reduce this noise by copper taping all connectors, power dividers, amplifier inputs with nonlocking BNC connectors. In addition, there were several possible sources of RF leakage in the area of the SPIRE Pulse 6000 convertor. An attempt to seal the convertor area with copper tape met with indifferent success. To be sure, the noise levels were about 200 μV which is admittedly small. However, in some cases the measured signals were only about 1 mV in amplitude. While the net contribution of the tails to the total charge emitted is relatively small, it is clear that one must be careful about making statements about the nature of the processes determining the net radiation response based on pulse shapes under the exposure conditions without taking into account the effect of system-generated noise.

In any further cable tests, it is desirable that great pains should be taken to eliminate RF coupling into the measurement system. Possible steps that could be taken to eliminate such noise include: (1) the exclusive use of semi-rigid cables and locking connectors (GR, SMA or N and not BNC) for cable runs, (2) positioning scopes and amplifiers away from the convertor area, i.e., back toward the operator to take advantage of the $1/r^2$ fall in radiated power, (3) to provide better RF shielding for the machine; especially at the converter area, and (4) to put the scopes and amplifiers in some sort of screened enclosure and to provide for isolation of these instruments.

4.5 MACHINE CHARACTERIZATION - DOSIMETRY

Great pains were taken to provide an active dose and fluence map for each pulse. For nearly all shots, data from two gold foil calorimeters provided by SPIRE was taken as well as that for two PIN diodes. The former yielded the total fluence per shot while the latter yielded radiation pulse shape and total dose [rads(Si)] external to the cable jacket. The diagnostic sensors were placed as indicated in Section 4.4 to yield a mapping of machine output.

The gold-foil calorimeters had 0.051 cm of foil with a thickness of about 1.0 gm/cm^2 so that essentially all of the x-ray beam was stopped. Calibration of those devices was provided by SPIRE. At the same total energy, this response is essentially spectrum/independent.

The PIN diodes were from Quantrad (model 025-PIN-125) and had an active area of 25 mm^2 (uncollimated) and a depth of 125 μm. For the most part, they were collimated with a 3.2 mm thick lead collimator which had a 2.29 mm diameter hole in it and shielded with 25 μm of Al foil to keep out scattered photoelectrons. The output from the PIN diodes were integrated either manually or, on at least one channel, with an RC integrator to yield a total dose directly. The SPIRE pulse shape, as recorded by a PIN diode is shown in Figure 7(c). The pulse typically had a FWHM of about 70 to 100 nsec, a corresponding peak dose rate of about 2.5×10^8 rads(Si)/sec, and a mean dose rate about 1/2 of that.

The PIN diodes were calibrated in a variety of ways including exposure to Co^{60} at a dose rate of 11 rads (PTFE:CaF_2 TLD)/sec, 12 MeV electrons at about 2×10^7 rads(Si)/sec, light from a He-Ne laser (0.6328 μm), a GaAs laser (0.9 μm), and light from a 2K tungsten light filtered by 0.5 mm of Si. Results are summarized in Table V. Based on the calibrations, a conversion factor of $2.7 \pm 0.3 \times 10^{-8}$ and $2.14 \pm 0.14 \times 10^{-8}$ C/rads(Si) were adopted for diodes 2 and 3 respectively when uncollimated and 4.3×10^{-9} rads(Si) and 3.4×10^{-9} C/rads(Si) with the 2.29 mm collimator in place.

In order to predict the response of the cables to the SPIRE Pulse 6000 radiation, both the incident fluence and spectrum must be known. At our request, SPIRE did some first-order characterization of the Pulse 6000 under the charging conditions (300 kV), gap widths, and cathodes that were used. The results of this characterization are shown in Figure 8. These measurements were done relatively quickly and may not be very accurate (Bill Siedler and Bob Lowell, SPIRE, private communication).

In order to calculate the dose equivalent to the fluence of the SPIRE 6000 pulse, QUICKE2 runs were carried out for the spectra shown in Figure 8. The results of these calibrations are

Linear Cathode: 1 $mcal/cm^2$ = 97 rads(Si)
Circular Cathode: 1 $mcal/cm^2$ = 178 rads(Si)

If one compares these fluences to dose conversion to the actual calorimeter/PIN data, one finds a disagreement. The mean experimental values are:

TABLE V. CALIBRATION OF PIN DIODES (UNCOLLIMATED)

Radiation	[Sensitivity C/rad(Si)] Diode 2	Diode 3	Relative Output Diode 2/Diode 3
Theoretical[a]	2.0×10^{-8}	2.0×10^{-8}	1
^{60}Co	2.4×10^{-8}	2.0×10^{-8}	1.20
12 MeV Electrons	2.99×10^{-8}	2.28×10^{-8}	1.31
Si Filtered Light			1.16
He-Ne Laser			1.0
GaAs Laser			1.3

[a]Based on a generation rate of 4×10^{13} e-h pairs/cm^3·rad(Si) and an active diode volume of 3.125×10^{-3} cm^3.

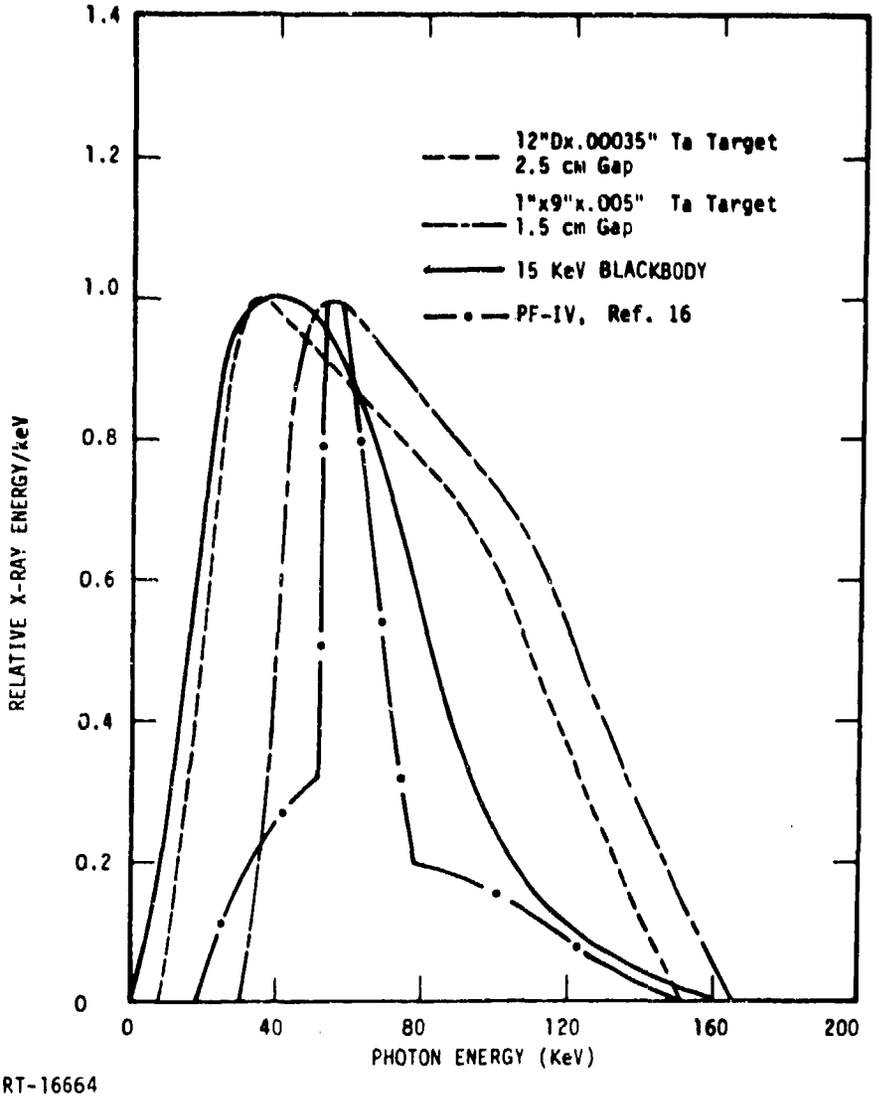

Figure 8. Representative SPIRE-PULSE 6000 Bremsstrahlung Energy Spectrum for a charging voltage of 300 kV. The 12 inch cathode is circular while the 1 inch x 9 inch cathode is linear. For reference, a 15 keV blackbody spectrum and the Aerospace Dense Plasma Focus IV spectrum (Ref 16) are also shown.

Linear Cathode:	64.5 rads(Si)	= 1 mcal/cm^2 (Pin 2)
	65.9 rads(Si)	= 1 mcal/cm^2 (Pin 3)
Circular Cathode:	136 rads(Si)	= 1 mcal/cm^2 (Pin 2)
	123 rads(Si)	= 1 mcal/cm^2 (Pin 3)

These values are about 70 percent of the predicted calibrations. It is to be noted that PIN 2 was in the center of both cathodes while PIN 3 is on the horizontal axis, about 4-1/2 inches to the left of center. That PINS 2 and 3 have about the same conversion factor for the linear cathode is evidence of the relative uniformity of the fluence along the cathode axis. That the center PIN shows a higher conversion factor than the left-most PIN for a given average fluence is probably evidence of a falling off of fluence away from the center of the circular cathode.

There is some evidence that there is a correlation between average fluence measured and the measured dose-to-fluence conversion constant for the linear cathode. As the measured fluence for a selected group of shots increases from 0.24 mcal/cm^2 to 0.32 mcal/cm^2, the conversion constant decreased monotomically from 91.9 to 56.7 rads(Si)/cal/cm^2 which suggests that, for given charging voltage and gap spectrums, the mean photon energy for dosimetry increases with increasing output. Clearly, to resolve the discrepancy, a more careful characterization of the SPIRE 6000 Pulse output for the experimental conditions should be carried out.

5. ANALYSES OF DATA

5.1 INTRODUCTION

This section presents the data obtained during photon tests and summarizes the significant results for each cable type tested. The data is presented in summary tables and the shot-to-shot response of each cable tested is presented in a series of plots which forms Appendix E. For each shot series, the response per unit fluence and per unit dose are given. The dose is expressed in rads(Si) and is the dose measured by the PIN diode external to the sample. A positive response is defined as one in which the net charge flow is from the center conductor through the 50 ohm termination to the outer shield.

Possible mechanisms for creating anomalous behavior (i.e., significantly varying response from shot to shot) are examined to explain the observed cable responses. These mechanisms include gaps, range shortening due to charge buildup in the dielectric, reduction in the number of photoelectrons crossing the gaps because of opposing fields due to previously trapped charge, reduction in gaps due to elastic deformation of the dielectric by electrostatic forces, radiation-induced conductivity in the dielectric, relaxation of stored charge in the dielectric as a consequence of irradiation, and ionization of air trapped in gaps. For the conditions under which data is taken [low fluence (<0.35 mcal/cm^2) x-ray irradiation of samples in vacuum], the predominant mechanism for creating "anomalous" behavior appears to be the presence of air trapped in gaps and ionized by the pulse. Taking the semirigid cables as an ideal case, the calculational method predicts the response of an ideal cable to within a factor of two or so. The accuracy of the calculation could be increased by taking more photon paths through the cable and summing. Basically, where one sees an enhanced but constant response above that predicted for an ideal gapless cable (or of opposite sign), the effect is due to gaps between the conductor and the dielectric. If the response varies significantly from shot to shot, currents created by ionized trapped air in gaps oppose and diminish the net vacuum cable response.

Our overall assessment of the importance of stored charge effects and methods for predicting and testing cable responses are given in Section 6.

5.2 SUMMARY OF PRESENT TEST DATA

5.2.1 Semirigid Coaxial Cable SR086

Data for this cable is summarized in Table VI and Figures E-1 through E-12 in Appendix E. Because independent measurement of both fluence and dose were made, results are presented in terms of the response per unit incident fluence and response per unit incident dose. The predicted responses for 1 μm inner or outer gaps are incremental, being the additional response per μm which is added to the gapless response in the low dose approximation (q.v. Section 3.3). For the unbent as-received cables, the experimental data and predictions (assuming no gaps between the conductors and the dielectric) agree in sign (positive) and in magnitude within a factor of 2 for all three manufacturers. There was little shot-to-shot variation in the responses.

Annealing the unbent cables produced little change in the response and again there was little shot-to-shot variation.

Bending the cables, with annealing either before or after the bending, made the responses for this cable always much larger while remaining positive. This change can be explained by assuming that the bending introduced gaps between the conductors and the dielectric. Because the net response is still positive in the present case, the average inner gaps (between the shield and the dielectric) must be larger than the average outer gaps (between the shield and the dielectric). For the annealed-then-bent samples, assuming that no outer gaps were created, the magnitudes of the observed responses can be attributed to range enhancement of electrons emitted from the inner conductor across inner gaps with widths on the order of 20 μm. This gap size is obtained by using the calculated responses presented in Table VI for the gapless cable and the contribution due to an inner gap. For bent-then-annealed samples, the inner gaps may be as large as 150 μm. When the cable was annealed before bending, there was little shot-to-shot variation in response. However, when the annealing followed the bending, the responses decreased gradually by about a factor of five in 6 to 8 radiation pulses, corresponding to a total fluence of 1 mcal/cm^2 and an external dose of about 120 rads(Si). Thus, annealing-after-bending appeared to increase the size of the inner gaps and made them more sensitive to successive pulses. A possible reason for this effect is given in Section 5.5.6.

5.2.2 Semirigid Coaxial Cable SR141

The data for the SR141 samples are summarized in Table VII and presented in detail in Figures E-13 to E-24 in Appendix E. As with the SR086 cable, the

TABLE VI. SR086 RESPONSE

	Predicted[a]				
Linear Cathode	3.5(-10)[b]	3.6(-15)[c]	Circular Cathode	2.9(-10)[b]	1.65(-15)[c]
1 μm outer gap	-2.1(-11)	-2.2(-16)		-2.2(-11)	-1.2(-16)
1 μm inner gap	5.8(-11)	5.9(-16)		5.8(-11)	3.3(-16)

Sample	Measured Response 1st	Measured Response nth	Ratio	Measured Response 1st	Measured Response nth	Ratio
	[coul/(cal/cm^2)•cm]			[coul/rad(Si)•cm]		
1. Uniform Tube - As Received[e]						
4	2.5(-10)	2.8(-10)(9)[d]	0.89	4.1(-15)	5.3(-15)	0.78
5	3.7(-10)	3.7(-10)(9)	1.0	6.0(-15)	7.1(-15)	0.85
6	1.9(-10)	2.0(-10)(9)	0.95	3.1(-15)	3.8(-15)	0.82
2. Precision Tube - As Received[e]						
5	6.5(-10)	7.4(-10)(8)	0.88	1.1(-14)	0.98(-14)	1.1
6	6.2(-10)	5.9(-10)(8)	1.05	1.1(-14)	0.89(-14)	1.24
4	7.7(-10)	8.2(-10)(8)	0.94	1.3(-14)	1.1(-14)	1.2
3. Cablewave - As Received[f]						
1	4.45(-10)(2)[g]	4.2(-10)(9)	1.1	7.0(-15)	7.96(-15)	0.88
2	4.4(-10)	2.9(-10)(9)	1.5	7.6(-15)	5.0(-15)	1.5
3	4.45(-10)	3.1(-10)(9)	1.5	7.7(-15)	5.8(-15)	1.3
4. Uniform Tube - Annealed[e]						
1	1.9(-10)	1.9(-10)(8)	1.0	3.9(-15)	3.4(-15)	0.88
2	2.6(-10)	2.0(-10)(8)	1.3	4.2(-15)	3.6(-15)	1.2
3	2.4(-10)	1.8(-10)(8)	1.3	3.9(-15)	3.2(-15)	1.2
5. Precision Tube - Annealed and Bent[e]						
2-2	1.4(-9)	1.2(-9)(6)	1.1	1.1(-14)	1.1(-14)	1.0
2-1	1.6(-9)	1.4(-9)(6)	1.1	1.3(-14)	1.2(-14)	1.0
2-3	1.3(-9)	1.1(-9)(6)	1.2	1.0(-14)	0.90(-14)	1.1
6. Precision Tube - Bent and Annealed[e]						
1	2.6(-9)	3.8(-10)(6)	6.8	2.1(-14)	3.4(-15)	6.2
2	1.3(-8)	2.5(-9)(6)	5.2	1.0(-13)	2.1(-14)	5.0
3	9.3(-9)	2.7(-9)(6)	3.4	7.4(-14)	2.3(-14)	3.2

[a] See Table B-1

[b] Number in parenthesis is the exponent to base 10, i.e. 3.5(-10)=3.5x10^{-10}. Units are (coul/(cal/cm^2)•cm)

[c] Exposed with linear cathode

[d] Last shot recorded

[e] Circular cathode exposure

[f] coul/(rad(Si)•cm); theoretical conversion factors from cal/cm^2 to rads(Si) based on QUICKE2 calculations (Section 4.5).

[g] A (i) after exponent means that the ith shot was the first recorded.

TABLE VII. SR141 RESPONSE

		Predicted[d]					
Predicted[a]	Linear Cathode	3.5(-10)[b]	2.6(-15)[f]	Circular Cathode	2.9(-10)[b]	1.2(-15)[f]
	1 μm outer gap	-2.1(-11)	-2.0(-16)		-2.2(-11)	-1.1(-16)
	1 μm inner gap	5.0(-11)	5.2(-16)		5.0(-11)	2.8(-16)

Sample	Measured Response 1st	nth	Ratio	Measured Response 1st	nth	Ratio
	[coul/(cal/cm^2)•cm]			[coul/rad(Si)•cm]		
1. Uniform Tube - As Received[c]						
4	1.5(-10)(2)[g]	1.9(-10)(9)[d]	0.79	4.4(-15)	4.4(-15)	1.0
5	2.3(-10)(1)	1.9(-10)(9)	1.2	5.9(-15)	4.4(-15)	1.3
6	2.6(-10)(3)	2.3(-10)(9)	1.1	6.0(-15)	5.4(-15)	1.1
2. Precision Tube - As Received[c]						
4	4.8(-10)	2.5(-10)(8)	1.9	7.1(-15)	4.1(-15)	1.8
3	3.0(-10)(2)[g]	3.0(-10)(8)	1.0	4.6(-15)	4.7(-15)	0.97
6	3.0(-10)(2)	3.2(-10)(8)	0.94	5.2(-15)	5.4(-15)	0.97
3. Cablewave - As Received[c]						
4	2.2(-10)	2.8(-10)(6)	0.79	3.5(-15)	4.4(-15)	0.78
5	5.9(-10)	3.4(-10)(6)	1.7	9.4(-15)	5.4(-15)	1.7
6	2.9(-10)	3.0(-10)(6)	0.98	4.6(-15)	4.7(-15)	0.98
4. Cablewave - Second Irradiation +16h[c]						
4	3.1(-10)(7)[d]	2.7(-10)(11)	1.15	3.3(-15)	4.0(-15)	0.83
5	3.5(-10)(7)	3.9(-10)(11)	1.0	4.2(-15)	5.6(-15)	0.74
6	3.9(-10)(7)	4.2(-10)(11)	0.92	5.6(-15)	6.1(-15)	0.93
5. Cablewave - Annealed[e]						
1	-1.6(-10)	-1.4(-10)(7)		-2.1(-15)	-2.4(-15)	0.86
2	-6.8(-10)	-7.6(-10)(7)	0.89	-1.2(-14)	-1.3(-14)	0.90
3	-2.5(-10)	-2.1(-10)(7)	1.2	-4.3(-15)	-3.6(-15)	1.2
6. Uniform Tube - Annealed and Bent[e]						
2.2	-4.6(-10)	<-5.6(-11)(10)	8.2	-4.4(-15)	<-5.6(-16)	7.8
2.3	4.5(-9)	2.2(-9)(10)	2.0	4.5(-14)	2.3(-14)	2.0
2.1	6.1(-9)	2.0(-9)(10)	3.0	6.1(-14)	2.4(-14)	2.5
7. Uniform Tube - Bent and Annealed[e]						
1	1.7(-9)	9.8(-10)(12)	1.7	1.3(-14)	6.7(-15)	1.9
2	6.2(-9)	1.9(-9)(12)	3.2	4.7(-14)	1.3(-14)	3.6
3	-4.2(10)(2)	-5.4(-10)(12)	0.78	-4.3(-15)	-3.7(-15)	1.2

[a] See Table B-1

[b] Number in parenthesis is exponent to base 10. Units for prediction are [coul/(cal/cm^2)•cm]

[c] Exposed in linear cathode

[d] Las. shot recorded

[e] Exposed with circular cathode

[f] coul/(rad(Si)•cm); theoretical conversion factors from cal/cm^2 to rads(Si) based on QUICKL2 calculations (Section 4.5).

[g] First recorded shot

experimental data and predictions (assuming no gaps) for the unbent as-received cables agree in sign (positive) and in magnitude within about a factor of 2 for all three manufacturers and there was little shot-to-shot variation in the responses. For one set of cables (Cablewave as-received), there was a 15 hour pause after the sixth shot. The response after the pause continued with about the same amplitudes.

Annealing one set of unbent cables changed the signs of the cable responses to negative but the absolute magnitudes were about the same as before annealing. The reversal of sign could be explained by assuming that the annealing introduced a gap between the shield and the dielectric of about 25 to 50 μm. Again there was little shot-to-shot variation in the response.

Bending the cable, with annealing either before or after the bending, made the originally positive responses much larger for about two out of three cables in each of the two sets (bent-annealed and annealed-bent). The magnitude of the response can be explained by assuming that the bending introduced inner gaps of about 100 μm, but negligible outer gaps. The cables with the largest initial positive response showed a decrease in response of about a factor of three after 10 to 12 pulses corresponding to a total fluence of about 1.5 mcal/cm^2. One cable with a somewhat smaller initial response decreased only about a factor of 2 with successive pulses. The order of bending and annealing had little effect on these cables. For the third cable in each of the two sets, the initial response had about the same absolute magnitude as for the unbent cables, but the signs were changed to negative, similar to what happened when this cable was annealed only. This change in response could be explained by assuming a net outer gap which is of the order of 30 μm larger than the net inner gaps. For the bent-annealed case, there was little shot-to-shot variation in the response but, for the annealed-bent case, the response decreased about an order of magnitude with accumulated pulses, but retained its negative sign.

5.2.3 Flexible, Braided-Shield Coaxial Cable, RG-178 B/U

The results for this cable type are summarized in Table VIII and in Figures E-25 to E-32 in Appendix E. The predicted first-pulse responses for as-received cables using an estimated outer gap size of 38 μm (which is based on measurements on a cross-sectioned cable) had the correct sign (negative) but were low by about a factor of 2 for the Belden Cable and by about 5 for the TIMES cable. For the Belden cable, there was little shot-to-shot variation. However, the TIMES cable showed considerable decrease (about a factor of 2.8 after several shots). Annealing and annealing-plus-flexing the

TABLE VIII. RG-178B/U RESPONSE

Predicted[a]							
		Linear Cathode	-1.7(-11)[b]	-1.8(-16)[c]	Circular Cathode	-1.7(-11)[b]	-9.6(-17)[c]
		1 μm outer gap	-8.1(-11)	-8.3(-16)		-8.1(-11)	-4.6(-16)
Including[d] Gaps	Belden	38 μm outer gap	-3.1(-9)	-3.2(-14)			
	Times	46 μm outer gap	-3.3(-9)	-3.3(-14)			

Measured

Sample	Response (coul/(cal/cm²)•cm) 1st	nth	Ratio	Response (coul/rad(Si)•cm) 1st	nth	Ratio
1. Belden - As Received[e]						
4	-6.5(-9)	-4.8(-9)(8)[f]	1.1	-1.1(-13)	-8.9(-14)	1.3
5	-6.3(-9)	-4.8(-9)(8)	1.4	-1.1(-13)	-9.0(-14)	1.3
6	-5.1(-9)	-3.8(-9)(8)	1.3	-8.9(-14)	-7.1(-14)	1.2
2. Times As Received[e] 7	-1.78(-8)	-7.0(-9)(21)	2.5	-1.81(-13)	-7.8(-14)	2.3
8	-1.68(-8)	-6.1(-9)(22)	2.8	-1.67(-13)	-6.8(-14)	2.5
9	-1.73(-8)	-6.2(-9)(22)	2.8	-1.70(-13)	-6.1(-14)	2.8
3. Times after 15h Pause						
7	-7.4(-9)	-4.2(-9)(6)	1.8	-8.0(-14)	-4.4(-14)	1.8
8	-6.2(-9)(2)	-5.0(-9)(6)	1.2	-5.8(-14)	-5.3(-14)	1.1
9	-7.0(-9)	-5.2(-9)(6)	1.3	-7.6(-14)	-5.5(-14)	1.4
4. Times - Annealed[e]						
1	-4.9(-9)(2)[g]	-4.4(-9)(7)	1.1	-7.7(-14)	-6.6(-14)	1.3
2	-7.7(-9)	-5.1(-9)(7)	1.5	-1.2(-13)	-6.9(-14)	1.7
3	-5.4(-9)(2)	-4.9(-9)(7)	1.1	-8.5(-14)	-6.7(-14)	1.3
5. Times- Annealed and Flexed[e]						
4	-4.0(-9)(2)	3.1(-9)(7)	1.3	-6.6(-14)	-5.6(-14)	1.2
5	-6.7(-9)	6.5(-9)(7)	1.0	-1.3(-13)	-1.2(-13)	1.1
6	-3.8(-9)	2.8(-9)(7)	1.4	-7.5(-14)	-5.1(-14)	1.5

[a] See Table B-1

[b] Number in parenthesis is exponent to base 10. Units for prediction are (coul/(cal/cm²)•cm)

[c] Linear cathode

[d] Last shot recorded

[e] (coul/(rad(Si)•cm); theoretical conversion factors from cal/cm² to rads(Si) based on QUICKL2 calculations (Section 4.5).

[f] First recorded shot

[g] From cross sectioning one cable

TIMES cable reduced the response approximately to the response of the Belden cable and the asymptotic response for the TIMES cable. It also removed most of the shot-to-shot variation. A possible reason for this latter effect is discussed in Section 5.5.6.

5.2.4 Flexible, Single Conductor, Braided-Shield Wire, SPEC 44/

The data for this cable type is summarized in Table IX and Figures E-33 to E-36 in Appendix E. For this cable, reliable data was obtained for only two as-received samples. The predicted first-pulse response (using the measured gap of 30 μm) has the right sign (negative) for both cables and is very close in magnitude for one but is low by about a factor of 2.5 for the other. It would take an outer gap of about 85 μm to fit the higher data if the gapless cable predictions were exact. Of three annealed cables, two responses were less (factor of two) than the predictions using the 30 μm outer gap, and one was about the same as the large response for unannealed samples, i.e., high by about a factor of 2.5. There was no significant shot-to-shot variation for any of these cables.

5.2.5 Flexible, Braided-Shield Wire, SPEC 88B

The data for this cable type is summarized in Table X and Figures E-37 through E-42 in Appendix E. The predicted first-pulse responses (using the measured outer gap of 8.6 μm) agreed in sign (negative) and quite well in magnitude with the responses for as-received cables. There was a significant decrease in response for the first few pulses and then the response nearly leveled off. However, one sample went bipolar at the highest doses delivered.

For the annealed-and-flexed samples, the first-pulse responses were slightly below predictions. For annealed only, two samples gave responses comparable to the predictions while another was high by about a factor of 4. However, it would take an outer gap of only 47 μm, assuming negligible inner gaps, to produce this response. All of these annealed samples showed shot-to-shot decreases of as much as a factor of 10 and the sample with the largest initial negative response went completely positive, with a substantial magnitude, at large fluences. Possible reasons for these trends are discussed in Section 5.5.6.

For the annealed-and-flexed samples, the tests were interrupted for 40 hours after the 13th shot. The samples remained in vacuum during this time. The responses for shot 14 (first shot after the interruption) were comparable to the responses for shot 1 -

TABLE IX. SPEC 44/RESPONSE

Predicted[a]						
Including[g]	Linear Cathode	-5.7(-10)[b]	-6.9(-15)[e]	Circular Cathode	-5.8(-10)[b]	-3.3(-15)[e]
	1 μm outer gap	-2.3(-10)	-2.4(-15)		-2.3(-10)	-1.3(-15)
	30 μm outer gap	-7.6(-9)	-7.8(-18)			

Measured

Sample	Response[c]			Response		
	1st	nth	Ratio	1st	nth	Ratio
	(coul/(cal/cm^2)•cm)			(coul/rad(Si)•cm)		
1. As Received[d] 4						
6	-1.8(-8)(4)[f]	-1.7(-8)(12)		-2.3(-13)	-2.3(-13)	
9	-8.1(-9)(5)	-7.9(-9)(11)		-1.2(-13)	-1.4(-13)	
2. Annealed[d]						
6	-4.4(-9)	-4.1(-9)(7)	1.1	-6.5(-14)	-5.5(-14)	1.2
9	-1.6(-8)(2)	-1.9(-8)(7)	0.84	-2.9(-13)	-2.6(-13)	1.1
12	-4.0(-9)(2)	-4.2(-9)(7)	0.96	-7.1(-14)	-5.7(-14)	1.2

[a] See Table B-1

[b] The number in parenthesis is the exponent to base 10. Units are coul/(cal/cm^2)•cm

[c] Linear Cathode

[d] Last recorded shot

[e] coul/(rad(Si)•cm); theoretical conversion factors from cal/cm^2 to rads(Si) based on QUICKE2 calculations (Section 4.5).

[f] First recorded shot

[g] From cross section measurements on one cable

TABLE X. SPEC 88B RESPONSE

			Predicted[a]			
		Linear Cathode	-1.33(-9)[b]	-1.4(-14)[c]	Circular Cathode	-1.09(-9)[b] -6.1(-15)[c]
		1 μm outer gap	-3.54(-10)	-3.6(-15)		-3.63(-10) -2.0(-15)
	Including[g] Gaps	8.6 μm outer	-4.3(-9)	-4.4(-14)		
		18.3 μm inner	+1.7(-9)	1.8(-14)		

		Measured					
	Sample	Response 1st	nth	Ratio	Response 1st	nth	Ratio
		[coul/(cal/cm²)•cm]			[coul/rad(Si)•cm]		
1.	As received[e] 10	-2.8(-9)(2)	+1.1(-10)(18)	-25.4	-4.0(-14)	1.4(-15)	-28.5
	11	-3.6(-9)(2)	-2.4(-9)(18)	1.5	-5.1(-14)	-3.4(-14)	1.5
	12	-3.2(-9)(2)	-2.3(-9)(17)	1.4	-4.5(-14)	-3.2(-14)	1.4
2.	Annealed[f]						
	8	-3.9(-9)	-6.9(-10)(15)[d]	5.6	-7.0(-14)	-1.1(-14)	6.4
	7	-1.8(-8)	+7.6(-9)(15)	-2.3	-4.5(-13)	+1.2(-13)	-3.7
	9	-3.2(-9)	-9.7(-10)(15)	2.2	-3.9(-14)	-1.6(-14)	2.5
3.	Annealed and Flexed[f]						
	18	-1.3(-9)(2)	-9.2(-11)(13)	14.2	-2.2(-14)	-1.6(-15)	14.0
	17	-3.2(-9)	-2.9(-10)(13)	11.0	-4.6(-14)	-7.4(-15)	6.1
4.	Second Irradiation +40h[f]						
	18	-9.8(-10)(14)	-1.2(-10)(30)	8.2	-1.3(-14)	-1.6(-15)	8.1
	17	-2.3(-9)(14)	-5.4(-10)(30)	4.2	-2.9(-14)	-8.0(-15)	3.7

[a] See Table B-1

[b] Number in parenthesis is exponent to base 10. Units for prediction are [coul/(cal/cm²)•cm]

[c] Linear Cathode

[d] Last Recorded shot

[e] coul/(rad(Si)•cm); theoretical conversion factors from cal/cm² to rads(Si) based on QUICKE2 calculations (Section 4.5).

[f] First recorded shot

[g] From cross section measurement of one cable

that is, the cable recovered to its pre-irradiation condition. The subsequent shot-to-shot decrease in response also followed the initial decrease.

5.3 DISCUSSION OF DATA

Several conclusions can be drawn from these results.

1. Of the identified factors that affect cable responses to x rays, gaps of the size typically found in cables are probably the most important parameter which determines the magnitude, and even the sign, of the response of a cable.

2. For unbent semirigid cables, responses can be predicted reasonably well (factor of two or so) assuming no gaps. Even this discrepancy may be partly due to the fact that the spectrum furnished by SPIRE and used for calculations may not be an accurate characterization of the real spectrum. The discrepancy between the calculated and measured dose discussed in Section 4 is evidence of this.

3. Bending semirigid cables creates significant gaps between the dielectric and both the center conductor and the shield. For the samples tested, the center gaps usually dominated the response. Occasionally the outer gaps were more important.

4. Most braided-shield cables contain large gaps (compared to photoelectron ranges) which is the most important factor in determining their response.

5. Annealing and flexing of braided-shield cables can alter the magnitude and shot-to-shot decrease of their responses. However, these changes appear to be related more to changes in the gaps, and perhaps outgassing, than to stored-charge effects.

6. Sectioning and photomicrographing braided-shield conductors will give a rough estimate of the gap sizes. However, the accuracy of the estimate is not good and sizable differences between predicted responses, using these measured gaps, and measured results can be expected. Some of these differences can be attributed to the relative accuracy of the computational method used. Based on a comparison between calculation and the response of straight semirigid cables, the calculations are probably good to a factor of two or so.

7. There is little, if any, conclusive evidence for stored-charge effects on the first-pulse anomalies.

8. In cables with large first-pulse responses, presumably due mainly to gaps, there is often a large progressive decrease in response for repeated pulses. However, some cables, with a variety of thermal annealing and mechanical treatments, show little change in the response with repeated pulses. The reason for this decrease (or absence of decrease) is not absolutely clear. Various mechanisms that have been proposed to explain these shot-to-shot variations are discussed in Section 5.5 and their relative importance is assessed. A possible model to explain the decreases with repeated pulses is described in Section 5.5.6 in relation to the observed data trends.

5.4 COMPARISON OF PRESENT DATA WITH RESULTS OF OTHER INVESTIGATORS

It is always interesting to compare one's results with those of other investigators. Unfortunately, most cable data was taken under different test conditions, such as state of cable (gaps), photon spectra, air or vacuum, etc., so that a direct one-to-one comparison cannot be made without evaluating how the conditions of irradiation affects the response. Therefore, in the following, comparisons are made only on the basis of cable type (or class) and differences in response due to difference in photon spectra and air/vacuum conditions are discussed.

Three sources of data are presented for comparison: (a) the experiments also performed on the SPIRE 6000 machine by D. Clement et al. of TRW,[3] (b) the summary report of cable response by F. Hai of Aerospace[16] and (c) the older data by J. Notthoff of McDonnell Douglas.[31]

Since the experiments of Reference 3 were performed with the same radiation source (however for slightly different x-ray spectra) from the present tests, the results should be fairly comparable for the same cable types in vacuum. Their tests included samples of some of the same SR086, SR141 and Spec 44 cables tested in this program.

The experiments of Reference 16 were performed both in air and in vacuum (~10 μm) using two versions of the Aerospace dense plasma focus (DPF) machine (MK IV and MK V). The MK IV spectrum is comparable to the spectrum of the SPIRE pulse 6000

[31] J. K. Notthoff, Coaxial Cable Responses to Ionizing Radiation from FX-100 and PR-1590 Flash X-Ray Machines, McDonnell Douglas Astronautics Company paper 1621, July 1971.

machine but the MK V spectrum is somewhat harder (Figure 5). Within the accuracy of the present comparisons, these differences in spectra will be ignored. Reference 16 includes data for the SR086, SR141, and Spec 44 cables and several other braid-shield coaxial cables which are included here for comparison.

There are two major differences between the experiments in Reference 31 and the present experiments; namely, the experiments in Reference 31 were performed in air and the photon spectrum was much harder, ranging from approximately 200 keV to 6 MeV with the most probable energy at 400 keV. Both of these differences could produce major changes in the cable responses. Most importantly, as the range of the photoelectrons is much greater, the effect of small gaps found in cable is much less important. To understand any differences in observed response, one would have to know the structure of the cable tested in these experiments and carry out an analysis similar to that in Appendix A for the relevant spectrum. There are three cables in Reference 31 that are of the same generic type as those examined in the present tests (RG-178 B/U, SR086, and SR141). The responses for RG-178 B/U and SR086 are bipolar. It is not possible in these cases to define a simple conversion factor from the data of Reference 31 to obtain response in coul/rad(Si)-cm. Therefore, these data are omitted from the comparison and only the data for SR141 is given.

Another difficulty in making these comparisons is that the results are often not presented in the same units. The data in Reference 3 are given as peak voltage across a 50 ohm resistor. Fortunately one is given simple conversion factors from mV to Coul-cm/cal and Coul/rad(Aℓ)-cm based on the relatively constant pulse shape and spectrum. The data in Reference 16 are presented in units of Coul/rad(Si)-cm, which is the same as that used to present the results of this study. The data in Reference 31 are given in terms of peak current (mA) per foot of cable for a peak dose rate of 10^{10} rad(Si)/sec. If the cable response and the gamma pulse had the same pulse shapes, amps per rad(Si)/sec would be the same as Coul/rad(Si). Unfortunately, many of the responses did not follow the beam pulse so this simple approach is not uniformly applicable to the data of Reference 31. However, for the unipolar responses it is a reasonable approximation. Therefore, this assumption will be used and the comparisons will be restricted to unipolar responses. To obtain units of Coul/rad(Si)-cm, the data of Reference 31 were multiplied by

$$F = \frac{10^{-13}}{(12)(2.54)} = 3.28 \times 10^{-15} \qquad (6)$$

to convert to Coul/rad(Si)-cm.

The comparison of the data is shown in Table XI. In general, the present data are in reasonably good agreement with the results of Clement et al. as one would expect since the test conditions are very similar. The data of Hai are consistently lower, while that of Notthoff is comparable for the SR141. The agreement with Notthoff's data could be fortuitous considering the much hotter photon spectrum that he used. Perhaps one of the more surprising results is that the responses from Reference 3 for the unbent, as-received, semirigid cables (SR086 and SR141) are negative while the present data, the data of Reference 3, and theoretical calculations by IRT and also by the authors of Reference 3 indicate that the responses should be positive. We have no definite explanation of this discrepancy. However, it is interesting that annealing the straight SR141 cables caused their responses to become negative (Section 5.2.2) and about the magnitude reported in Reference 3 (see Table VII). It is possible that the cable tested by the author of Reference 3 had sufficiently large outer gaps (caused by bending) to change the sign of the response.

5.5 MODEL FOR SHOT-TO-SHOT VARIATIONS

It is evident that the enhanced response of the cables tested (above that predicted for the idealized gap free cable) is attributable to the presence of gaps between conductors and the dielectric whose size is comparable to or larger than the range of the photoelectrons created by the simulator x-ray pulses. It remains to account for the variation in response from shot to shot seen in some cases in these measurements and by others.[3] Several hypothetical mechanisms are presented below and an assessment is made of their relative effectiveness in producing the observed behavior for the given conditions of irradiation (spectrum, fluence, possible presence of air trapped in gaps). The most likely origin of the varying response is shown to be electrical currents in ionized air that is trapped in gaps.

5.5.1 Range Shortening in Dielectrics Due to Buildup of Electric Fields

Typical ranges in dielectrics for emitted photoelectrons with energies in the range of 10 to 30 keV are on the order of 10^{-3} cm. The amount of charge emitted in, say, 20 pulses of the SPIRE pulse 6000 machine (if trapped in the dielectric) corresponds to an electric field $\sigma/\kappa\epsilon_0$ = (2 x 10^{-7} Coul/cal) (0.25 x 10^{-3} cal/cm^2-pulse) (20 pulses)/(2 x 10^{-13} f/cm) = 5 x 10^3 V/cm where σ is the charge density, κ the relative dielectric constant and ϵ_0 the permittivity of free space. The maximum decrease in energy of an

TABLE XI. COMPARISON OF PRESENT EXPERIMENTAL RESULTS WITH OTHER DATA

Cables and Treatments	IRT (Vacuum)		Clement et al.[a] (Vacuum)		Hai[b] (Vacuum)	Notthoff[c] (Air)
	$\frac{10^{-10}\ \text{coul-cm}}{\text{cal}}$	$\frac{10^{-15}\ \text{coul}}{\text{rad(Si)}\cdot\text{cm}}$	$\frac{10^{-10}\ \text{coul-cm}}{\text{cal}}$	$\frac{10^{-15}\ \text{coul}}{\text{rad(Al)}\cdot\text{cm}}$	$\frac{10^{-15}\ \text{coul}}{\text{rad(Si)}\cdot\text{cm}}$	$\frac{10^{-15}\ \text{coul}}{\text{rad(Si)}\cdot\text{cm}}$
SR086						
As-received, straight						
Uniform Tube	+1.9 to +3.7	+3.1 to +6	-3.2	-3.1	+0.14 to +1.5	
Precision Tube	+6.2 to +7.7	+11 to +13				
Cablewave	+4.4 to +4.6	+7.0 to +7.7				
Phelps Dodge						*
Bent or coiled	+13 to +130	+10 to +100	+53	+51		
SR141						
As-received, straight						
Uniform Tube	+1.5 to +2.6	+4.4 to +6	-4	-3.8	-0.18 to +0.93	
Precision Tube	+3.0 to +4.8	+4.6 to +7.1				
Cablewave	+2.2 to +5.9	+3.5 to +9.4				
Phelps Dodge						-2.6
Bent or coiled	-4.2 to +62	-6 to +63	-8.6	-8.4		
Spec 44						
As-received	-81 to -180	-12 to -230	-72	-70	-37	
Other braided-shield coaxial cables	-28 to -180	-40 to -180			-1 to -89	*

*Responses for SR086 and RG-178B/U are bipolar so the conversion factor is not valid.

[a]Reference 3

[b]Reference 16

[c]Reference 31

electron traversing this field before stopping is only 5 eV. In other words, the electron stopping power is far greater than the field produced by the trapped photocharge. Since this energy is negligible, for present purposes, compared to the initial energies of the electrons, the effect of range-shortening in the dielectric because of trapped protocharge must also be negligible.

5.5.2 Reduction in Driven-Electron Currents Across the Gaps Due to Buildup of Electric Fields in Dielectrics

If the electrostatic potential across a gap is greater than the kinetic energy of some of the emitted electrons, then these electrons will be turned back to the emitting surface and the net driven current across the gap will be less. Assuming a rather wide gap of 200 μm and the electric field (5×10^3 V/cm) calculated above, the voltage across the gaps is 100 V. If one could measure or calculate accurately the energy spectrum of the emitted electrons, then one could calculate the fraction of the electrons with energies less than 100 eV and, therefore, the percent reduction in the current transmitted across the gap. Unfortunately, the codes for calculating emission spectra are not very accurate for energies below 1 keV. However, one can make an estimate based on the following. Reference 32 reports the amount of charge collected from a gold plate that is irradiated with a pulse of photons from an exploding-wire source as a function of the bias applied to the plate. Biases on the order of kilovolts produced less than an order of magnitude change in the collected charge while a 100 volt bias produced only a few percent change. Since the SPIRE 6000 spectrum is much harder than the photon spectrum of the source used to carry out the experiments reported in Reference 32, there will be a lower percentage of low-energy emitted electrons in the present experiments than in the experiments of Reference 32. Therefore, the effect of a 100 volt field in reducing transport of photoelectrons across the gap in the experiment should be even less than for the case discussed in Reference 32. Thus, any electric field buildup across the gaps should have little effect on the gap-related cable responses in vacuum.

[32] D. A. Fromme et al., IEEE Trans. Nucl. Sci. NS-24, 2371 (1977).

5.5.3 Reduction in Gap Width Due to Elastic Deformation of Dielectrics by Electrostatic Forces

This effect is negligible since the electric field of 5×10^3 V/cm estimated in Section 5.5.1 corresponds to a pressure of less than 1 lb/in^2. Assuming a rather low value of 105 lbs/in^2 for Young's modulus of polymer dielectrics, this pressure produces to a structural deformation of only 10^{-5} cm for a dielectric thickness of 0.1 cm. This change is negligible compared to gap sizes of interest (a few μm).

5.5.4 Radiation-Induced Electrical Conductivity in Cable Dielectrics

In Section 3.3 and Appendix C of this report, the model of Chadsey[7] regarding the effects of radiation-induced electrical conductivity on cable responses was discussed. The analysis in Appendix C, which was for a semirigid coaxial cable (SR086) with no gaps, indicates that effects of the electric fields and radiation-induced conductivity would start to become significant for a 15 keV blackbody incident spectrum around 20 to 50 mcal/cm^2 (see Figure C-3 of Appendix C), depending on the value of K_p, the proportionality factor between the radiation-induced conductivity and the dose rate. Using an average fluence per pulse of 0.25 mcal/cm^2, ten pulses, would deposit only 2.5 mcal/cm^2, which is considerably less than the threshold range of about 20 mcal/cm^2, even using the largest probable value for K_p. Therefore, this mechanism does not appear to be the cause of the observed response decreases. If it were, one would expect to see shot-to-shot decreases for the unbent, semirigid cables, especially since their dielectric is Teflon, which has one of the largest values of K_p for polymer dielectrics. Large decreases were not seen in these unbent cables.

Moreover, the invocation of this mechanism cannot explain why the largest decreases with accumulated dose occur in cables with large gap effects. This is especially evident for the bent, semirigid cables where the bending apparently introduced gaps which increased the first-pulse responses and usually caused large decreases in response with accumulated dose. In general, this mechanism would not be expected to be very effective in reducing the response associated with the gaps for the following reasons. The decrease in response calculated in Section 3.3 and Appendix C results because the dose-created electric fields in the dielectric cause a return current of electrons to the surface of the dielectric, which reduces the effect of the driven charge. The amount of reduction depends on how close these returning electrons can come to the emitting conducting surface where the compensating positive charges are located. For a cable with no gaps, this charge returns to the conducting surface so the

fractional change is large. However, when there are vacuum gaps between the conductor and the dielectric, the electrons in the dielectric can only return to the dielectric-gap interface. The fractional reduction in the response is then, at most, the ratio of the electron range in the dielectric ($\simeq$10 μm) to the gap width (say, 10 to 100 μm). Therefore, the reduction would be only 10 to 50 percent which is much less than observed. One might argue that the return current in the dielectric could flow around the sides of the gap to the points where the dielectric again contacts the conductor. However, these path lengths are relatively long and the electric fields are not in the optimum direction to expedite such a flow. Therefore, the electrons flowing in the dielectric would normally become trapped long before they reached the conductor.

One final argument against radiation-induced conductivity as the mechanism that causes the response reduction in cables with gaps is that the tendency for the reduction to occur can apparently be greatly influenced by cable treatments which should have no bearing on the radiation-induced conductivity effect. For SR086 cables, bending, followed by annealing, resulted in large decreases in response with dose whereas the cables that were bent after annealing had little shot-to-shot variations in response.

5.5.5 Relaxation of Stored Charge in Dielectrics

It has been argued that anomalous first-pulse responses are due to relaxation of charge that was stored in the cable dielectric by pre-irradiation processes and subsequently released by the deposited dose in the first pulse, or first few pulses. Presumably, after this charge is released, the subsequent responses of the cable are the "true" responses. This hypothesis is the basis for radiation annealing of cables to produce a so-called normal state.

On the basis of our present work, and the results of the TRW investigations[3] it appears that stored-charge effects are much less important than previously believed in contributing to the anomalous response of outgassed cables exposed in vacuum. The reason for this conclusion is that the observed changes in response with accumulated dose cannot be explained by the probable modification of driven charge responses by stored charge in the amounts given as upper limits in Section 2.

The results of Reference 18 indicate that the persistent surface charge densities of the order of 5×10^{-11} and 5×10^{-9} Coul/cm^2 can be introduced by extrusion. The charge introduced by other processes is comparable. By comparison, a 0.25 mcal/cm^2 x-ray pulse with a spectrum comparable to that of the SPIRE pulse 6000 machine causes

the emission of electronic charge of about 5×10^{-11} Coul/cm^2 from the cable shield into the dielectric. For 20 pulses this would amount to $\sim 10^{-9}$ Coul/cm^2.

If there were a sizable stored charge in the bulk of the dielectric (even just 10 μm into the dielectric from the conductor (see Section 2.2)), one would expect a considerable shot-to-shot decrease in response for the straight semirigid cables. There would be large built-in electric fields in the dose-enhancement regions near the metal-dielectric interfaces and these would produce internal electric currents which would either add to or subtract from the driven-charge effect, depending on the sign of the stored charge. If they added to the driven charge effect (which would require a positive stored charge), the responses to successive pulses should decrease. If the stored charge were negative, the currents due to the built-in fields would oppose the driven charge. If the radiation pulses somehow relaxed this retarding field, as postulated, the cable response should actually increase for successive shots as the built-in fields are washed out and the retardation effect is reduced. Neither of these response changes were observed for the straight semirigid cables.

It could be argued that the stored charge is very close to the surface of the dielectric ($\ll$ dose enhancement distance) and consequently its effect would only be observable when there are gaps to separate the charged surface of the dielectric from the conductor. For this case, consider two magnitudes of the stored charge density, $\simeq 5 \times 10^{-10}$ Coul/cm^2 which is comparable to the emitted charge for 10 pulses and 5×10^{-9} Coul/cm^2 which is much larger than the emitted charge for the exposures of these experiments.

If the shot-to-shot reduction in responses is due to the fields from the stored charge, one would not expect to notice an effect until the total density of emitted charge was comparable to the stored charge. Thus, if the stored charge is 5×10^{-9} Coul/cm^2, it would take 100 pulses to see a 50 percent effect, and even for 5×10^{-10} Coul/cm^2, it would take 10 pulses. The observed effects are much larger than that. On that other hand, if the density of stored charge is less than 5×10^{-10} Coul/cm^2, the resulting fields and potentials are too small to have a noticeable effect on the driven charge. The argument is exactly the same as the one given in Section 5.5.2 in regard to the effect of the charge buildup across a gap due to the total emitted charge.

Therefore, it appears that stored charge does not have a significant effect on the response of cables in vacuum.

5.5.6 Ionization of Air Trapped in Gaps

The most probable mechanism that could cause the decrease in amplitude, and sometimes even a change of sign, which characterizes the anomalous response of cables with accumulated dose appears to be ionization of air that is trapped in gaps between conductors and dielectrics. The electrical conductivity of the ionized air, combined with electric fields across the gap whose source is the driven charge that is imbedded in the dielectric, produces a return current which opposes the effect of the driven charge.

According to this model, the decrease in response amplitude with successive pulses occurs in the following way. At the beginning of the first pulse, the electric field across the gap is zero, assuming negligible stored charge in the dielectric (Section 5.5.5). Therefore, the return current during the first small pulse is insignificant and the cable response should be comparable to the response with completely evacuated gaps. Moreover, because the return current is small, the driven charge that crosses the gap will not be fully neutralized by the return current. A small electric field develops across the gap. Thus, on the second shot, there is a small return current which cancels part of the driven current and reduces the net cable response. On successive pulses, the electric fields across the gap, and likewise the return currents, gradually increase even more and the net cable response continues to decrease. This model is very similar to the one proposed by TRW[3] to explain certain anomalous bipolar responses for cables with gaps when irradiated in air. However, there are a few differences between the models, as discussed later.

For most of the cables that showed a shot-to-shot decrease in response, the response after several pulses approached an asymptotic value with the same sign as the first-pulse response. However, for a few cables, the response after several pulses first became bipolar and then completely changed sign from the first-pulse response. If the electric fields across the gaps increased continuously and at the same rate for gaps close to the shield and close to the center conductor, the response should approach an asymptotic value of zero. However, after a pulse is over, there are still positive ions in the air in the gaps. On a time scale that is long compared to a pulse width but short compared to the time between pulses, the ions will migrate to the walls of the gap and partially neutralize the electric fields. The asymptotic situation occurs when the amount of neutralization after a pulse just equals the buildup of field during the pulse. Since the net cable response is the difference between a positive contribution due to emission from the inner conductor and a negative contribution due mainly to emission from the shield (Section 3.1), the magnitude and sign of the asymptotic response

depends on the relative decrease of the positive and negative contributions. For example, suppose the first-pulse response is dominated by emission across gaps between the shield and the dielectric. For purposes of discussion, suppose the relative magnitude of the first-pulse response due to the gaps is -10 and the magnitude due to the inner conductor is +1. The net response is -9. Now suppose the asymptotic response due to the gap is -3 and due to the inner conductor is still +1. The net asymptotic response is -2, a factor of 4.5 reduction from the first pulse. As a counter example, suppose the contribution from the inner conductor is constant and +4 for all pulses and the gap contribution again goes from -9 to -3. The first pulse response would be -5 and the asymptotic response would be +1 -that is, the response changes sign.

The above model can explain all of the data given in Section 5.2 and Appendix E with suitable assumptions about gap locations and the presence or absence of air in the gaps. However, it needs to be verified with detailed transport calculations in a model which correctly accounts for air chemistry as a function of air pressure and fluence.

For the semirigid cables (SR086 and SR141), the responses were small and fairly constant with dose until they were bent. It is fairly clear that the bending introduces gaps which increases the first pulse responses. According to this model, those cables which showed significant decreases in response with accumulated dose had air trapped in the gaps. Those semirigid cables that showed little change with dose after bending apparently either were so tight that no air ever got into the gaps or else they were so porous that the gas could easily escape during the pumpdown.

For the braided-shield cables, large gaps are present in the as-received samples between the outer braid and the dielectric. The only question to be answered is whether annealing and/or flexing increased or decreased the trapping of air in the gaps. The one conclusion that appears definite is that Spec 44/ cable apparently has a very porous construction so that the gaps are easily evacuated and the responses are constant with dose. For the RG-178B/U cable manufactured by Times, the as-received samples appear to have gaps that tightly trap the air and cause large decreases in response. Annealing and/or flexing the cables produces changes in the dielectric which unseals the gaps and allows the air to escape during pumpdown. The Belden cables are apparently more porous and trap less air. Finally, for the Spec 88 cables, the change in response with accumulated dose is large and similar for the as-received, annealed, and annealed-and flexed cables so these cables are apparently very airtight, even after the annealing and flexing.

Since the outer shield and jacket are placed on the cable while it is in air, it is certainly plausible that trapped pockets of air can exist. Any conclusions regarding outgassing rates are specific not only to cable type but also installation. It is conceivable that long lengths of cable (compared to the approximately one-foot samples tested), terminated in a different manner, could show significantly different outgassing behavior.

Perhaps the most convincing argument for this model is the fact that, in the annealed-and-bent Spec 88B cables, the response after a 40 hour interruption in the tests essentially repeated the responses for the initial radiation pulses on that cable. According to the present model, the field that is built up across the gap in the first few pulses, and which causes the decrease in the responses for subsequent pulses, could bleed off during the 40 hour period due to delayed electrical conductivity in the dielectric and even in the air. If the decrease in responses with accumulated dose were due to persistent stored charge from manufacturing or handling processes that was being neutralized by the radiation pulses, one would not expect the stored-charge condition to recover during the interruption.

If the above model is correct, it means that the decreased response with dose would not occur in a true space environment if the gaps can become completely evacuated before the arrival of the incident photon pulse. Of course, as stated previously, for system-length cables, the outgassing time could be fairly long. Therefore, one should not count on the relieving effect of the air ionization for design purposes.

On the other hand, it is conceivable that this effect could actually increase the cable response over the first-pulse magnitude. This result would occur if the positive and negative contributions to the response initially cancelled each other almost exactly and then one contribution decreased significantly with successive pulses while the other remained essentially constant. However, it appears unlikely that this scenario would result in very large ial responses. By assumption, any cable that shows a large shot-to-shot change in response has large air-filled gaps. Normally, these gaps will be near either the shield or the inner conductor, but not in both places simultaneously with equal magnitudes. Therefore, the first-pulse response will usually be large due to gaps near one of the conductors. Then, as the response contribution from the gaps decreases with successive pulses, at worst one will be left with just the contribution from the zero-gap regions, which should be much smaller than the first-pulse gap effect. This conclusion is borne out by the data in Appendix E in that response of opposite sign from the first-pulse response are always considerably smaller in magnitude than the

maximum first-pulse responses for each cable type. Thus, a conservative approach is to use the normalized first-pulse response to obtain the response at larger doses, whether with trapped air or completely evacuated gaps.

Since TRW also assumed air ionization in gaps to model the effect of stored charge in cables,[3] some comments about the similarities and differences in results are warranted. The data that they try to explain had a positive response for the initial pulse. This response decreased in amplitude for a few shots and then became bipolar (first positive, then negative). To explain this result, they proposed a model that had gaps between the shield and the dielectric and a surface density of negative stored charge on the dielectric side of the gap. This charge causes an electric field which opposes the emitted current. They then postulate that the first effect of the radiation pulse is to ionize the air in the gap, thus allowing a current to flow across the gap from the dielectric to the shield. This return current gives a positive response in the exterior circuit. For the first few pulses, this return current dominates the driven current, so the total response is positive. Later, when some of the stored change is neutralized, the driven charge will dominate at the end of the pulse, creating the negative half of the bipolar response. Eventually, when all of the stored charge is neutralized, the response returns to the normal unipolar negative situation.

The main difference in our models is their assumption of a stored charge layer in the dielectric. However, they make the additional assumption that the air is quickly ionized during the pulse. This early ionization allows the reverse current to flow first to give the initial positive response opposing the driven charge effect and only later the driven charge dominates. In all of our data, the initial responses agree in sign with the response to the driven charge. The reversal in sign for the bipolar responses occurs, in our model, when the initially dominant driven-charge effect decreases sufficiently and then the driven charge from the other conductor (with a response of opposite sign) takes over. It may be that both models are basically correct but they occur in different ranges of air pressure. The data that TRW analyzed with their model was obtained in air at 1 atmosphere of pressure, whereas the air in the gaps in our experiments could well be at much less than one atmosphere. Since our data indicates that air in the gaps reduces the maximum cable response, it is not too important whether or not our models are in full agreement with each other.

There are two important questions concerning this model. First, is there enough charge in the ionized air in the gap due to one pulse to approximately counteract the driven charge? Second, is the response time of the electrons in the ionized air fast

compared to the pulse width and the electron attachment time so that the electrons can move a significant distance across the gap during the pulse and before they attach to a molecule?

The emission density per pulse is approximately

$$\sigma = (2 \times 10^{-7}\ \text{C/cal})\,(0.25 \times 10^{-3}\ \text{cal/cm}^2)/1.6 \times 10^{-19}\ \text{C/e}$$

$$\simeq 3 \times 10^{8}\ \text{e/cm}^2,$$

for a pulse with the spectral characteristics of the SPIRE Pulse 6000 machine. The unenhanced deposited dose is about 20 rads(Si)/pulse. However, dose enhancement in a low-Z material (air) due electrons emitted from a higher Z material (copper) can increase the deposited dose in the low-Z material by a factor of several hundred.[7] For this calculation, an enhancement factor of 100 is used, giving a deposited dose D = 2 krads (air). From Reference 33, the density of electrons created in air per deposited rad is $K_g \cong 3 \times 10^6$ P e/cm^3-rad (air). The quantity P is the air pressure in Torr. The density of ionized electrons due to one pulse is

$$n = K_g D = 6 \times 10^9 P\ \text{e/cm}^3. \qquad (7)$$

On the average, the ionized electrons only travel half the width of the gaps, d, whereas the driven electrons traverse the full width. Therefore, for full cancellation of the fields due to the driven charge σ,

$$n\frac{d}{2} = 3 \times 10^9\ Pd = \sigma = 3 \times 10^8\ \text{e/cm}^2 \quad .$$

For a typical value of $d = 10^{-2}$ cm, P = 10 Torr. Below this pressure, there would not be enough ionized electrons to counterbalance the driven charge.

From Reference 33, the mobility for the ionized electrons is

$$\mu \cong \frac{10^6}{P}\ \text{cm}^2\text{/V-sec} \qquad (8)$$

and the attachment time (electron lifetime) is

---

[33] V. A. J. van Lint, Mechanisms of Transient Radiation Effects, Gulf Radiation Technology Report GA-8810, Aug 28, 1968.

$$\tau \cong 10^{-2}/P^2 \quad \text{sec.} \tag{9}$$

From the discussion in Section 5.5.1, the electric field across the gap after a few pulses would be about 10^3 V/cm, assuming no return currents. If this field exists, the transit time across the gap is

$$t_t = \frac{d}{\mu E} = \frac{10^{-2}}{10^6 (10^3)} P = 10^{-11} P \text{ (sec)} \quad . \tag{10}$$

Even for atmospheric pressure (P = 760 Torr), t_t is much less than the pulse width (≈60 nsec). For P = 760 Torr, the attachment time is $\tau \cong 17$ nsec and it is even longer at lower pressures.

In summary, it appears that there is enough ionization, even down to 10 Torr, to counterbalance the driven charge and only a relatively small field ($<10^3$ V/cm) is required to sweep the electrons out of the gap before they recombine and before the end of the pulse. It is interesting that Clement et al.[34] found that air conductivity effects disappear at about 4 Torr for braided and semirigid cables, in reasonable agreement with this order-of-magnitude calculation.

[34] D. M. Clement and R. A. Lowell, The Hardening of Satellite Cables to X-Rays, TRW Final Report for the Defense Nuclear Agency under Contract DNA 001-77-C-0084, Feb 1978.

6. ASSESSMENT

This section contains an assessment of several aspects of the response to x rays of satellite cables based on our studies. These are:

1. The relative importance of stored charge in determining the behavior of cables in (a) an x-ray simulator, (b) the space electron environment, and (c) high fluence environment.
2. The origin of the so-called first-pulse anomaly seen in simulator tests.
3. Factors to be taken into account in predicting cable response both in a simulator and in a high fluence environment.
4. How to test satellite cables.
5. Production of low-response cables.

The principal findings of our study are contained in the executive summary presented at the beginning of this report.

6.1 RELATIVE IMPORTANCE OF STORED CHARGE EFFECTS

As discussed in Section 5.5.5, the presence of stored charge in the amount evidently present in cables does not seem to be as important a factor in determining cable responses as was surmised at the beginning of the program, at least for vacuum conditions. This is in contradiction to the behavior of capacitors where persistent internal polarization significantly enhances response.[30] Given the probable magnitudes of the stored charge surface density ($<5 \times 10^{-10}$ Coul/cm^2) present in the cables, the fields created by this charge are too small to significantly affect the cable response associated with gaps, which is the dominant factor in determining the behavior of many cables.

In Appendix D, it is shown that, whatever the initial stored charge distribution present, it will be replaced by that due to the natural or artificial trapped radiation environment in a time relatively short compared to satellite lifetimes. For many satellite threat scenarios, the density of emitted charge due to the x-ray pulse will completely overwhelm the stored charge and consequently make its effect negligible.

Thus, we have found no evidence that stored charge (in the sense that it might be introduced through manufacturing processes or handling) will significantly affect cable response. On the other hand, handling, especially bending of semirigid cables, will significantly enhance their response because of the creation of gaps. While stored charge may have an initial effect in contributing to the anomalous response of a cable with air-filled gaps, the amount of charge that may be present is comparable to that produced by the pulse in a simulator environment, and much less than in high fluence cases. Its net effect is to diminish the enhanced response which is due to the presence of gaps. The first pulse response in this case will be typical of the cable with evacuated gaps, if slightly diminished.

6.2 "ANOMALOUS" FIRST-PULSE RESPONSES

It appears that the so-called anomalous first-pulse cable responses observed in x-ray simulator tests are associated with the ionization of air trapped in the cable gaps, whether the anomaly consists of a bipolar first-pulse response to a small dose of x-rays, the decrease in cable responses for successive low-dose pulses, or the appearance of a pulse of opposite sign to that expected. The implications are that a completely outgassed cable would not show these anomalies. It is the large and unipolar first pulse response which is probably more representative of what the cable response would be in a fully outgassed condition than the asymptotic responses after several pulses. Moreover, the actual response with no air trapped in the gaps will be at least as large, if not larger, for most cases.

The net response of an ideal coaxial cable is due primarily to the difference between two comparable drivers, created by the motion of charge into the dielectric from the inner and outer conductor. Gaps, where present, enhance the magnitude of each of these terms. In the cables examined, gaps large enough to determine the cable response tended to be found at only one of the two interfaces. This was typically between the outer braid and the dielectric of the flexible cables. For the semirigid cables, such gaps could appear at either interface.

The mechanism proposed in Section 5.5.6 for the anomalous response of a cable predicts that the net response will diminish and may change sign because of a reduction in magnitude of the dominant driver across the gap. The net cable response of the cables studied, where a sign change was observed, was never larger than the initial response. This is largely because asymptotic response of the cable in this case is primarily due to the transport of charge across an interface which had no, or only relatively small, gaps. Thus our conclusion that the first shot response is, in most cases,

true in practice because of the structure of real cables. One could conceive of pathological cases where there were large gaps at both interfaces. It would be possible, in such a case, for the response to change sign and become larger in magnitude. In practice, this does not seem to be a realistic case.

In the above discussion, low-dose conditions were emphasized because all experiments, except for those conducted as part of a few underground tests, have necessarily been conducted at simulators. There are real high-dose effects which make cable responses scale sublinearly at high fluences, as discussed in Section 3.3, which should not be confused with these anomalies. Specifically, after a cable has been subjected to a relatively large dose, its response to a subsequent photon pulse will usually be considerably reduced due to the resulting built-in fields. Thus, "radiation-annealing" does not actually anneal a cable to restore its original as-received state, but instead creates a space-charge polarization that can significantly change the subsequent responses. Whether this radiation annealing effect occurs is dependent on the time between pulses and on the magnitude of the delayed conductivity which tends to relax the trapped charge. The effect should be most noticeable in cables with no, or only small, gaps because the field-generated currents can return completely to the metal conductor, However, for sufficiently large doses, it should also become noticeable in cables whose responses are normally dominated by gap effects. With very large fields present, the return currents can flow around the gaps to the conductors. Note that the presence of large gaps will diminish the effect of radiation-induced relaxation so that departures from linear response in each cable will occur at higher fluences than in the gap free case. Thus, predictions of the type made in Reference 7 must be viewed critically.

6.3 METHODS FOR ESTIMATING CABLE RESPONSES

It appears that reasonable estimates can be made for the response of short sections of cables to low fluence x-ray pulses in vacuum by considering only the emission current of electrons from the cable conductors and dielectrics (including interface enhancement effects), the range of the emitted electrons in the dielectric, the buildup of charge in the dielectric due to the divergence of the photon-driven electron current, and the average size and locations of the gaps in the cables. To model foam dielectrics which contain gaps, the gaps would be spread throughout the dielectric. Their size would be an adjustable parameter estimated from photomicrography. Stored charge effects can be ignored if the cable is completely outgassed.

If the cable has been subjected to a previous irradiation, from space electrons, for example, which cause large built-in fields, the electrical currents due to these fields and the radiation-induced conductivity should be considered. However, one must take into account the irradiation time history. For example, a cable exposed to a uniform and relatively constant space electron flux will reach an equilibrium state. On the other hand, precharging a cable in a simulator test may not be a valid simulation of space radiation conditions. This is true not only because the correct mix of particles and photons with the proper energy distribution will not be simulated, but also because the injected electron distribution starts to relax as soon as the electron beam is turned off as a consequence of the not-insignificant delayed conductivity of the polymer dielectric.

The biggest uncertainty in calculating cable response is related to prediction of gap size. Sectioning and photomicrographing cables can give a rough estimate of the gap sizes. Because of the irregular shape of gaps, estimating a mean gap size is difficult. Nor is the resolution of the structure very good. A possible technique for producing better photomicrographing, which was only conceived while this report was being written, is the following. The cables are potted in a low viscosity epoxy which would be colored or doped with a fluorescent compound to provide a clear contrast between gaps and the conductors and dielectrics. The resultant sample would then be polished and photographed in color under an arc light source, polarized if such enhances the contrast. One might also want to cross section a few cables samples after representative handling to obtain a range of possible gap sizes to be found in real cables.

If cables are to be used in air, or on a short flight (for example, missiles) where outgassing may not be complete, ionization of the air in the gaps should be considered in response predictions. However, it appears that the air ionization will normally reduce the magnitude of the response since it provides a shunt leakage path for return currents. Thus, for worst-case estimates, air ionization can usually be ignored.

For large-dose pulses, the effects of the electric fields generated by the pulse itself and the radiation-induced conductivity should be considered. It is conservative to neglect this effect, i.e., to extrapolate linearly with fluence from simulator cases, but the penalty may be overly severe. This effect should be largest in cables with no gaps. For very large cables, it can become important even with gaps, as explained in Section 6.2.

When the length of the cable is long compared to the characteristic wavelength of the incident pulse, transmission line effects should be considered in determine the signal

that impinges on the electronic system at the end of the cable. The responses that are predicted (or measured) for short sections of cables can be converted to driving functions per unit length of cable for a transmission line analysis, as is commonly done with existing cable codes.

6.4 EXTRAPOLATION OF LABORATORY DATA TO THREAT CONDITIONS

The recommended procedure for predicting the response of cables to a threat environment is to use a combination of analysis, simulator testing, and measurement of cable properties. In order to make such response predictions, one needs to know the cable structure, including representative gap sizes, materials of construction, including plating on conductors, and outgassing behavior. It is important to minimize the uncertainty involved in extrapolating by specifying the cable structure as completely as possible and by ensuring that the test procedures chosen do not lead to false conclusions about response (e.g. Section 6.5). One of course also needs to know the spectrum and flux of the exciting radiation pulses. Ideally, these predictions would be confirmed with test data in the real environment, both radiation and space. Unfortunately, such data cannot usually be provided. Therefore, one must rely on extrapolation from simulator tests.

The response of the cable would be determined for well-characterized samples in a simulator whose fluence, flux and spectrum are carefully determined. Such data would be compared to calculations which would be iterated until satisfactory agreement is achieved. This step would give one a warm feeling about the validity of predictions made for the threat environment. Next, calculations should be performed for the correct cable using the desired spectrum and both a low fluence, corresponding to that at which test data is taken, and the threat fluence level. There is not a rigorously correct procedure at present for going from the calculated charge transfer for the test spectrum and dose, which was adjusted to agree with experiment, to the calculated charge transfer at low dose with the desired spectrum, and finally to the threat dose and spectrum. A certain amount of judgement must always be used. The simplest method is just to scale up the calculated threat-level charge transfer from that measured and multiplying the ratio of the calculated low-dose charge transfer for the test and the desired spectrums at simulator fluences.

If there are no significant high-dose effects at the threat level, the response time history can be taken proportional to the deposition dose rate. However, if high-dose effects are important, the calculated charge transfer versus dose should be

differentiated versus dose and then multiplied by the dose rate time history to obtain the response time history. Finally, when the pulse width is short compared to cable length, transmission line effects must be taken into account by properly phasing the response of each small section of cable.

6.5 RECOMMENDED TESTING PROCEDURES

It is evident from the results of this work, and the companion effort to TRW, that the factors which determine the response of cables have been determined. It is possible, in principle, to calculate the response of a cable based on the procedure described in Chapter 3, which has been embodied in several codes, most notably, that of TRW (MCCABE),[35] and SAI (CHIC).[7] The predictive problem is reduced to (1) specifying the nature of the incident radiation, (2) the cable structure, especially mean gap sizes and locations, and (3) the degree to which air can be trapped in these gaps. These are parameters which must be determined experimentally as part of the test program. Once determined, care should be taken to ensure that the conditions under which the tests are carried out and the cable structure is not changed in an inadvertent manner.

In order to be sure that one understands the response of the cable, one needs to know the characteristics of the x-ray pulse driving that response. This means, in practice, determining the spectral characteristics of the machine for the particular charging and diode conditions employed during the test. Ideally, it would be desirable to do this for each shot with a series of x-ray diodes. However, a machine's output spectrum is probably a relatively constant function of charging conditions. More important, one needs to determine the x-ray fluence and flux through the use of calorimeters and PIN diodes. It was our experience in using the SPIRE Pulse 6000 that one observed significant variations in average fluence and pulse shape ($\pm$ 20%) over a series of ~300 shots, as well as fluctuations in these parameters over the cathodes face for a single shot. In order to obtain reasonable accuracy, multiple dosimeters should be employed to monitor the large area cathodes of the size useful in cable tests.

In order to predict the response of the cable, one needs to know its detailed structure, especially the presence and locations of gaps. At present, this is best done by cross sectioning, potting, and end-polishing. Since cable cross sections, except for semi-rigid cables, are somewhat irregular, one can usually make only a guess as to mean

[35] D. M. Clement et al., IEEE Trans. Nucl. Sci. NS-23, 1946 (1976).

gap size. Moreover, this size may vary from cable to cable, or as a function of handling. Therefore, it is reasonable to test several cables of each history of interest to bound the range of responses. It was an attempt to determine some inefficient statistics on response range that led to our choice of three samples. Clearly, the more of each cable type that can be tested, the better defined is the standard deviation bounding the response of each type. Moreover, those cable samples which show an anomalously large or small response (based on test data and correct predictions) should be cross sectioned and examined for structural anomalies.

The test setup should not itself contribute to an altered response. For example, in past tests, cable samples have been tightly coiled to permit exposure of the largest possible samples in the smallest possible area. As we have seen, tight bending can drastically alter the response of semi-rigid cables. On the other hand, if the cables are to be bent in practice as part of fabrication into cable harnesses, which may affect their response, a simulation of their layout in the harness should be made where possible. Our test data have made clear that installation practices where cables, expecially semi-rigid, are tightly coiled to provide slack or strain relief should be avoided where possible.

The most significant unknown factor in determining cable response is the amount of air which may be trapped in gaps. At present, this is best determined experimentally. It is usually obvious if a cable contains trapped air because an anomalous radiation response occurs (as opposed to gap induced enhancement) where the output changes from shot to shot. Therefore, it should be useful to determine the rate at which each cable type of interest outgasses. This should be done during the qualification tests performed on space-qualified cables to determine the rate at which it loses material in a vacuum environment. It may also be possible to do this during the radiation tests. One may find that some cables, like the Spec 88B or semi-rigids do not lose trapped air. This fact should be taken into account in predicting their response. Unfortunately, the outgassing rate may be a function of the structures of the actual cable harness, i.e., cable lengths, terminations, bending, etc. As a worst case, one can assume no air is present in predicting response.

6.6 LOW RESPONSE CABLES

It is theoretically possible to design cables with a low radiation response based on an identification of each factor which determines their response. Whether such designs are practicable is another matter.

Identified designs typically involve a trade off between radiation response and other factors which determine desired thermal, mechanical, or electrical behavior. We will only discuss these factors briefly. An excellent account of them can be found in Hai[16] and Clement et al.[34]

The net response of a satellite cable to x-radiation is due primarily to two terms, i.e., the difference between the charge emitted from the outer conductor into the dielectric and that emitted from the inner conductor into the dielectric. These two terms are comparable in magnitude for typical, relatively small, satellite cables. The magnitude of either one of these terms can be enhanced if gaps are present whose size is comparable to or greater than the range of a photoelectron in the dielectric. The magnitude of the net emitted charge across an interface is proportional to the difference in atomic number of the conductor and dielectric. Thus, net charge transfer in normal cables is from conductor to dielectric. The response produced by this material difference can be diminished if there is a relatively high conductivity path by which current can be returned to the conductor when driven by fields whose source is the driven charge deposited in the dielectric.

Postulated methods of producing low-response cables are based on reducing effects (1) and (2) and enhancing effect (3). In practice, the interface problem has been addressed by constructing cables whose conductors are made from low-Z metals such as aluminum whose atomic number is comparable to that for polymer dielectrics. Aluminum cables with Teflon dielectrics are now commonly used in SGEMP tests. While such cables do indeed show a diminished radiation response if compared to Cu cables of the same magnitude,[16] the use of aluminum conductors introduces handling problems. A better solution, according to Hai, is achieved with an Al-poly (chlorotrifluorethylene) Al construction. Unfortunately, such a dielectric (Kel-F) is more lossy than Teflon. Cables constructed with this material may not have the desired high frequency behavior. However, this may not be a problem for the short cable runs found in satellites, especially if used to transmit low-frequency data or power.

Even if one constructs a cable as described above to provide for balanced emission, the net cable response may be larger than predicted because of the presence of gaps between a conductor-dielectric interface. Enhanced response due to the presence of gaps can be minimized by using semi-rigid cables which tend to be gap free or at least have relatively small gap sizes compared to photoelectron ranges. Of course, one must be careful not to introduce such gaps because of handling or bending. Unfortunately, some bending of such cables in fabricating cable harnesses is probably unavoidable.

By nature, braided-shield cables have large gaps which determine their response. Various solutions have been proposed to reduce the responses, including filling of gaps with a fluid dielectric while under pressure which subsequently polymerizes and hardens. Whether this can be done practically for the lengths of cables found in a satellite or missile cable harness is a problem which should be looked at by cable manufacturers. An alternate solution may be to use a foil-tape wrap over a compound dielectric. The inner dielectric would be applied by extrusion. An outer dielectric would be applied as a thin coating of a viscous liquid which would become a rubber on polymerization. While the outer dielectric is still soft, the foil tape would be wrapped around. One problem with this technique may be in producing cables with uniform outer diameters. For shielded wires, the small variation in dimensions is probably not important. An alternate means of producing such a cable might be to make the outer conductor a foil-backed polymer tape where the polymer possesses a lower melting temperature than the inner dielectric. On heating, the tape would be fused to the inner dielectric.

Since gaps are important in determining the response of flexible cables, it would not be unreasonable to fund the manufacturers of satellite cables to attack the problem based on one of the solutions described above or some alternative chosen to achieve the same result.

An alternative and complementary approach to producing low-response cables is to dope the inner and outer surfaces of the dielectric with a low-Z material (over a thickness comparable to the range of photoelectrons emitted into the dielectric from both conductors), such as carbon black, to enhance the conductivity of a thin layer of the polymer. This technique is used to produce low noise electrometer cables. The resultant conductivity of the doped layer is comparable to that of a semiconductor. Clement, et al.[36] has shown that such cables do indeed show a diminished response. This is for much the same reason that those cable which have anomalous behavior also do, i.e., because of return conductivity currents. To be most effective, cables treated in this manner should be gap free, and have the dopant deposited in the dielectric not only near the outer shield, as is done for electrometer cables, but also near the center conductor.

LITERATURE CITED

1. MIL-W-83575, Military Specification, Wiring Harness, Space Vehicle, Design and Testing, 1 March 1973.

2. J. M. Wilkenfeld and R. E. Leadon, Research on the Physics of Transient Radiation Effects in Coaxial Cables, Monthly Progress Reports for Harry Diamond Laboratories Contract DAAG39-77-C-0089, IRT Documents 8148-011 and 8148-015, March 1977, May 1977.

3. D. M. Clement, L. C. Nielsen, T. J. Sheppard, and C. E. Wuller, Stored Charge Release in Cables in Low Fluence X-Ray Environments, Topical report prepared on DNA Contract DNA001-77-C-0084, 9 April 1977.

4. D. M. Clement and Charles E. Wuller, Cable Parameter and Photon Source Parameter Sensitivity in Low Fluence X-Ray Environments, Topical report on Contract DNA001-77-C-0084, 8 April 1977.

5. R. L. Fitzwilson, M. J. Bernstein, and T. E. Alston, "Radiation-Induced Currents in Subminiature Coaxial Cables," IEEE Trans. Nucl. Sci., NS-20, 58 (1973).

6. F. Hai, P. A. Beemer, C. E. Wuller, and D. M. Clement, "Measured and Predicted Radiation-Induced Currents in Semi-Rigid Coaxial Cables," Paper, IEEE Trans. Nucl. Sci. NS-24, (1977).

7. W. Chadsey, B. L. Beers, V. W. Pine, and C. W. Wilson, "Radiation-Induced Signals in Cables," IEEE Trans. Nucl. Sci., NS-23, 1933 (1976).

8. J. Wilkenfeld and V. Junkkarinen, Thermal and Radiation Depolarization of Persistent Charge Stored in Polymer Dielectrics, IRT Document INTEL-RT 8124-005, August 1976.

9. R. Leadon, Effect of Trapped Space Electrons on Cable Responses, Topical report prepared for Computer Sciences Corporation under Contract F29601-76-C-0014, 26 May 1977, IRT Document 0031-067.

10. D. M. Clement and C. E. Wuller, Assessment of Cable Response Sensitivity to Cable and Source Parameters in Low Fluence X-ray Environments, DNA Topical Report 4407T, 8 April 1977.

11. Singley and J. J. Vettie, A Model Environment for Outer Space Electrons, NCSDS Report 72-13, Dec 1972.

12. C. E. Wuller, L. C. Nielsen, D. M. Clement, Definition of the Linear Response Region of X-ray Induced Cable Response, DNA Topical Report 4405T, 13 May 1977.

13. J. Van Turnhout, Thermally Stimulated Discharge of Polymer Electrets, Elsevier, Amsterdam 1975, Chapter 10.

14. E. Sacher, J. Macromol Sci-Phys. B6, 151 (1972).

15. MIL-C-27500D (USAF), Cable, Electrical, Shielded and Unshielded, Aerospace.

16. F. Hai, Summary of Cable Response Experiments, SAMSO-TR-77-151, 15 July 1977.

17. J. Wilkenfeld, Radiation Effects in Insulator Materials, Final Report HDL-CR-77-089-1, IRT Report INTEL-RT 8148-011, 1977.

18. D. M. Taylor, T. J. Lewis, and T. P. T. Williams, J. Phys. D: Appl. Phys. 7, 1756 (1974).

19. D. M. Taylor and T. J. Lewis, Proceedings 2nd International Conference on Static Electricity, Frankfurt, FRG (1973); Dechema Monograph, Vol. 72 (1974).

20. A. Wintle, J. Appl. Phys. 43, 2927 (1972).

21. D. K. Davies, J. Phys. D: Appl. Phys. 2, 1533 (1979).

22. P. Ong and J. van Turnhout, in Proceedings 2nd International Conference on Static Electricity, Frankfurt, FRG (1973); Dechema Monograph, Vol. 72 (1974).

23. R. O. Bolt and J. G. Carroll, Radiation Effects on Organic Materials, Academic Press, New York (1963), p. 545.

24. T. A. Dellin and C. J. MacCallum, IEEE Trans. Nucl. Sci. NS-20, 91, (1973).

25. S. H. Rogers and A. J. Woods, Multiple-Plate Modification of QUICKE2 Analytical Electron Emission Code, IRT Report INTEL-RT 8141-026, 15 June 1976, prepared for Defense Nuclear Agency under Contract DNA001-76-C-0068.

26. T. A. Dellin and C. J. MacCallum, IEEE Trans. Nucl. Sci. NS-23, p. 1844, December 1976.

27. H. H. Colbert, SANDYL, Sandia Laboratories Report SLL-74-0012, May 1972.

28. W. L. Chadsey, POEM, AFCRL Report TS-75-0324 (1975).

29. E. A. Burke and J. C. Garth, IEEE Trans. Nucl. Sci. NS-23, 1838 (1976).

30. R. E. Leadon, D. P. Snowden, and J. M. Wilkenfeld, Radiation Effects in Semiconductor and Insulator Materials, HDL-CR-76-152-1, IRT Report INTEL-RT 8124-004, 1 April 1976.

31. J. K. Notthoff, Coaxial Cable Responses to Ionizing Radiation from FX-100 and PR-1590 Flash X-Ray Machines, McDonnell Douglas Astronautics Company paper 1621, July 1971.

32. D. A. Fromme et al., IEEE Trans. Nucl. Sci. NS-24, 2371 (1977).

33. V. A. J. van Lint, Mechanisms of Transient Radiation Effects, Gulf Radiation Technology Report GA-8810, 28 August 1968.

34. D. M. Clement and R. A. Lowell, The Hardening of Satellite Cables to X-Rays, TRW Final Report for the Defense Nuclear Agency under Contract DNA001-77-C-0084, February 1978.

35. D. M. Clement et al., IEEE Trans. Nucl. Sci. NS-23, 1946 (1976).

APPENDIX A. ILLUSTRATION OF CABLE RESPONSE CALCULATIONS FOR LOW-FLUENCE PULSES

The calculational techniques described in Sections 3.1 and 3.2 of this report are applied to a typical coaxial cable behind a 0.0508 cm layer of Aℓ which approximates the walls of a satellite. The selected cable is 2.18 mm (0.086-inch) od, copper jacketed, semirigid, 50-ohm type. It was chosen because it is commonly used in systems and some radiation test data exist for it. Its geometry and the photon paths used in the calculations are those illustrated in Figure 2.

The charge transfer ΔQ that would occur in an exterior circuit per unit length of cable has been calculated for three blackbody spectra (5, 8, and 15 keV). Low-fluence pulses are assumed for the results in this appendix so that electrical conductivity in the interface region can be ignored. High-fluence results are given in Appendix C.

The calculations were first performed ignoring the silver plating on the center copper conductor because Reference 16 indicates that the Ag coating is ≤ 1 μm, which is considerably less than the range of most emitted electrons in Ag ($\leq$(2 to 4 μm)). If this information is correct, the net emission from the center conductor will correspond more closely to emission from the bulk copper than from the Ag plating. On the other hand, the relevant MIL spec (MIL-C-17E) requires the Ag coating to be >1 μm in accordance with ASTM B-298 and B-501. If we assume that the coating thickness is significantly more than the minimum requirement, say, a few μm, it would be comparable to an electron range. Then the electron emission from the center conductor would correspond more closely to emission from Ag than from copper. Therefore, the calculations were repeated using a Ag-coated center conductor for the 15 keV blackbody spectrum, which gave the largest responses without the Ag coating.

As noted in Section 3.1 of this report, there is little attenuation of the photons that reach the cable dielectric as they pass through the dielectric. Therefore, charge buildup in the bulk of the dielectric is negligible and has been ignored. The calculations for the gap used an arbitrary gap width of 2.54 μm . Since the effect of a vacuum gap is linear in the width for small doses, the response due to this effect can be scaled directly for any other width.

The calculated emitted charge and the first moments and centroids of the charge emitted from the conductors into the dielectric are summarized in Table A-1 for the four photon paths illustrated in Figure 3-1.

TABLE A-1. SUMMARY OF QUICKE2 RESULTS

PATH 1 [a]	5 keV (Without Ag Plating on Center Conductor)	8 keV (Without Ag Plating on Center Conductor)	15 keV (Without Ag Plating on Center Conductor)	15 keV With Ag Plating
(1) Forward charge emitted from outer copper [b]	1.451 (-8)	4.574 (-8)	6.90 (-8)	
(2) Moment of charge (1) in CF_2 [c]	3.53 (-12)	1.727 (-11)	4.777 (-11)	
(3) Centroid of (1) = (2)/(1) [d]	2.43	3.76	6.91	
(4) Reverse charge emitted from CF_2 into outer copper	2.09 (-10)	5.62 (-10)	7.58 (-10)	
(5) Forward charge emitted from CF_2 into inner conductor	4.06 (-10)	1.215 (-9)	2.138 (-9)	
(6) Reverse charge emitted from inner conductor (Cu or Ag)	9.70 (-9)	2.924 (-8)	4.152 (-8)	1.12 (-7)
(7) Moment of charge (6) in CF_2	2.01 (-12)	9.05 (-12)	2.242 (-11)	5.26 (-11)
(8) Centroid of (6) = (7)/(6)	2.07	3.1	5.4	4.7
(9) Forward charge emitted from inner conductor (Cu or Ag)	1.25 (-9)	8.90 (-9)	2.621 (-8)	4.88 (-8)
(10) Moment of charge (9) in CF_2	4.87 (-13)	5.25 (-12)	2.615 (-11)	4.5 (-11)
(11) Centroid of (9) = (10)/(9)	3.9	5.9	10.0	9.2
(12) Reverse charge emitted from CF_2 into inner conductor	1.50 (-11)	9.32 (-11)	2.663 (-10)	
(13) Forward charge emitted from CF_2 into outer copper	3.32 (-11)	2.39 (-10)	9.52 (-10)	
(14) Reverse charge emitted from outer copper	7.96 (-10)	5.37 (-9)	1.493 (-8)	
(15) Moment of charge (14) in CF_2	2.62 (-13)	2.587 (-12)	1.162 (-11)	
(16) Centroid of (14) = (15)/(14)	3.29	4.81	7.78	
PATH 2				
(17) Forward charge emitted from outer conductor	1.417 (-8)	4.505 (-8)	6.841 (-8)	
(18) Moment of charge (17) in CF_2	3.469 (-12)	1.709 (-11)	4.754 (-11)	
(19) Centroid of (17) = (18)/(17)	2.45	3.79	6.95	
(20) Reverse charge emitted from CF_2 into outer copper	2.04 (-10)	5.52 (-10)	7.507 (-10)	
(21) Forward charge emitted from CF_2 into inner conductor	3.95 (-10)	1.192 (-9)	2.116 (-9)	
(22) Reverse charge emitted from inner conductor (Cu or Ag)	9.43 (-9)	2.868 (-8)	4.101 (-8)	1.11 (-7)
(23) Moment of charge (22) in CF_2	1.96 (-12)	8.92 (-12)	2.22 (-11)	5.23 (-11)
(24) Centroid of (22) = (23)/(22)	2.08	3.11	5.42	4.7
(25) Forward charge emitted from inner conductor (Cu or Ag)	2.15 (-9)	1.275 (-8)	3.244 (-8)	4.83 (-8)
(26) Moment of charge (25) in CF_2	7.68 (-13)	6.90 (-12)	3.007 (-11)	4.48 (-11)
(27) Centroid of (25) = (26)/(25)	3.57	5.41	9.25	9.3
(28) Reverse charge emitted from CF_2 into inner copper	2.67 (-11)	1.37 (-10)	3.323 (-10)	
(29) Forward charge emitted from CF_2 into outer copper	5.74 (-11)	3.39 (-10)	1.127 (-9)	
(30) Reverse charge emitted from outer copper	1.38 (-9)	7.77 (-9)	1.864 (-8)	
(31) Moment of charge (30) in CF_2	4.17 (-13)	3.43 (-12)	1.349 (-11)	
(32) Centroid of (30) = (31)/(30)	3.03	4.4	7.23	

TABLE A-1 (Continued)

PATH 3	5 keV (Without Ag Plating on Center Conductor)	8 keV	15 keV	15 keV With Ag Plating
(33) Forward charge emitted from outer copper	1.28 (-8)	4.145 (-8)	6.521 (-8)	
(34) Moment of charge (33) in CF_2	3.154 (-12)	1.616 (-11)	4.629 (-11)	
(35) Centroid of (33) = (34)/(33)	2.47	3.88	7.1	
(36) Reverse charge emitted from CF_2 into outer copper	1.78 (-10)	5.03 (-10)	7.11 (-10)	
(37) Forward charge emitted from CF_2 into outer copper	3.26 (-10)	1.041 (-9)	1.952 (-9)	
(38) Reverse charge emitted from outer copper	7.80 (-9)	2.499 (-8)	3.739 (-8)	
(39) Moment of charge (38) in CF_2	1.686 (-12)	8.04 (-12)	2.085 (-11)	
(40) Centroid of (38) = (39)/(38)	2.16	3.22	5.58	
PATH 4				
(41) Forward charge emitted from outer copper	7.27 (-9)	2.89 (-8)	5.29 (-8)	
(42) Moment of charge (41) in CF_2	2.068 (-12)	1.259 (-11)	4.102 (-11)	
(43) Centroid of (41) = (42)/(41)	2.84	4.35	7.76	
(44) Reverse charge emitted from CF_2 into outer copper	9.87 (-11)	3.36 (-10)	5.62 (-10)	
(45) Forward charge emitted from CF_2 into outer copper	1.94 (-10)	7.49 (-10)	1.671 (-9)	
(46) Reverse charge emitted from outer copper	4.67 (-9)	1.778 (-8)	3.075 (-8)	
(47) Moment of charge (46) in CF_2	1.132 (-12)	6.36 (-12)	1.867 (-11)	
(48) Centroid of (46) = (47)/(46)	2.42	3.58	6.06	

a. Paths are defined in Figure 2

b. Emitted charge in coul/cal

c. Moments in coul-cm/cal

d. Centroids in μm from interface

For each photon spectrum, the open circuit voltages and the charge transfer resulting from the following effects or combinations of effects have been calculated for low-fluence pulses (no radiation-induced conductivity).

1. Driven charge from the outer conductor only for a cable with no gap.
2. Same as (1) but driven charge from center conductor only.
3. Driven charge from the dielectric into the inner and outer conductors.
4. Sum of (1), (2), and (3). This result is the normal driven-charge response for no gaps and neglecting induced conductivity.
5. Concentric vacuum gap between the outer conductor and the dielectric.

Since the above driven charge effects with no induced conductivity are directly proportional to the incident dose, the values in this appendix have been normalized to 1 cal/cm^2 incident on the 20 mils of Al. The responses per unit dose are summarized in Table A-2. The charge transfer for electron emission from the center conductor is opposite in sign to the charge transfer for emission from the outer conductor because the directions of emission are in radially opposite directions.

TABLE A-2. CALCULATED VOLTAGES AND CHARGE TRANSFER FOR 1 cal/cm^2 INCIDENT DOSE WITH NO INDUCED CONDUCTIVITY

	5 keV (Without Ag Plating on Center Conductor)	8 keV	15 keV	15 keV With Ag Plating
(1) Average $\frac{Q\bar{x}}{A}$ for charge emitted from outer copper[a]	1.73 (-12)	9.6 (-12)	2.94 (-11)	2.94 (-11)
(2) $\Delta V_1 \simeq -(1)/K\epsilon_0$	-9.56	-53.0	-162.0	-162.0
(3) $\Delta Q_1 = C\ \Delta V_1$[d]	-9.09 (-12)	-50.5 (-12)	-154.0 (-12)	-154.0 (-12)
(4) Average $\frac{Q\bar{x}}{A}$ for charge emitted from inner conductor (Cu or Ag)	1.37 (-12)	8.0 (-12)	2.62 (-11)	4.85 (-11)
(5) $\Delta V_2 \simeq +(4)/K\epsilon_0$[b]	+7.56	+44.2	+145.0	+268.0
(6) $\Delta Q_2 = C\ \Delta V_2$[d]	+7.16 (12)	+42.0 (-12)	+138.0 (-12)	+256 (-12)
(7) Total Q/L on center conductor due to charge from CF_2[c]	-8.53 (-12)	-2.34 (-11)	-3.1 (-11)	-3.1 (-11)
(8) $\Delta V_3 = \frac{(7)\ \ln(R_0/R_1)}{2\pi K\epsilon_0}$[b]	-8.95	-24.6	-32.6	-32.6
(9) $\Delta Q_3 = C\ \Delta V_3$[d]	-8.53 (-12)	-23.4 (-12)	-31.0 (-12)	-31.0 (-12)
(10) Total $\Delta V_{123} = \Delta V_1 + \Delta V_2 + \Delta V_3$[b]	-10.95	-33.4	-49.6	+73.4
(11) $\Delta Q_{123} = C\ \Delta V_{123}$[d]	-1.04 (-11)	-3.18 (-11)	-4.73 (-11)	+7.0 (-11)
(12) Average charge (Q/A) emitted from outer copper[e]	0.685 (-8)	2.43 (-8)	4.25 (-8)	4.25 (-8)
(13) ΔV_4 due to gap of 0.1 mil (2.54×10^{-4} cm) $\simeq -(9)\ 2.54 \times 10^{-4}/K\epsilon_0$	-9.6	-34.1	-59.5	-59.5
(14) $\Delta Q_4 = C\ \Delta V_4$[d]	-0.91 (-11)	-3.24 (-11)	-5.66 (-11)	-5.66 (-11)

NOTES TO TABLE A-2

$\ln(R_0/R_1) = 1.194$

$K\epsilon_0 = 2.0 \times 8.84 \times 10^{-14} = 1.81 \times 10^{-13}$ f/cm

$c = 9.51 \times 10^{-13}$ f/cm

(a) $\frac{Q}{A}\frac{\bar{x}}{}$ in units of $\frac{\text{(coul - cm/cm}^2\text{ of cable surface)}}{\text{(cal/cm}^2\text{ of beam area)}}$

(b) ΔV in units of volts/(cal/cm^2 of beam area)

(c) Q/L in units of (coul/cm of cable length)/(cal/cm^2 of beam area)

(d) ΔQ = change transfer in units of $\frac{\text{(coul/cm of cable length)}}{\text{(cal/cm}^2\text{ of beam area)}}$

(e) Q/A in units of (coul/cm^2 of cable surface)/(coul/cm^2 of beam area)

APPENDIX C. ILLUSTRATION OF HIGH-FLUENCE EFFECTS IN A TYPICAL CABLE

In Reference 7, Chadsey et al. show that radiation - induced conductivity in the interface enhancement regions between the cable conductors and dielectrics reduces the charge transfer in a cable caused by the driven charge. For a planar geometry, the incremental charge transfer (dQ) per incremental dose ($d\gamma$) is

$$\frac{dQ}{d\gamma} = \frac{dQ_0}{d\gamma} \; F(\gamma) \qquad \text{(C-1)}$$

where dQ_0 is the incremental charge transfer neglecting the conductivity effect and

$$F(\gamma) = \frac{1}{\bar{x}} \int_0^{r_e} R_c(x) \; e^{-\gamma \, K_p R_D(x)} \; dx \qquad \text{(C-2)}$$

In Equation C-2, r_e is the maximum range of the secondary electrons in the dielectric, $\bar{x}$ is the mean electron range, $R_c(x)$ and $R_D(x)$ are the relative current and dose deposition profiles, respectively, near the metal-dielectric interface, and K_p is the coefficient of the radiation-induced conductivity,

$$\frac{\sigma(x,t)}{\epsilon} = K_p R_D(x) \; d\gamma/dt \quad , \qquad \text{(C-3)}$$

where ϵ is the dielectric constant.

Note that the electron range r_e does not appear explicitly in Equation C-6, although it is contained in $dQ_0/d\gamma$. Thus, the electron range does not affect the percent reduction of $dQ_0/d\gamma$ due to conductivity.

For small γ_T,

$$\frac{Q}{\gamma_T} \cong \frac{dQ_0}{d\gamma} \quad , \tag{C-7}$$

while for large γ_T,

$$\frac{Q}{\gamma_T} \cong \frac{dQ_0}{d\gamma} \frac{2}{\gamma_T K_p R_D(0)} \quad . \tag{C-8}$$

Although the above results were derived for a planar geometry, they can be applied to a nonsymmetric cylindrical problem when the electron ranges r_e are small compared to the radius of the cable, as they are for the three blackbody spectra used in these calculations. In that case, each local dose-enhancement region is essentially planar and Equation C-8 can be used for the full cable response for the blackbody spectra considered at this time.

To illustrate the effect of the induced conductivity, it is convenient to plot the charge transfer divided by the total dose versus that dose. Since the charge transfer is proportional to dose in the absence of conductivity, $\Delta Q/\gamma$ is a constant versus γ in that case. The three contributions to the total response with no conductivity and their sum (items 3, 6, 9, and 11 in Table A-2 of Appendix A) are plotted in Figures C-1 through C-3 for the three blackbody spectra. Also shown in the figures is the high-dose approximation for the conductivity effect (Equation C-8). Two values of K_p were used corresponding approximately to Teflon and polyethylene (Reference C-1). $R_d(0)$ was arbitrarily taken to be 200 based on data such as Figure 1 of Reference C-1. This number is not crucial to the present analysis since uncertainty regarding its magnitude can be absorbed in the uncertainty for K_p. The conversion from cal/cm^2 incident on the satellite to dose in the polymer was based on QUICKE2 calculations of the dose in the polymer for each spectrum. The net response when conductivity is present is summarized in Figure C-4 for the three blackbody spectra and the larger value of K_p.

Integrating Equation C-1 from zero to the total dose γ_T gives the total charge transfer,

$$Q = \int_0^{\gamma_T} \frac{dQ}{d\gamma}\, d\gamma = \frac{dQ_0}{d\gamma} \int_0^{\gamma_T} F(\gamma)\, d\gamma$$

$$= \frac{dQ_0}{d\gamma}\, \frac{1}{\bar{x}} \int_0^{r_e} \frac{R_c(x)}{K_p R_D(x)} \left[1 - e^{-\gamma_T K_p R_D(x)}\right] dx \quad . \tag{C-4}$$

The distributions $R_c(x)$ and $R_D(x)$ can be obtained for any interface materials and photon spectra using codes such as SANDYL or POEM. However, for the present illustration, a rather crude approximation to $R_c(x)$ and $R_D(x)$ is used. In this approximation, R_c and R_D decrease linearly from the interface to zero at r_e,

$$\left.\begin{aligned} R_c(x) &= 1 - \frac{x}{r_e} \\ R_D(x) &= R_D(0)\ (1 - x/r_e) \\ \bar{x} &= \overline{R_c(x)} = r_e/2 \end{aligned}\right\} \tag{C-5}$$

It is recognized that the approximations in Equation C-5 undoubtedly introduce some inaccuracies into the results. However, for present illustrative purposes, it is felt that they demonstrate the desired effects reasonably well. In addition, their use allows the simplification of integrating the equations in closed form.

Substituting Equation C-5 into Equation C-4 and integrating yields

$$\frac{Q}{\gamma_T} = \frac{dQ_0}{d\gamma}\, \frac{2}{\gamma_T K_p R_D(0)} \left\{\left[1 - \frac{1}{\gamma_T K_p R_D(0)} \left(1 - e^{-\gamma_T K_p R_D(0)}\right)\right]\right\} . \tag{C-6}$$

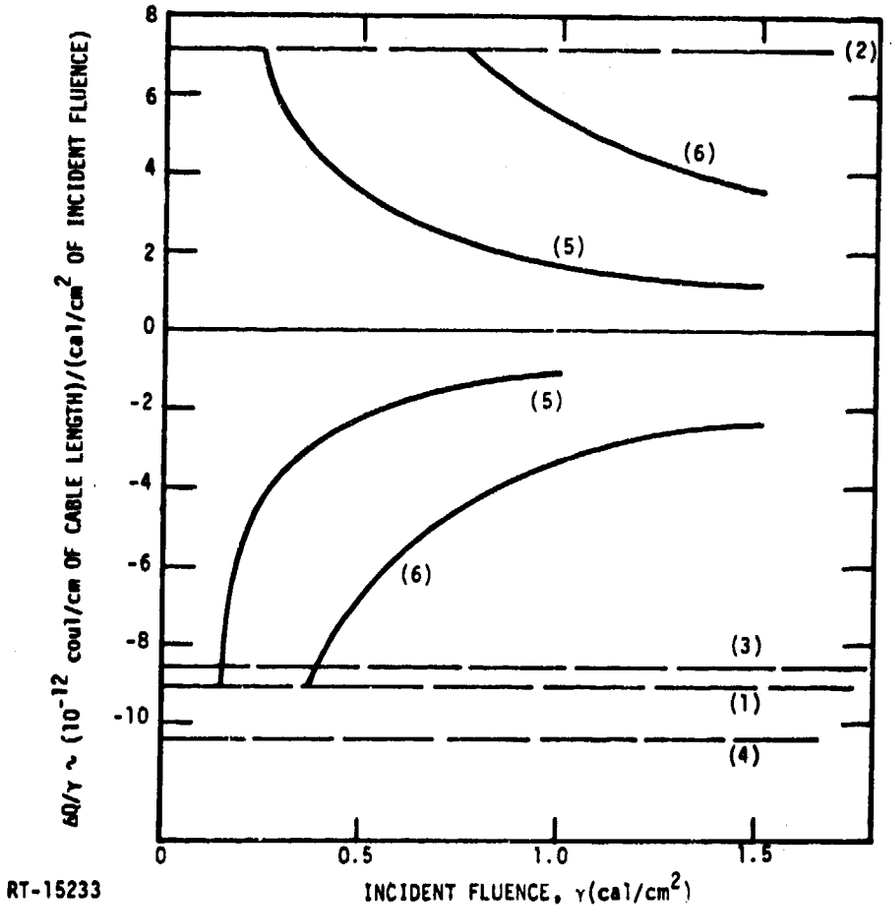

Figure C-1. $\Delta Q/\gamma$ versus γ for 5-keV blackbody incident spectrum. (1) $\Delta Q/\gamma$ for charge emitted from outer conductor, no conductivity; (2) $\Delta Q/\gamma$ for charge emitted from inner conductor, no conductivity; (3) $\Delta Q/\gamma$ for charge emitted from dielectric to conductor, no conductivity; (4) sum of (1), (2), and (3); (5) reduction in (1) and (2) due to conductivity, $K_p = 1.75 \times 10^{-5}$/rad ($CF_2$); (6) reduction in (1) and (2) due to conductivity, $K_p = 5.4 \times 10^{-6}$/rad (CF_2).

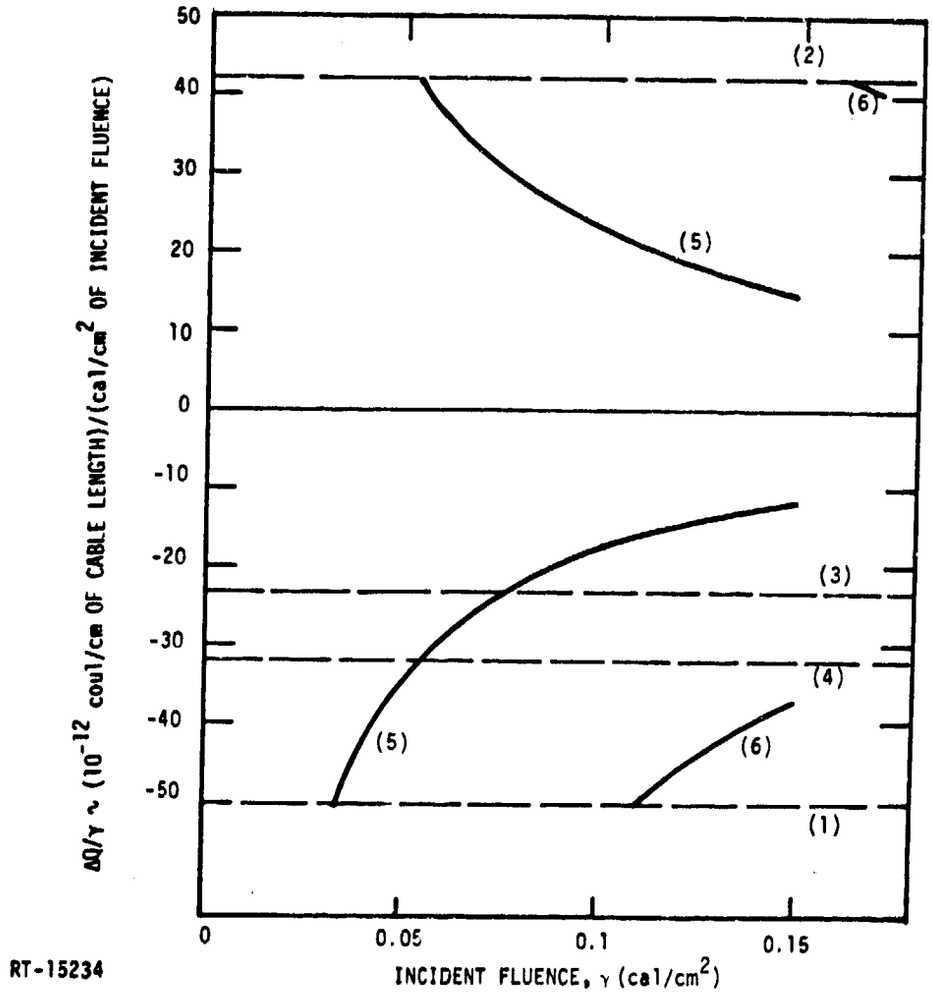

Figure C-2. $\Delta Q/\gamma$ versus γ for 8-keV blackbody incident spectrum. (1) $\Delta Q/\gamma$ for charge emitted from outer conductor, no conductivity; (2) $\Delta Q/\gamma$ for charge emitted from inner conductor, no conductivity; (3) $\Delta Q/\gamma$ for charge emitted from dielectric to conductor, no conductivity; (4) sum of (1), (2), and (3); (5) reduction in (1) and (2) due to conductivity, $K_p = 1.75 \times 10^{-5}$/rad ($CF_2$); (6) reduction in (1) and (2) due to conductivity, $K_p = 5.4 \times 10^{-6}$/rad (CF_2).

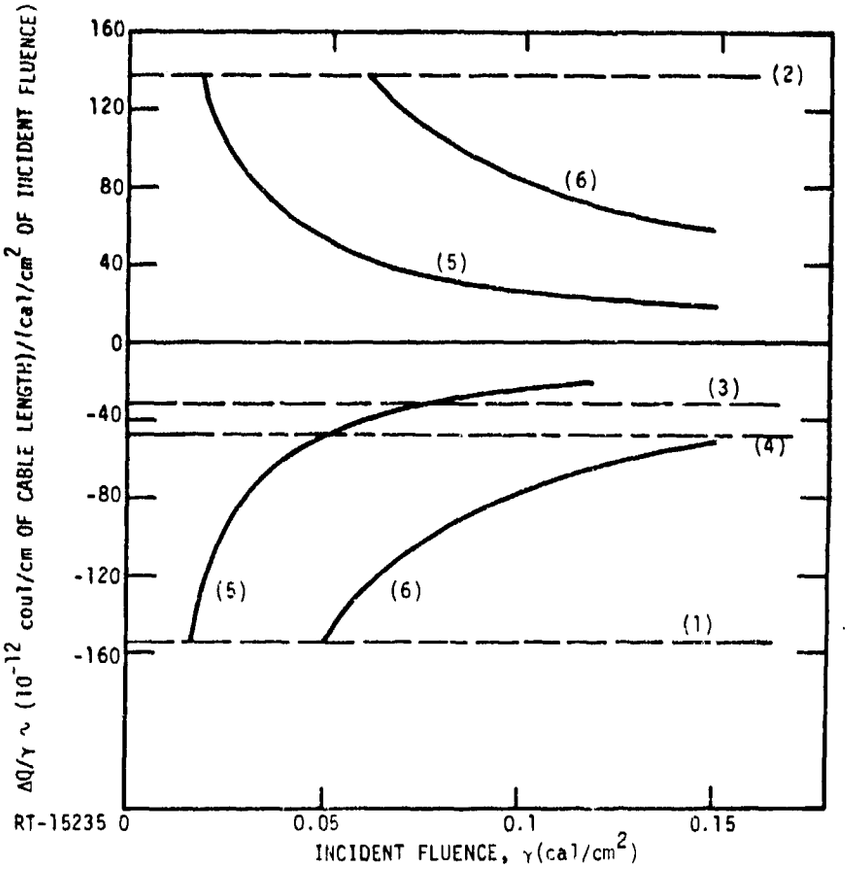

Figure C-3. $\Delta Q/\gamma$ versus γ for 15-keV blackbody incident spectrum. (1) $\Delta Q/\gamma$ for charge emitted from outer conductor, no conductivity; (2) $\Delta Q/\gamma$ for charge emitted from inner conductor, no conductivity; (3) $\Delta Q/\gamma$ for charge emitted from dielectric to conductor, no conductivity; (4) sum of (1), (2), and (3); (5) reduction in (1) and (2) due to conductivity, $K_p = 1.75 \times 10^{-5}$/rad ($CF_2$); (6) reduction in (1) and (2) due to conductivity, $K_p = 5.4 \times 10^{-6}$/rad (CF_2).

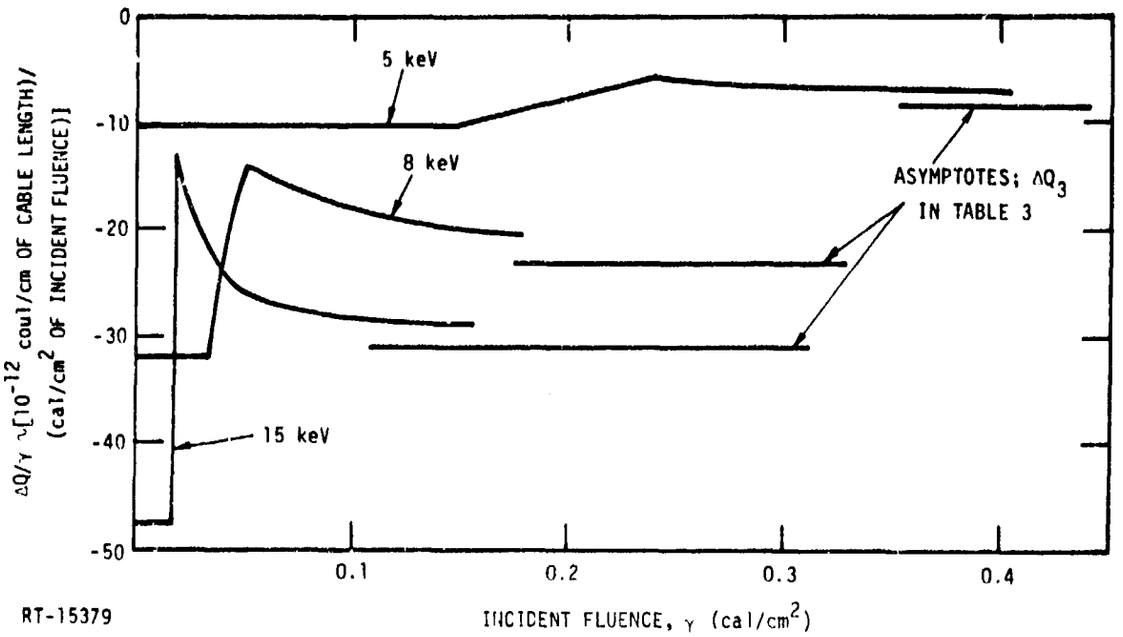

Figure C-4. Net charge transfer, including radiation-induced conductivity effect, versus dose for $K_p = 1.75 \times 10^{-5}$/rads ($CF_2$).

Sum of terms (3) and (5) in Figures C-1, C-2, and C-3.

The large decrease in the charge transfer per dose with increasing dose when induced conductivity is included (Figures C-1 through C-3) occurs because the driven charge produces electric fields in the enhanced dose regions. These electric fields combine with the induced conductivity to produce a current which opposes the driven current and thus reduces the open circuit voltage, and therefore, the charge transfer in the external circuit. For small doses, the electric fields are amall and the resulting opposing current is negligible compared to the driven current. However, the field increases at the larger doses and the opposing current is proportionately larger. At very large doses, an equilibrium is reached where the driven current is just balanced by the returning current. In this case, most of the charge transfer occurs near the beginning of the pulse before the field has built up to the equilibrium condition and the last part of the pulse produces little additional charge transfer, as pointed out in Reference 7.

The rather peculiar shape of the net curves with conductivity in Figure C-4 results because the onset of the conductivity effect at the outer and inner conductor occurs at different incident doses (see Figures C-1 through C-3). If the full equation for conductivity (Equation C-6) had been used instead of just the high-dose approximation (Equation C-8), the transitions between the low-dose and high-dose regions would have been smoother but the general shape would have been the same. Although it does not occur in the present calculations, it appears possible, with some combinations of cable types and photon spectra, for the response in Figure C-4 to cross the zero axis on the first sharp decrease, and then return to the original sign.

APPENDIX D. CALCULATED EFFECT OF TRAPPED SPACE ELECTRONS IN CABLES

When electrons from the earth radiation belts impinge on cables in space vehicles, the cables will capture some of these electrons and develop internal electric fields in their dielectrics. These electric fields have two possible detrimental consequences. First, the fields might become large enough to cause the dielectric of the cable to break down locally. This breakdown might cause electrical failure of the cable insulation and/or the discharge arc could induce large currents into electronics, or at least cause upset. The second possible effect of the internal electric fields is enhancement of the response of the cable to a threat photon pulse. The purpose of these calculations is a Quick-look estimate of both the magnitude of the internal fields due to the capture of space electrons and their effect on cable responses.

Calculations have been made for one typical coaxial cable geometry and material composition. The selected cable is the same one (SR086) used in the calculation of the driven-charge cable response (Figure 2 and Appendix A).

The SANDYL code was used to obtain the dose and charge deposition profiles inside the cable due to an incident spectrum of isotopic space electrons. The charge deposition was then converted to radial current density by integrating the continuity equation. A 0.020-inch Aℓ shield, simulating the satellite skin, was assumed between the electron source and the cable. Since the electron source and the shielding are assumed to be isotropic, the deposition profiles inside the cable due to the space electrons will be cylindrically symmetric. These calculations are discussed in Section D.1 of this appendix. Because of the anisotropy of shielding of a given cable in a real satellite, the deposition profile would also in practice be anisotropic.

If the incident electrons accumulated indefinitely, the fields inside the dielectric would always eventually exceed the dielectric breakdown strength. However, there is a relieving effect due to an electrical current which results from the radiation-induced conductivity and the internal electric fields created by the incident electrons. If the dielectric does not break down first, a steady-state condition will develop, where this relieving current exactly cancels the incident current everywhere in the dielectric. The corresponding steady-state field profile inside the cable dielectric can be determined

rigorously by a simple analytical calculation, given the incident dose and electron deposition profiles [D(r) and n(r)] due to the incident electrons and assuming a proportionally factor (K_σ) betweeen the radiation-induced electrical conductivity (σ) and the local dose rate [D(r)]. This calculation is described in Section D.2. For a given geometry with no, or only small, applied bias on the cable, the steady-state fields are functions only of the dose and charge deposition profiles and the induced-conductivity factor (K_σ). They are not a function of the incident dose rate. Therefore, the fact that the incident dose rate of space electrons varies with time during an orbit does not affect the steady-state fields, provided the electron energy spectrum is reasonably constant with time.

The analysis described in Section D.2 only gives the steady-state condition, which will be approached asymptotically in time (or dose). It does not say how much fluence is required to approach within some percentage of this steady-state condition. In Section D.3, an approximate analytical estimate is made of the fluence required to approach steady state.

The above analyses are sufficient to estimate whether the dielectric will break down merely due to the accumulation of the space electrons. However, to determine the effect of these space charges on the cable response to a photon puise, the radiation-induced conductivity due to the photon pulse must be combined with the above built-in electric fields due to the incident space electrons. The induced conductivity due to the photons was obtained from the calculated dose profiles for the various photon paths through the cable cross section that were used in the driven charge calculations. The estimated change in photon-generated cable response due to the built-in electric field is given in Section D.4.

Section D.5 summarizes the conclusions of this analysis.

D.1 SANDYL CALCULATIONS OF DEPOSITION PROFILES

The driving functions for the development of a steady-state charge distribution in a cable are the dose and electron-current profiles due to an incident isotropic electron spectrum. As stated previously, the resulting profiles should be cylindrically symmetric for the assumed geometry.

The SANDYL code was run with a cylindrical grid system concentric with the cable axis and using an isotropic point source of incident electrons at one point on the 0.020-inch A shield which was assumed to be concentric around the cable for convenience of calculation. For these SANDYL calculations, a 1-μm thickness of Ag was

assumed on the center copper conductor. The resulting dose [D(r)] and charge [n(r)] in the concentric grid regions, averaged around the circumference, were obtained. These average values are the same as would occur for an isotropic electron source completely around the cable. However, the present approach appears to be computationally more efficient to obtain good Monte Carlo statistics.

The electron spectrum that was used to generate the curves in the appendix is the equilibrium fission electron spectrum[D-1] shown in Figure D-1. Under a different program,[9] similar calculations were made using a natural space electron spectrum but these results are not reproduced in this report. The resulting cylindrically symmetric dose and electron-current profiles (Equation D-3 in Section D.2) are shown in Figure D-2. The values in Figure D-2 are for one incident electron/cm^2 on the surface of the Aℓ shield.

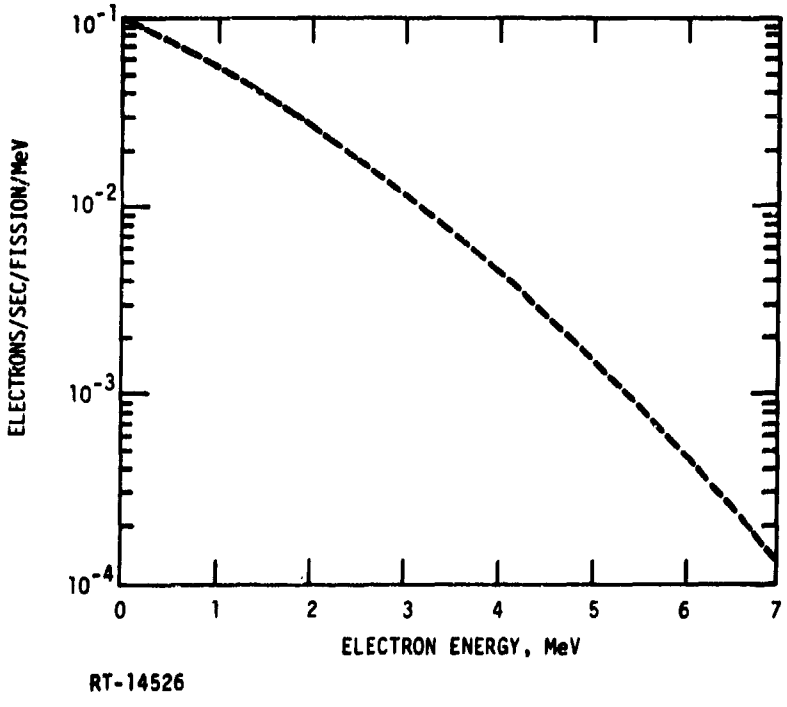

Figure D-1. Equilibrium fission electron spectrum

D-1 The Trapped Radiation Handbook, DNA-25244, December 1971, p. 11-3.

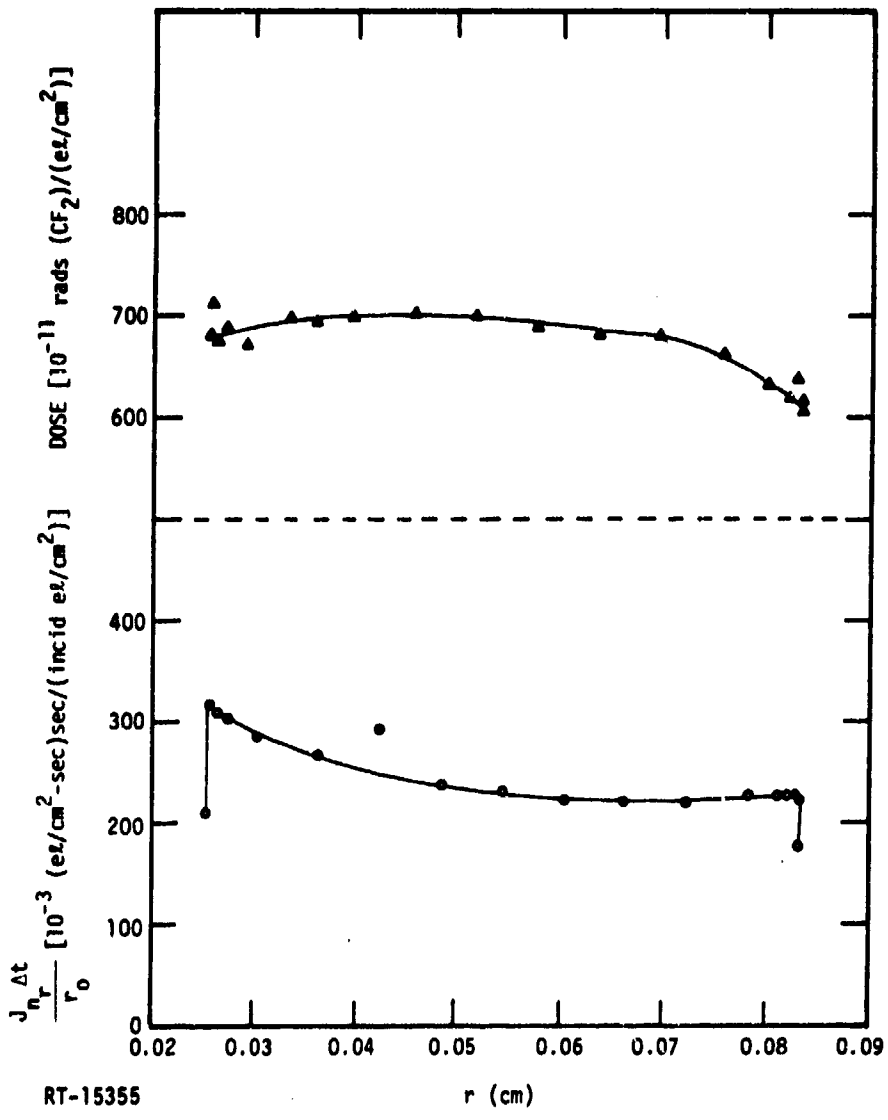

Figure D-2. Dose and current profiles due to incident isotropic fission electrons

D.2 METHOD OF CALCULATING STEADY-STATE FIELDS

The incident electron particle current density $J_n(r)$ at each radial position can be obtained by integrating the continuity equation and using the distribution n(r) from Section D.1.

$$\nabla_r \cdot J_n(r) = \frac{1}{r} \frac{\partial [r J_n(r)]}{\partial r} = - \frac{dn(r)}{dt} \qquad \text{(D-1)}$$

or

$$\frac{\partial [r J_n(r)]}{\partial r} = -r \frac{dn(r)}{dt} \quad . \qquad \text{(D-2)}$$

(Positive vectors, e.g., J_n and E_r, are radially outward.)

Integration of Equation D-2 from the radius of the inner conductor (R_i) to an arbitrary radius r′ gives

$$J_n(r') = \frac{-1}{r'} \left[\int_{R_i}^{r'} \frac{r dn(r)}{dt} dr - R_i J_n(R_i) \right] . \qquad \text{(D-3)}$$

This equation gives the incident electron current density corresponding to the deposition rate of n(r).

In steady state, the incident electron current density (Equation D-3) plus the current density due to the radiation-induced conductivity $[J_\sigma(r')]$ must equal the total current density (J_T) through the dielectric, which is unknown at this time.

$$J_n(r') + J_\sigma(r') = J_T \quad . \qquad \text{(D-4)}$$

The electron particle current density due to conductivity is

$$J_\sigma(r') = -E_r(r') \frac{\sigma}{q} = -E_r(r') \frac{K_\sigma \dot{D}(r')}{q} \qquad \text{(D-5)}$$

where σ is the induced electrical conductivity, $\dot{D}(r')$ is the local dose rate, and q is the absolute value of the electronic charge. Substituting Equation D-5 into Equation D-4 and solving for E_r gives

$$E_r(r') = \frac{q[J_n(r') - J_T]}{K_\sigma \dot{D}(r')} \quad . \tag{D-6}$$

For a given applied voltage, V_A (positive on the center conductor),

$$V_A = \int_{R_i}^{R_0} E_r(r')dr' = \frac{q}{K_\sigma} \int_{R_i}^{R_0} \frac{J_n(r')}{\dot{D}(r')} dr' - \frac{qJ_T}{K_\sigma} \int_{R_i}^{R_0} \frac{dr'}{\dot{D}(r')} \tag{D-7}$$

where R_0 is the inner radius of the outer conductor. Everything in Equation D-7 is assumed to be known except the total current density J_T. Solving for J_T and substituting into Equation D-5 gives the equation for the electric field profile in terms of all known, calculated, or assumed quantities.

$$E_r(r') = \frac{q\left[J_n(r') - \dfrac{\displaystyle\int_{R_i}^{R_0} \frac{J_n(r)dr}{\dot{D}(r)} - \frac{K_\sigma V_A}{q}}{\displaystyle\int_{R_i}^{R_0} \frac{dr}{\dot{D}(r)}}\right]}{K_\sigma \dot{D}(r')} \tag{D-8}$$

Since both $J_n(r)$ and D(r) are obtained from n(r) and $\dot{D}(r)$ by dividing by the same pulsewidth, the steady-state field in Equation D-8 is independent of the pulsewidth (i.e., the dose rate) for zero applied bias V_A. Moreover, with $V_A = 0$, the magnitudes of the electric fields are inversely proportional to the constant of proportionality (K_σ) for the induced conductivity. Therefore, as one would expect, a material with a large radiation-induced conductivity is less likely to break down due to trapped charge, assuming the breakdown strengths of the different dielectrics are comparable in magnitude.

Using the dose and electron current profiles from Figure D-2 in Equation D-8, the resulting steady-state electric field profile is given in Figure D-3.

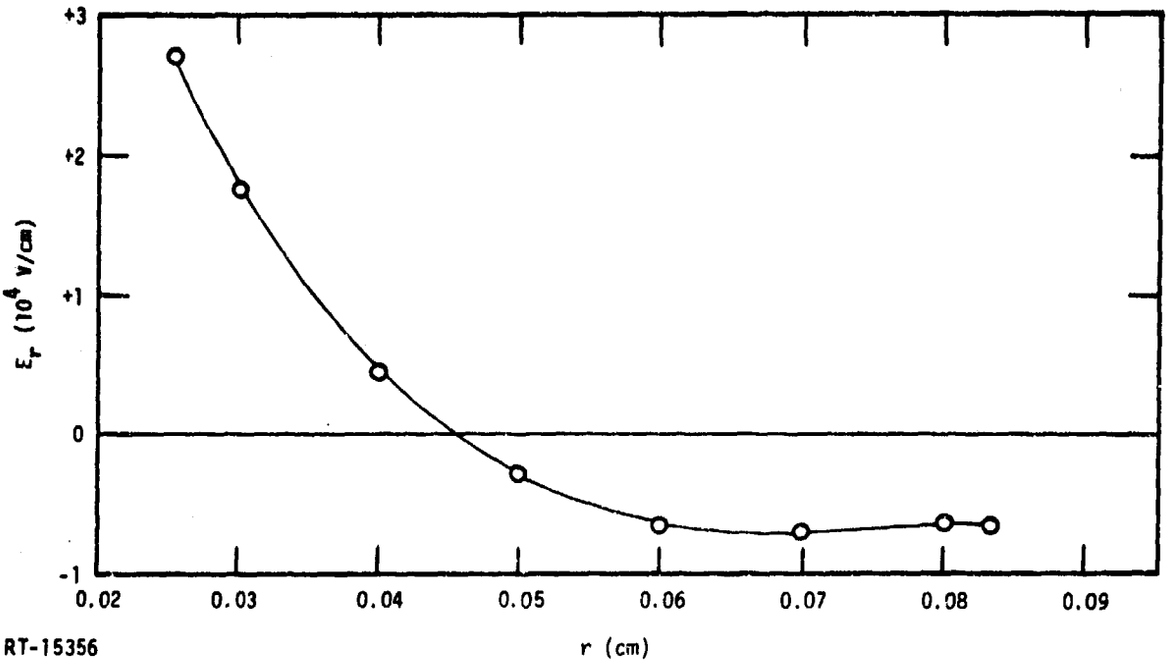

Figure D-3. Steady-state electric field in cable dielectric due to incident fission electrons

D.3 FLUENCE TO APPROACH STEADY-STATE CONDITION

The characteristic time to asymptotically approach steady state is the dielectric relaxation time, $\tau = \varepsilon/\sigma$. For simplicty, assume that the dose deposition is uniform throughout the dielectric. From Figure D-2, use $\dot{D}_{ave} = 13.6 \times 10^{-9}$ [rads (CF_2)/sec)/(e/cm^2-sec)]. For 1 e/cm^2-sec, and $K_\sigma = 10^{-17}$ [$(\Omega\text{-cm})^{-1}$/(rad/sec)],

$$\tau = \frac{\varepsilon}{K_\sigma \dot{D}} = \frac{8.84 \times 10^{-14}}{(10^{-17})(13.6 \times 10^{-9})} = 0.65 \times 10^{12} \text{ sec} \quad .$$

Therefore, to reach (1/e) of steady state with this value of K_σ requires an incident fluence of 0.65×10^{12} (e/cm^2). Using a typical flux of fission electrons of 3×10^{13} e/cm^2-day, the above fluence will be reached in 0.021 days $\simeq$1/2 hour.

Similar calculations using a natural, rather than a fission, electron spectrum shows that the energy spectrum makes a sizable difference on the steady state profile of the electric field. For one particular cable and natural spectrum, a fluence of about 4×10^{13} e/cm^2 was required to approach steady state. For some orbits, the flux of natural electrons can be as high as 5×10^{12} e/cm^2-day. At this flux, only twenty days would be required to approach steady state.

However, one should remember that this time to steady state varies inversely with K_σ so considerably longer times are required for dielectrics with smaller values of K_σ.

D.4 EFFECT OF BUILT-IN FIELDS ON CABLE RESPONSE TO A PHOTON PULSE

The total response of the cable to a photon pulse is the combined effect of the driven charge and the currents produced by the built-in fields. The total charge transfer in this cable due to the driven charge, assuming no initial built-in fields, was calculated in Appendix A for incident blackbody spectra of 5, 8, and 15 keV. The calculations in Appendix C gave an estimate of the effect of radiation-induced conductivity in the dose enhancement regions near the metal-dielectric interfaces. In the present section, the effect of radiation-induced conductivity in the region of the built-in fields due to captured space electrons will be estimated.

Since the incident photons are not cylindrically symmetric around the cable, the dose deposition profiles are also nonsymmetric. Therefore, for a rigorous calculation of the cable response, one should use a time-dependent, two-dimensional transport code. Since a suitable code is not available at this time, the following approximate approach was used.

If a radial current density J_r flows in the dielectric of a coaxial cable with radius R_i for the inner conductor and R_0 for the inner edge of the outer conductor, the corresponding rate of charge transfer from the inner to the outer conductor in short circuit is

$$\frac{dQ}{dt} = \frac{2\pi}{\ell n(R_0/R_i)} \int_{R_i}^{R_0} J_r(r)\,dr \quad . \tag{D-9}$$

To obtain the effect of the built-in electric field, we take J_r to be $J_\sigma = \sigma E_r$. If the dose, and therefore σ, were uniform in the dielectric, σ could be taken outside the

integral in Equation D-9 and the charge transfer would be proportional to

$$\int_{R_i}^{R_0} E_r \, dr \quad ,$$

which is zero in short circuit. Therefore, the only way that a built-in field can produce a charge transfer in short circuit is if the radiation-induced conductivity in the dielectric is nonuniform.

From the QUICKE2 runs used in Appendix A, the dose profiles in the dielectric vary by only about 5 percent for any path through the dielectric (Figure 3-1) for 15-keV blackbody photons and about 10 percent for 5-keV blackbody photons. The average doses were 3.7×10^4 and 4.4×10^3 [rads(CF_2)/(1 cal/cm^2)] for 15- and 5-keV spectra, respectively.

As a rough, hopefully upper-limit, estimate of the charge transfer due to the built-in fields, it is assumed that the dose in the region of negative fields (at large radii) in Figure D-3 is 5 percent above the average dose and the dose in the positive field region is 5 percent below the average dose, i.e., a 10 percent asymmetry. The absolute value of the integral of E_r from the zero field point in Figure D-3 to either end is about 210 volts. Inserting these values into Equation D-9, the total charge transfer (neglecting for the present any reduction in the electric field due to the charge transfer) is

$$\Delta Q = \frac{2\pi}{\ell n\left(\frac{0.0833}{0.0254}\right)} (0.1)\ 10^{-17}\ (3.7 \times 10^4)\ (210) \qquad \text{(D-10)}$$

$$= 4 \times 10^{-11} \text{ (coul/cm of length)/(cal/cm}^2 \text{ in beam)} \quad .$$

This value is for the average dose due to 15-keV blackbody spectrum [3.7×10^4 rads (CF_2)/(cal/cm^2)]. It is comparable to the total charge transfer due to the driven charge only, neglecting conductivity (ΔQ_{123} in Table A-2 of Appendix A). Although a value of $K_\sigma = 10^{-17}$ $(\Omega\text{-cm})^{-1}$/(rad/sec) was used in Equation D-10, it is interesting that ΔQ is actually independent of the value of K_σ, assuming that the steady-state fields do not exceed the dielectric breakdown strength. If a smaller value of K_σ had been used in

these calculations, the steady-state electric fields in Figure D-3 and the value of 210 volts would have been proportionately larger, exactly canceling the smaller value of K_σ in Equation D-10.

As stated before Equation D-10, the above calculation neglects the reduction in the built-in field due to the charge transfer. Therefore, the charge transfer from Equation D-10 is valid only for sufficiently small doses. For larger doses, the maximum charge transfer that could occur is a fraction (perhaps 10 percent) of the actual charge stored in the dielectric by the space electrons.

D.5 CONCLUSIONS

1. For a typical fission electron environment, the cable used in this study reaches a steady-state charge condition after about 1/2-hour exposure, when $K_\sigma = 10^{-17}$ $(\Omega\text{-cm})^{-1}/(\text{rad/sec})$ and after about 20 days for some natural environments.

2. The peak electric field for this K_σ is about 2.7×10^4 V/cm.

3. Both the peak field and the time to steady state vary inversely with K_σ, for zero applied biases.

4. For an incident 15-keV blackbody photon spectrum, the charge transfer due to the steady-state built-in change in fields is about 4×10^{-11} $(\text{coul/cm})/(\text{cal/cm}^2)$, which is comparable to the charge transfer due to the driven charge only (neglecting induced-conductivity effects; i.e., for small doses). This charge transfer is independent of K_σ because σ is proportional to K_σ and the built-in fields are inversely proportional to K_σ.

5. The rate of charge transfer in (4) is valid only for small doses because it neglects the reduction in the initial built-in fields due to the charge transfer.

6. At larger photon doses, the average rate of charge transfer per dose due to the built-in fields decreases. The maximum charge transfer would be some fraction less than unity (about 0.1 for the present example) times the total charge stored in the dielectric by the incident space electrons.

7. A precharged coaxial cable without gaps could show slightly anomalous first-pulse responses (on the order of factors of 2) until enough dose is

accumulated to wash out the initial charge stored in the dielectric. Conversely, after a cable is exposed to space electrons for a few days, all previous stored charge should be washed out and superceded by the trapped space electrons.

APPENDIX E. MEASURED SHOT-TO-SHOT RESPONSE DATA FOR EACH TEST SERIES

The measured shot-to-shot variation in response for successive pulses is contained in Figures E-1 through E-42 for the five cable types and various pre-irradiation treatments. The normalized responses are plotted versus both measured accumulated fluence (mcal/cm^2) and measured accumulated external dose [rads(Si)] as each quantity was measured independently (q. v. Section 4.5).

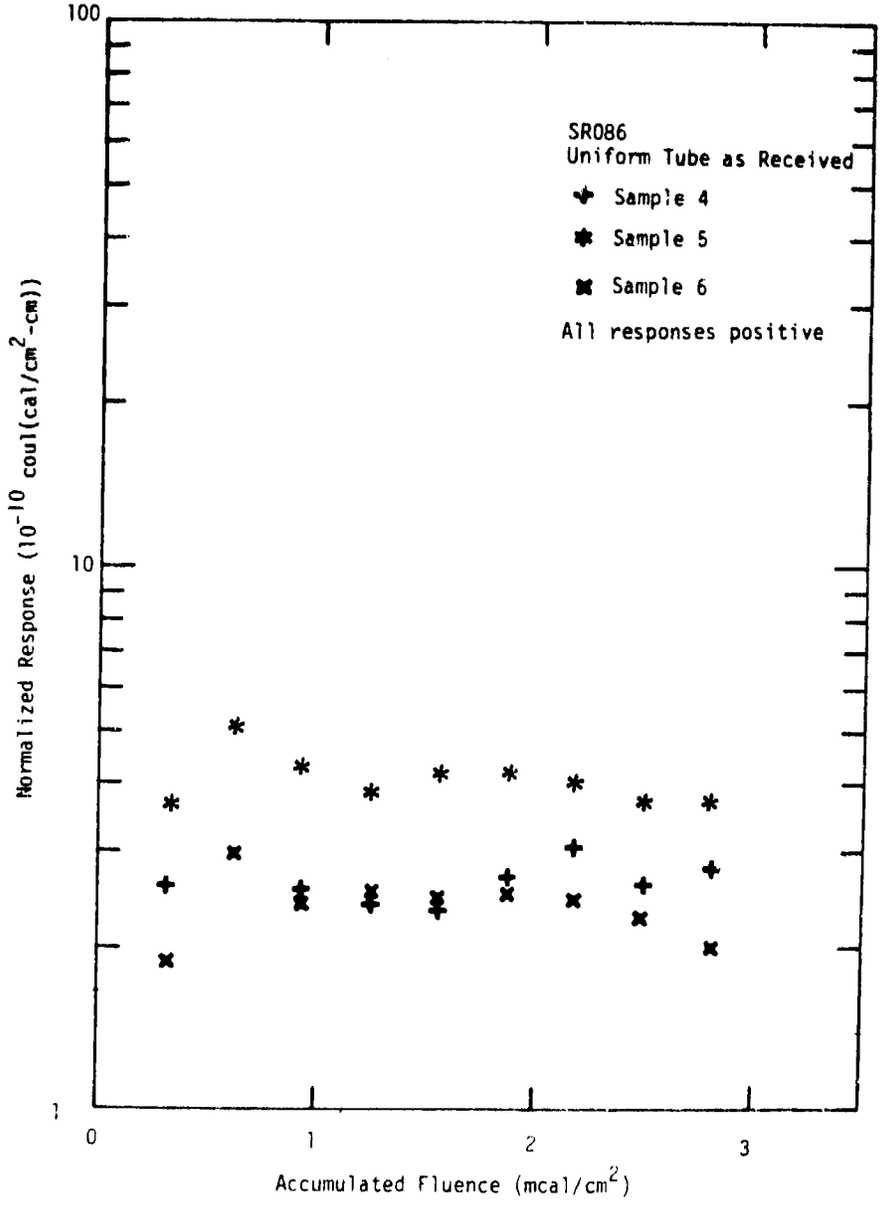

Figure E-1. Shot-to-shot responses of Uniform Tube SR086 cables as received versus total fluence. All responses were positive.

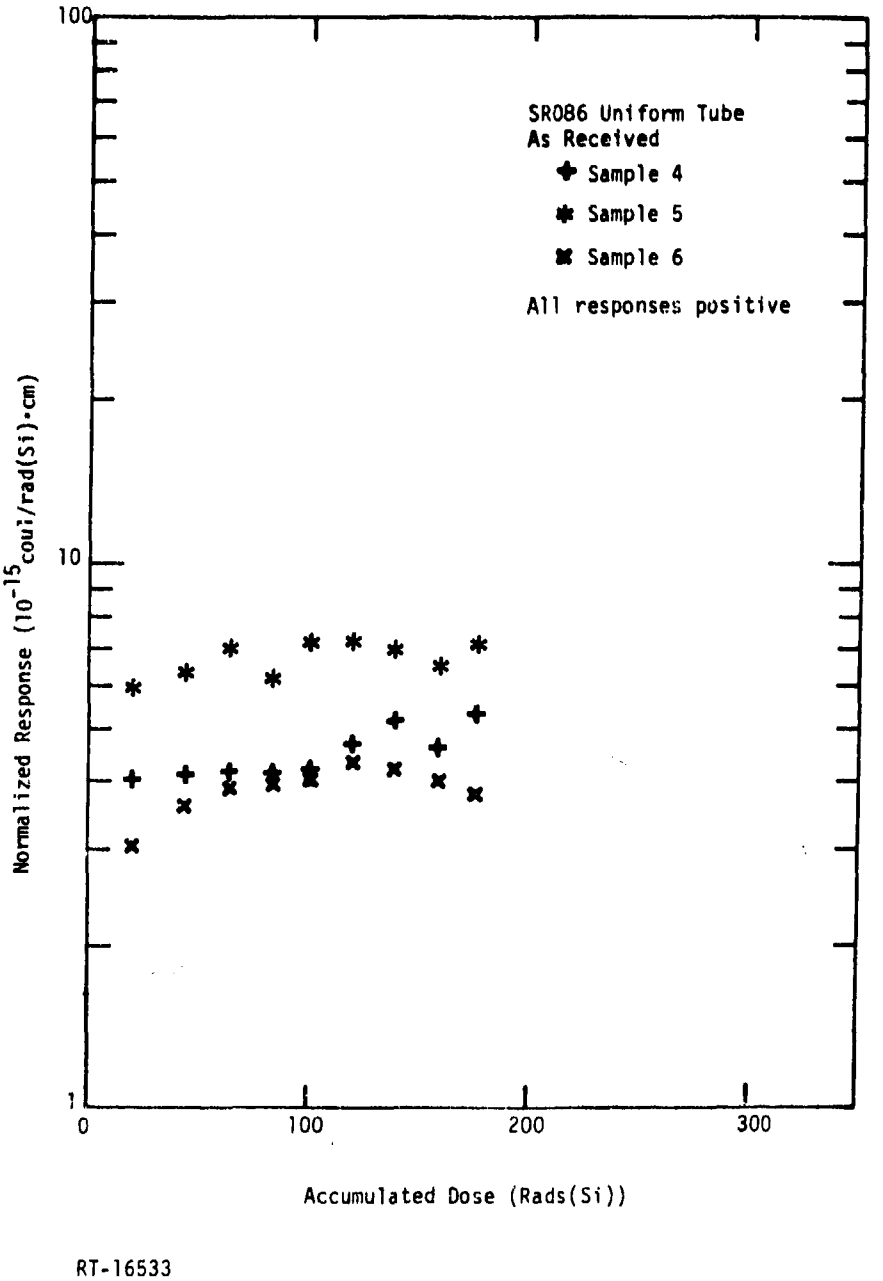

Figure E-2. Shot-to-shot responses of Uniform Tube SR086 cables as received versus total dose. All responses were positive.

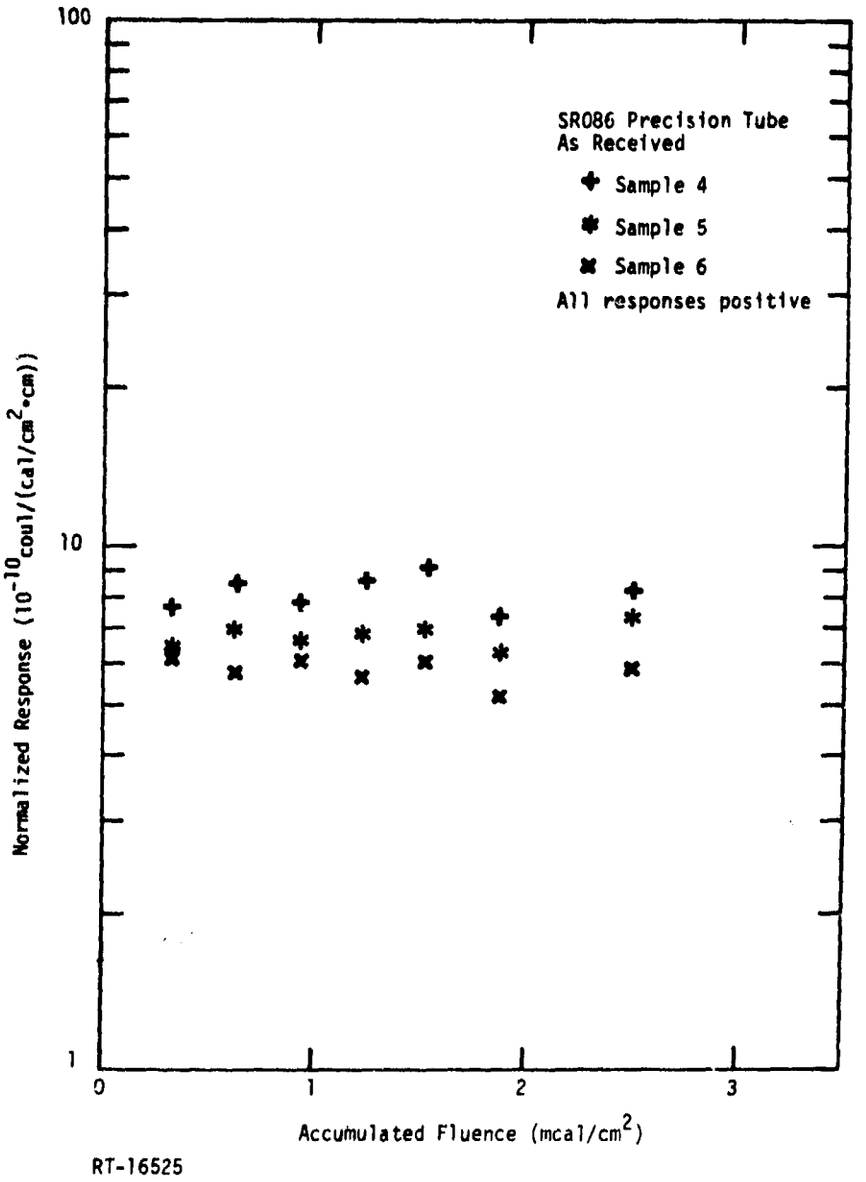

Figure E-3. Shot-to-shot responses of Precision Tube SR086 cables as received versus total fluence. All responses were positive.

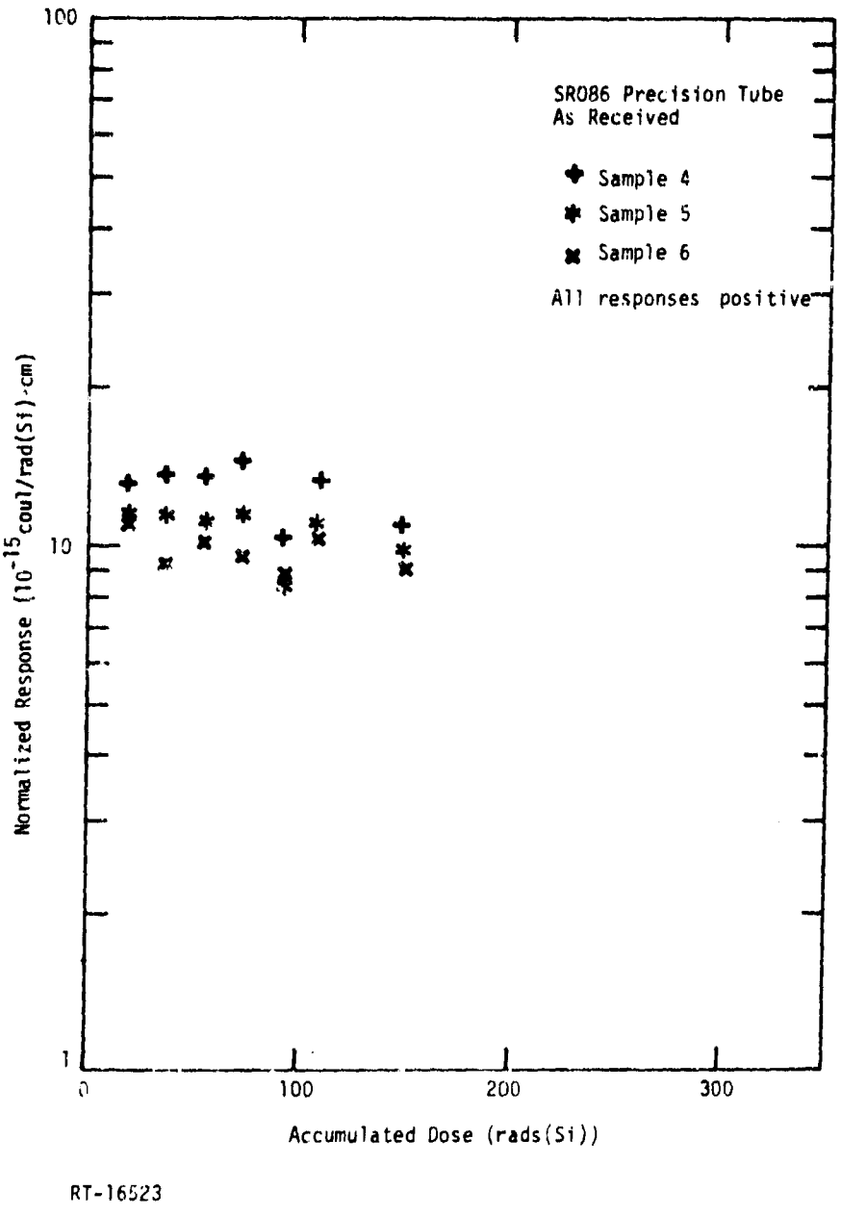

Figure E-4. Shot-to-shot responses of Precision Tube SR086 cables as received versus total dose. All responses were positive.

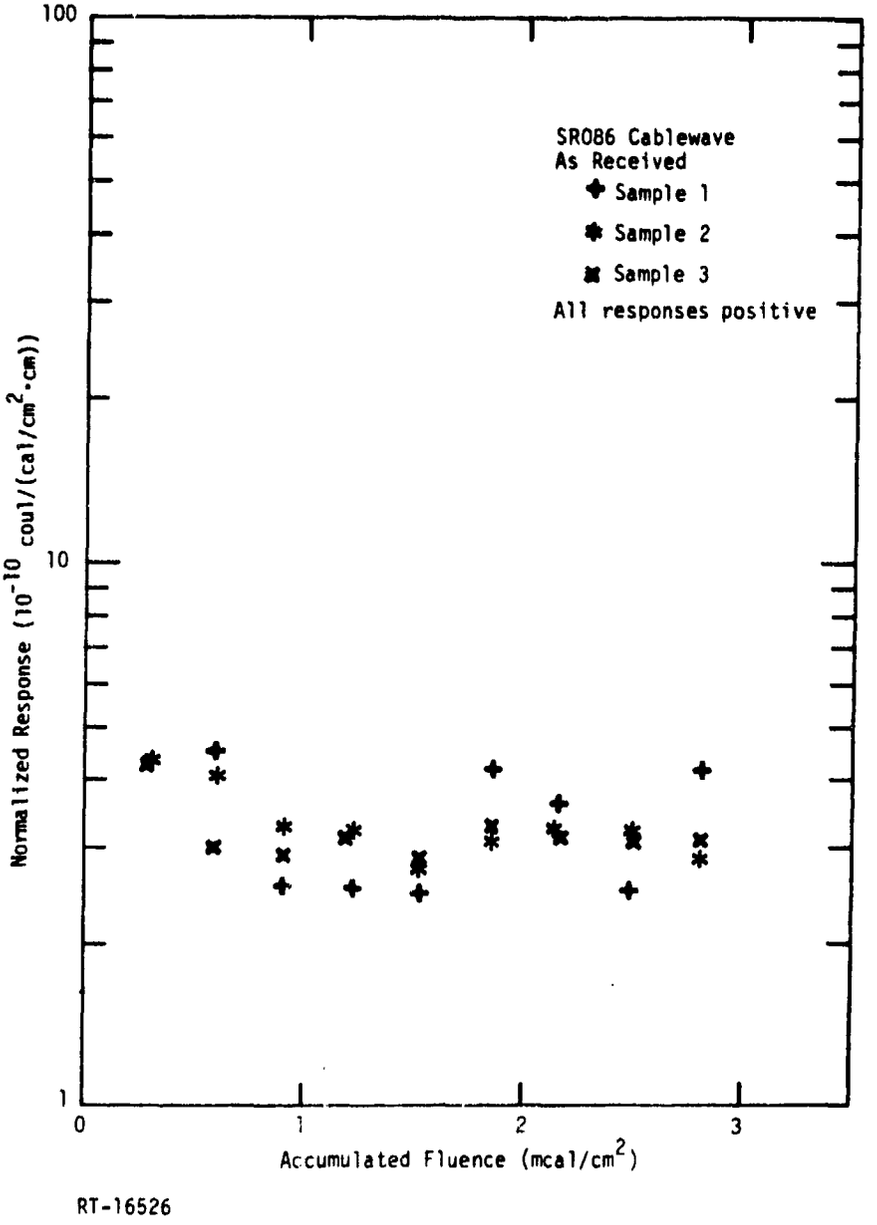

Figure E-5. Shot-to-shot responses of Cablewave SR086 cables as received versus total fluence. All responses were positive.

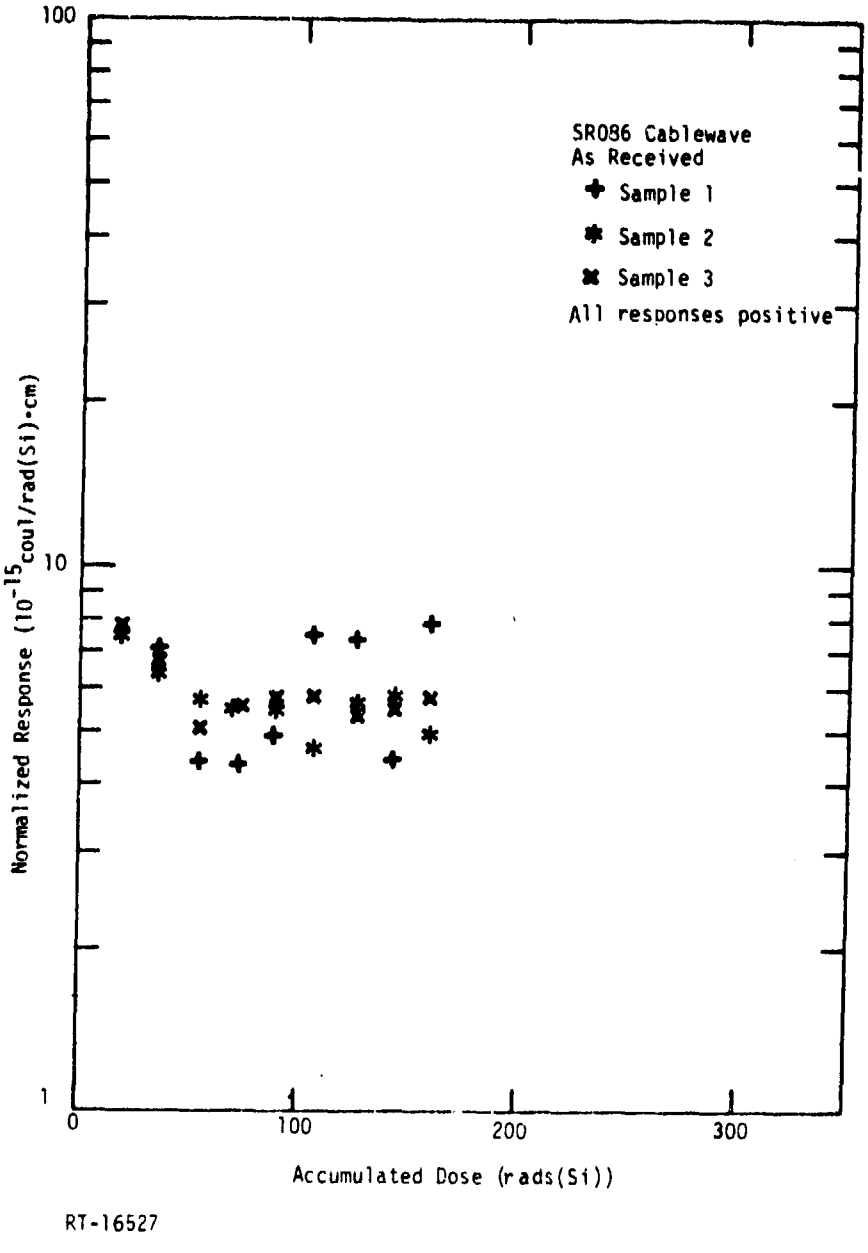

Figure E-6. Shot-to-shot responses of Cablewave SR086 cables as received versus total dose. All responses were positive.

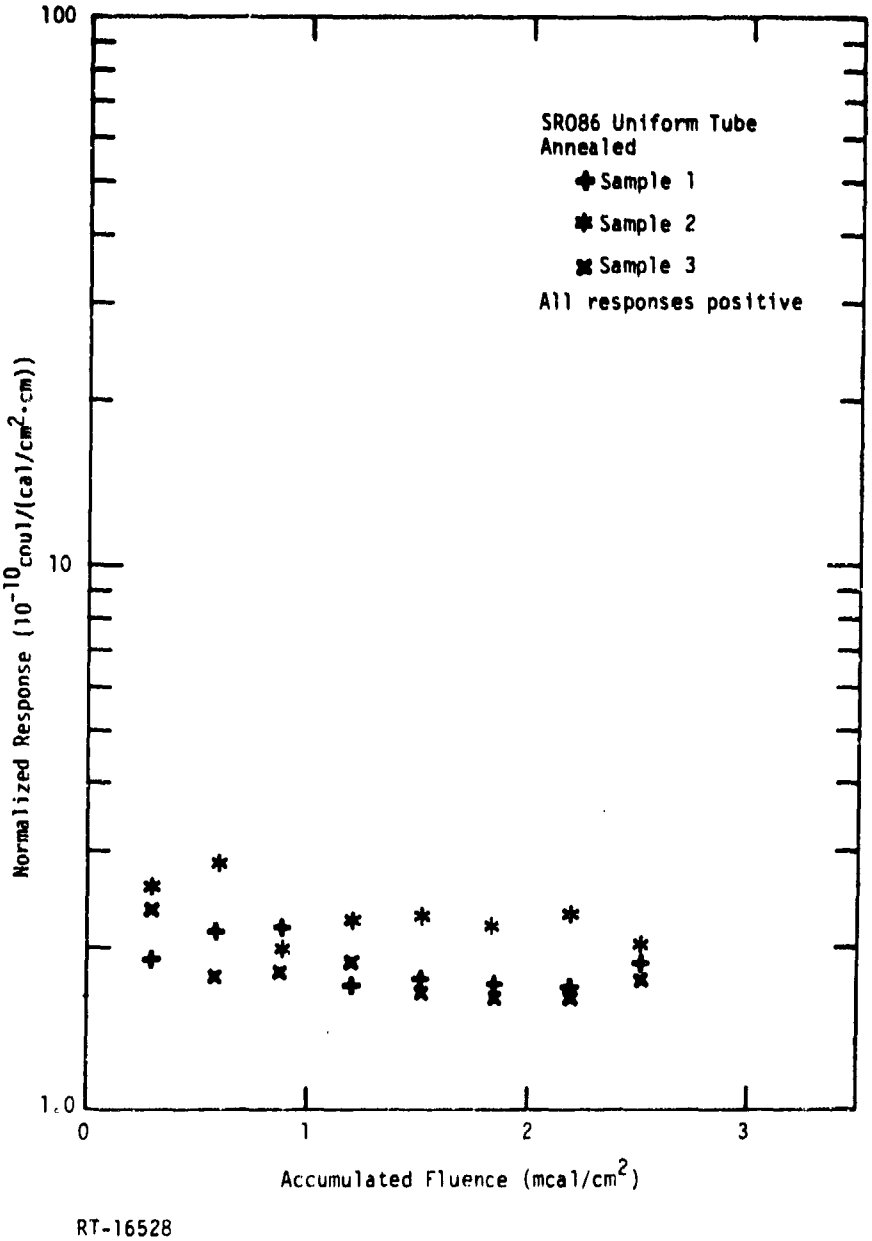

Figure E-7. Shot-to-shot responses of Uniform Tube SR086 cables annealed for 12 hours at 150°C versus total fluence

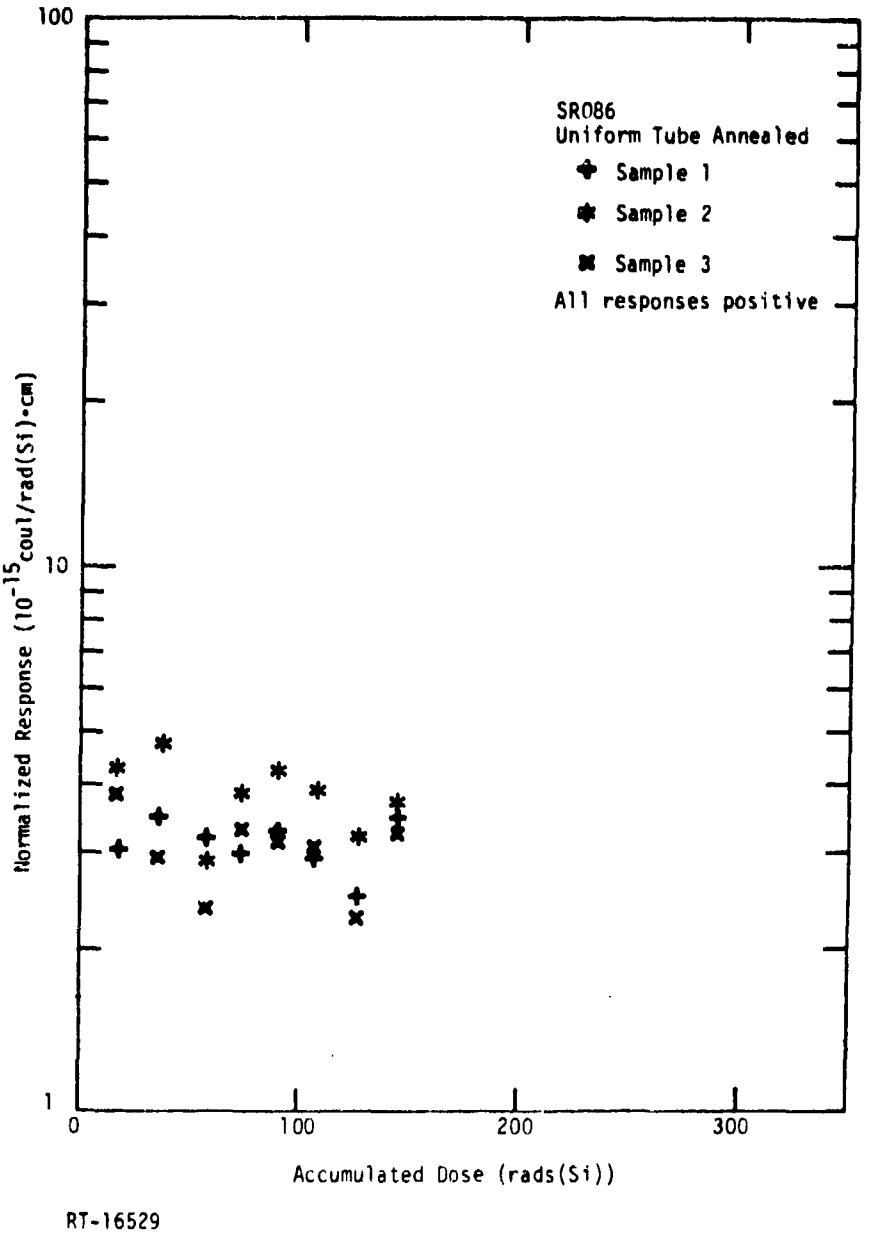

Figure E-8. Shot-to-shot responses of Uniform Tube SR086 cables annealed for 12 hours at 150°C versus total dose

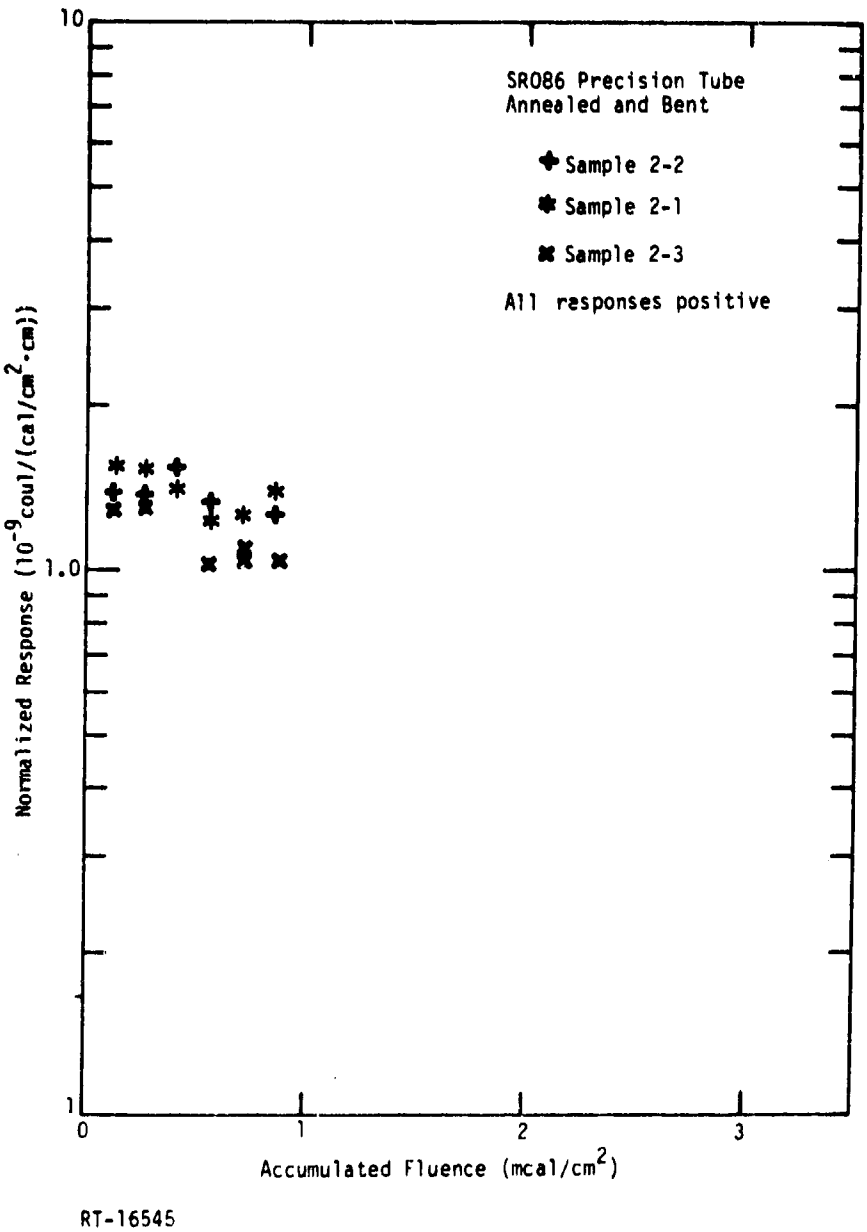

Figure E-9. Shot-to-shot responses of Precision Tube SR086 cables annealed for 12 hours at 150°C and bent into approximately 11 one-inch diameter u-shaped bends versus total fluence. All responses were positive.

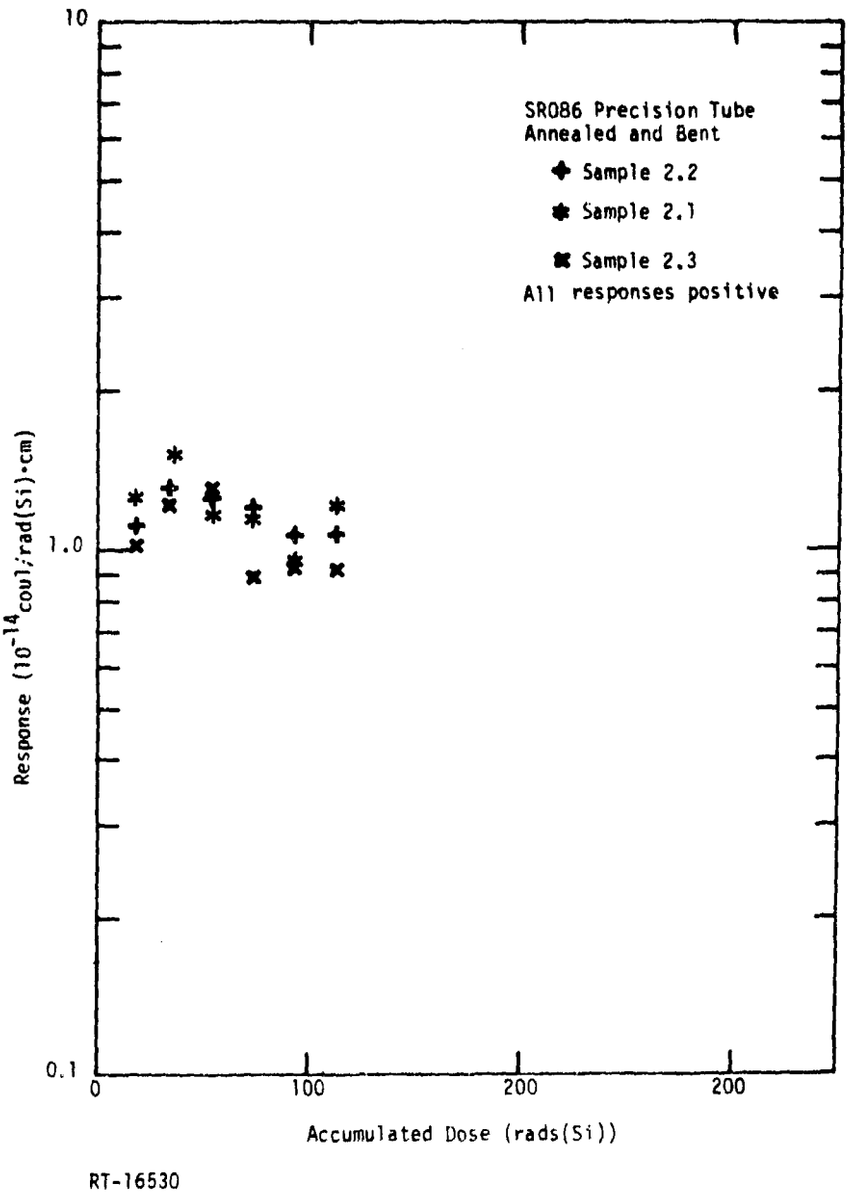

Figure E-10. Shot-to-shot responses of Precision Tube SR086 cables annealed for 12 hours at 150°C and bent into approximately 11 one-inch diameter u-shaped bends versus total dose. All responses were positive.

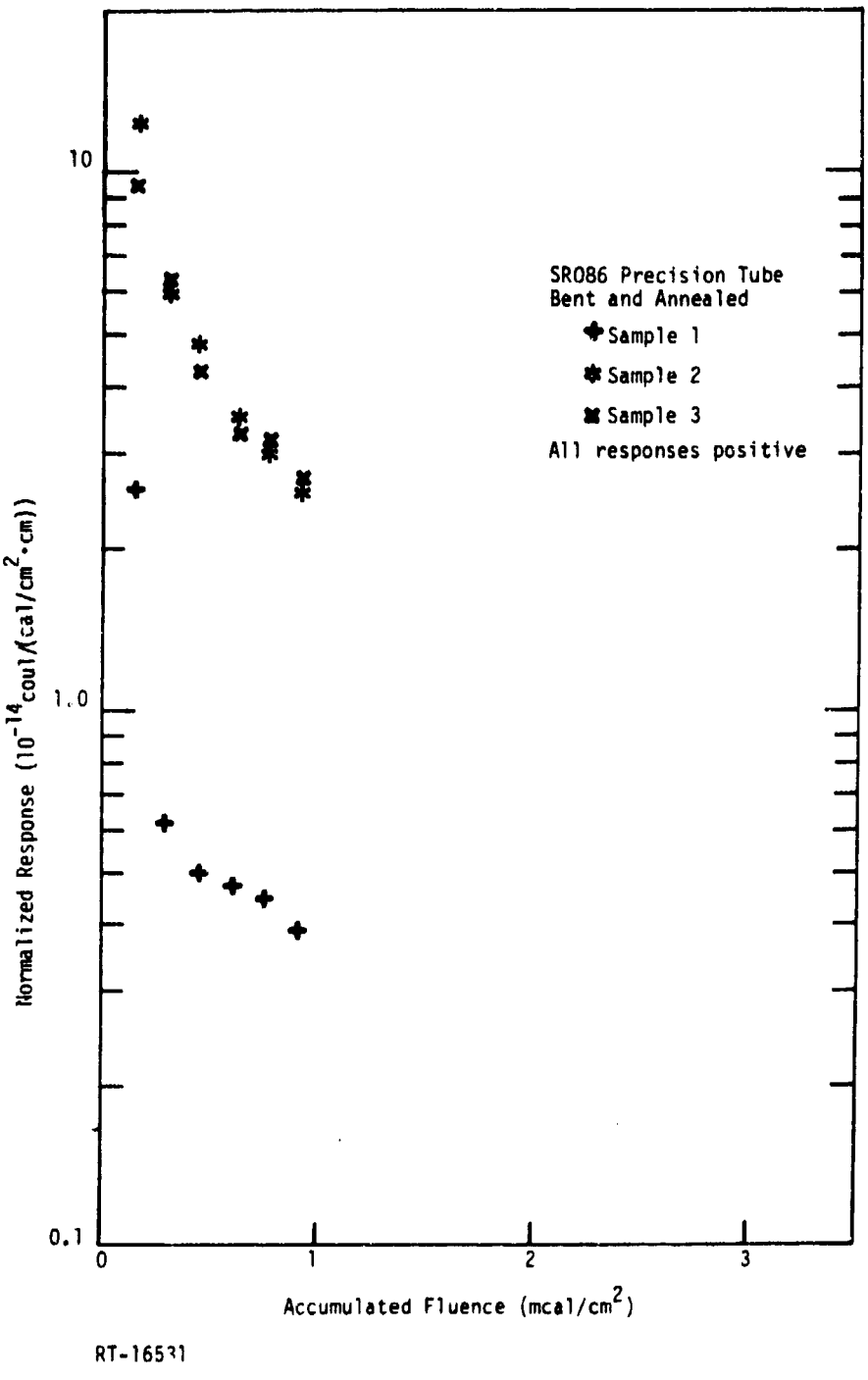

Figure E-11. Shot-to-shot responses of Precision Tube SR086 cables bent into approximately 11 one-inch diameter u-shaped bends and then annealed at 150°C for 12 hours versus total fluence. All responses were positive.

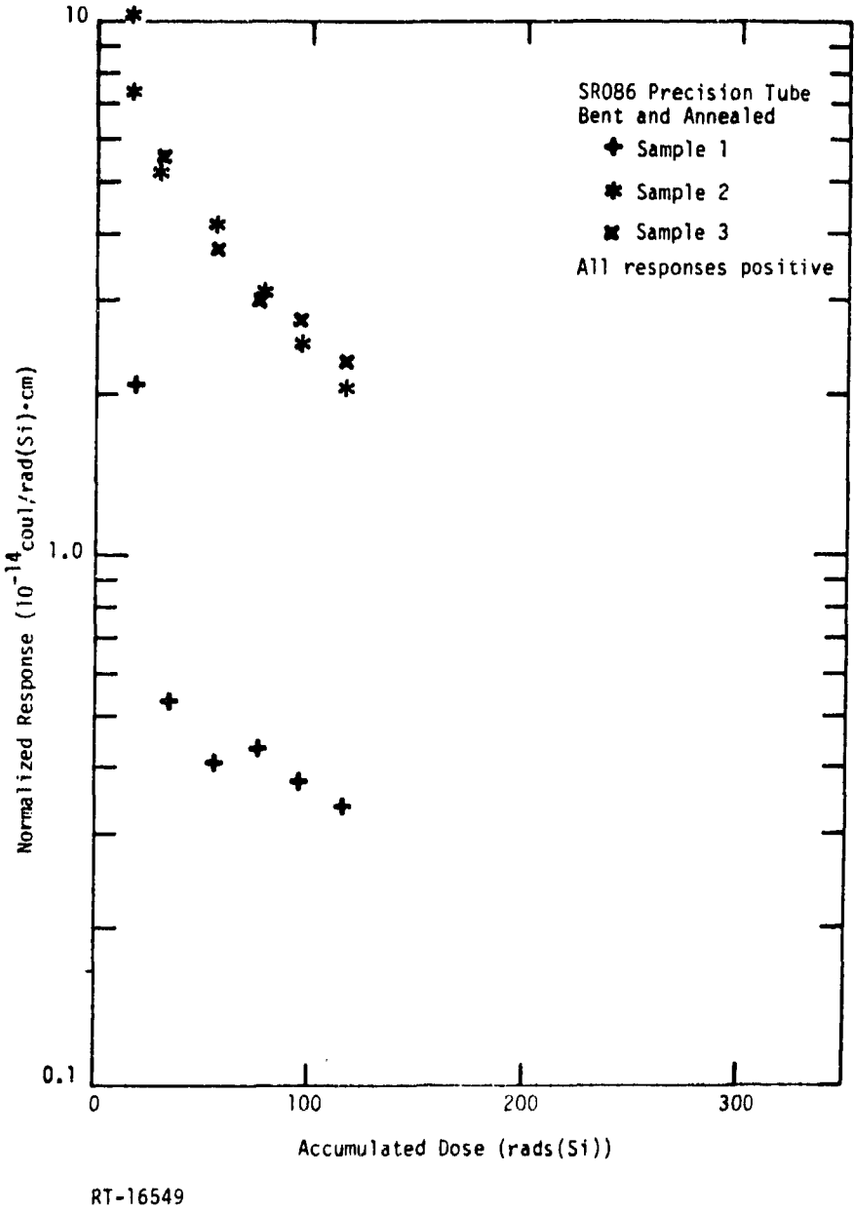

Figure E-12. Shot-to-shot responses of Precision Tube SR086 cables bent into approximately 11 u-shaped bends and annealed at 150°C versus total dose. All responses were positive.

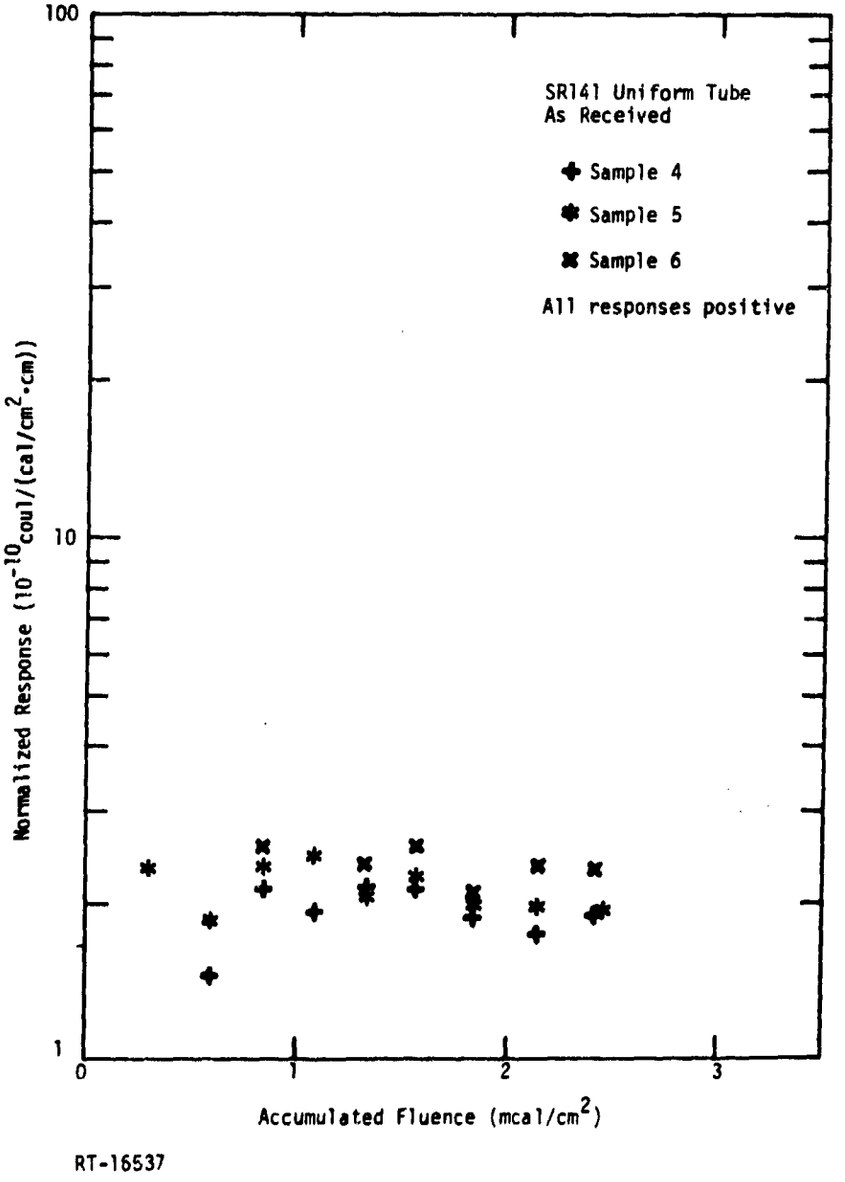

Figure E-13. Shot-to-shot responses of Uniform Tube SR141 cables as received versus total fluence. All responses were positive.

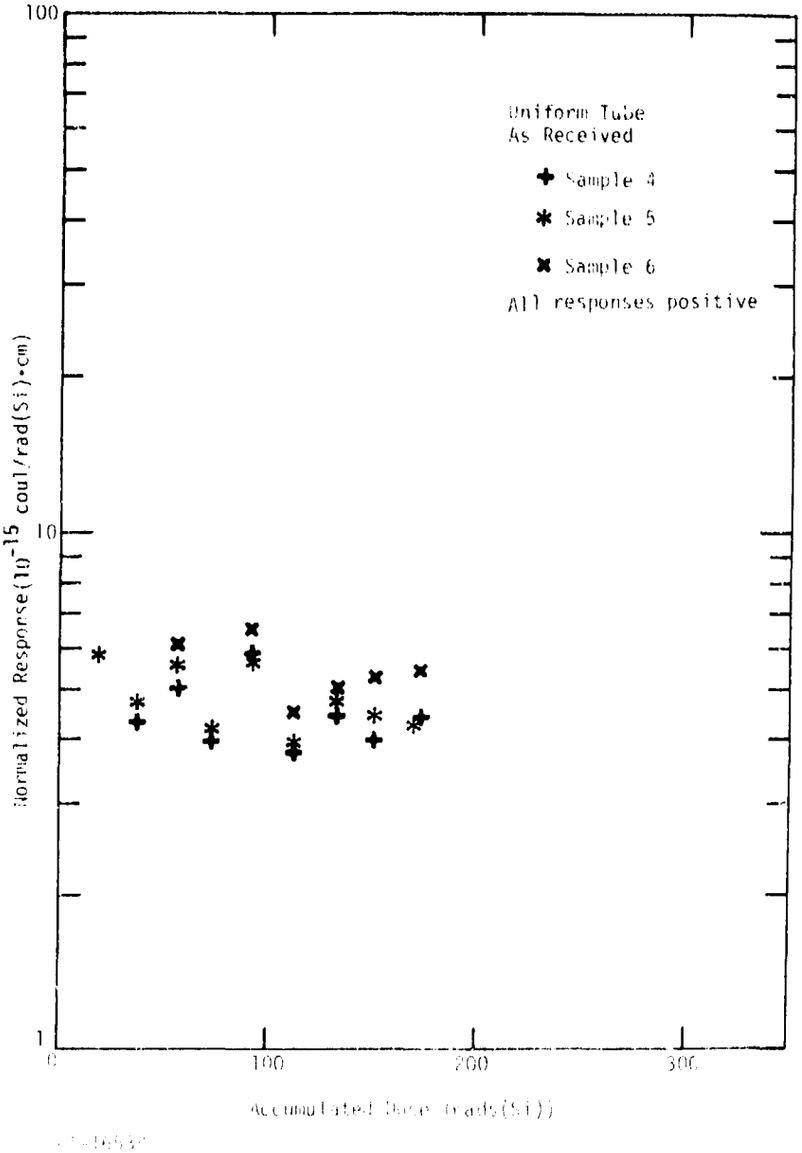

Figure E-14. Shot-to-shot responses of Uniform Tube SR141 cables as received versus total dose. All responses were positive.

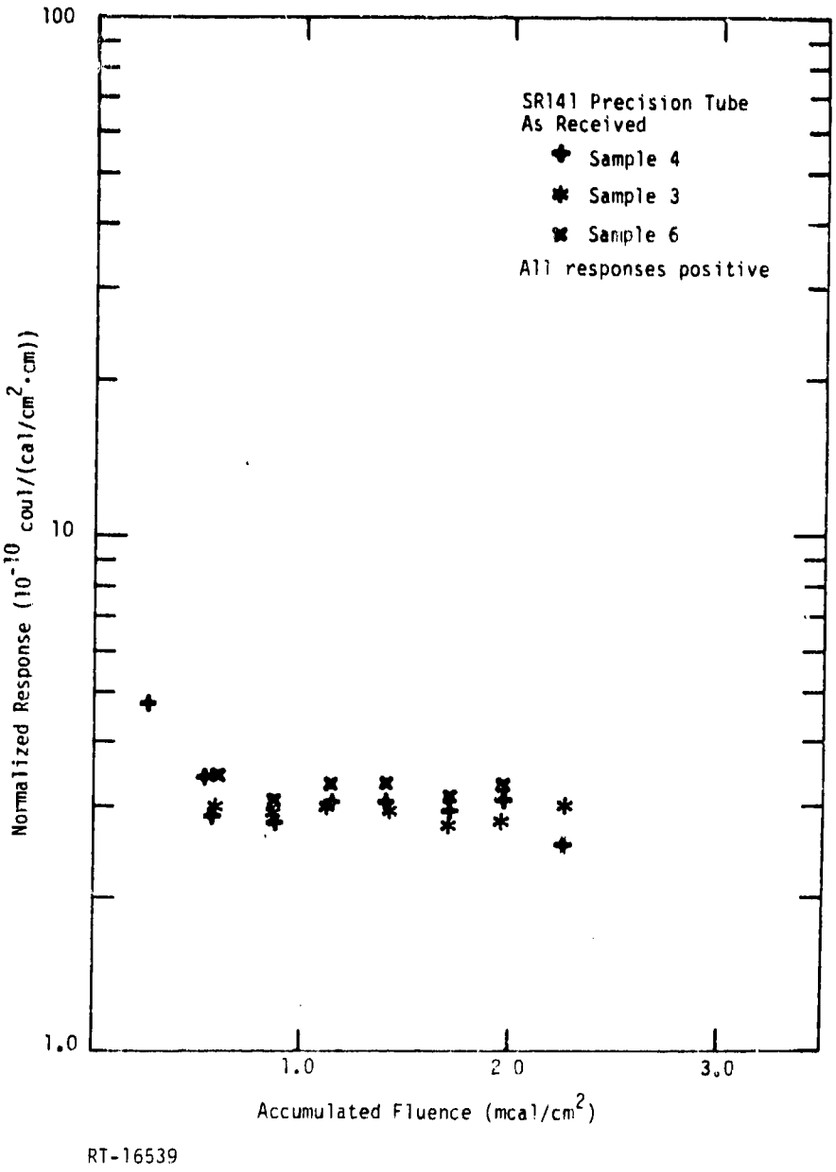

Figure E-15. Shot-to-shot responses of Precision Tube SR141 cables as received versus total fluence. All responses were positive.

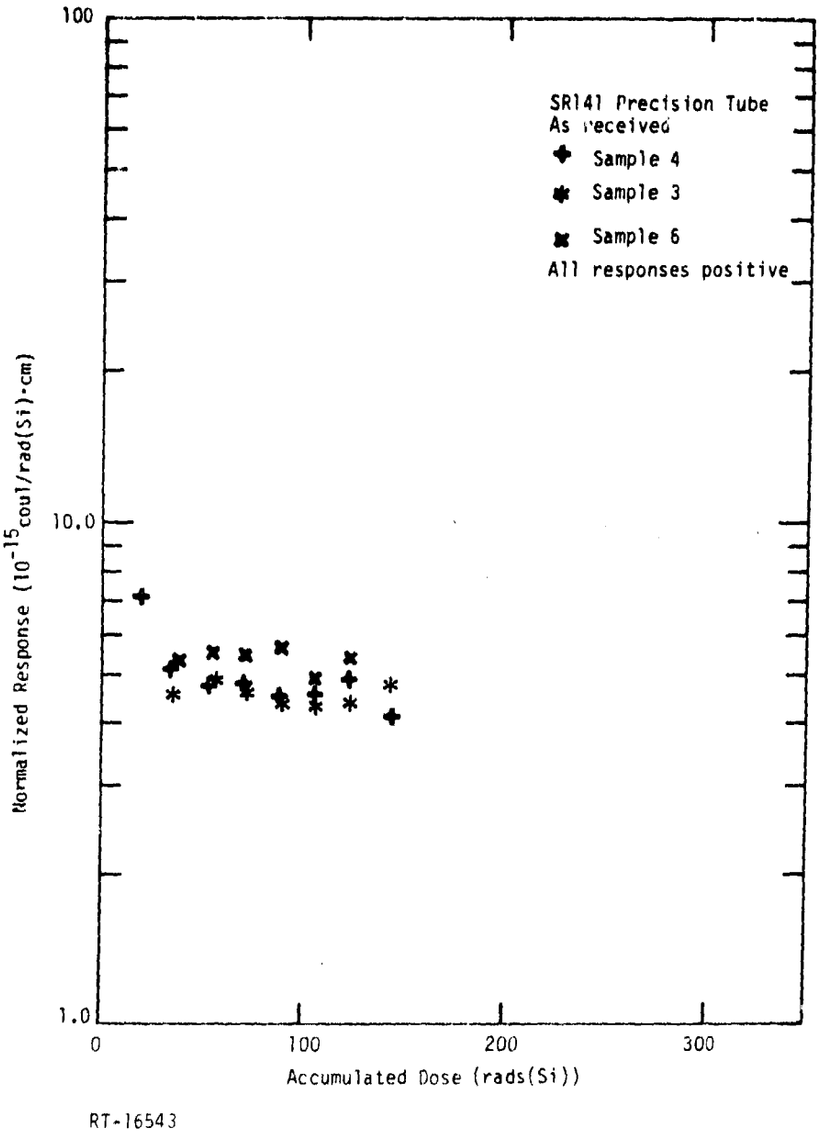

Figure E-16. Shot-to-shot responses of Precision Tube SR141 cables as received versus total dose. All responses were positive.

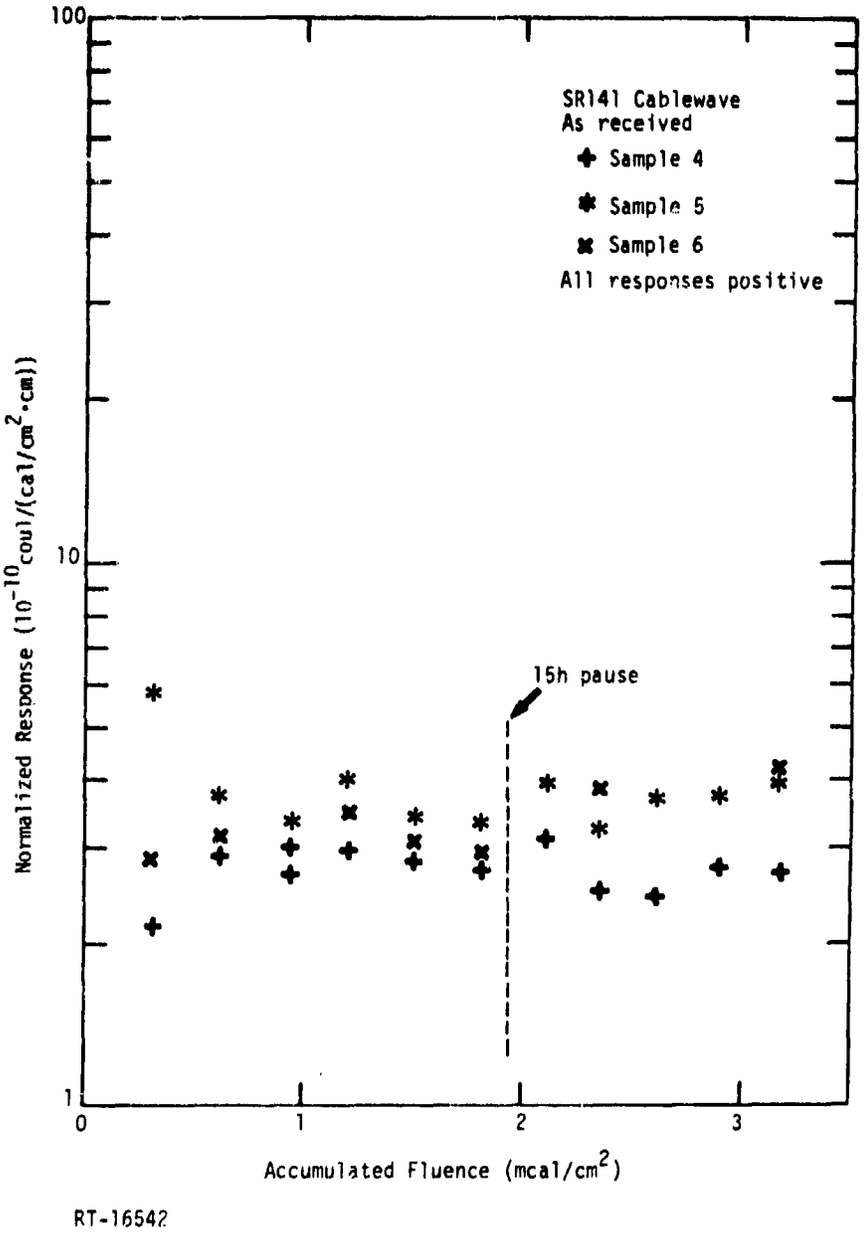

Figure E-17. Shot-to-shot responses of Cablewave SR141 cables as received versus total fluence. All responses were positive. Irradiation was stopped after shot 6 and resumed 15 hours later.

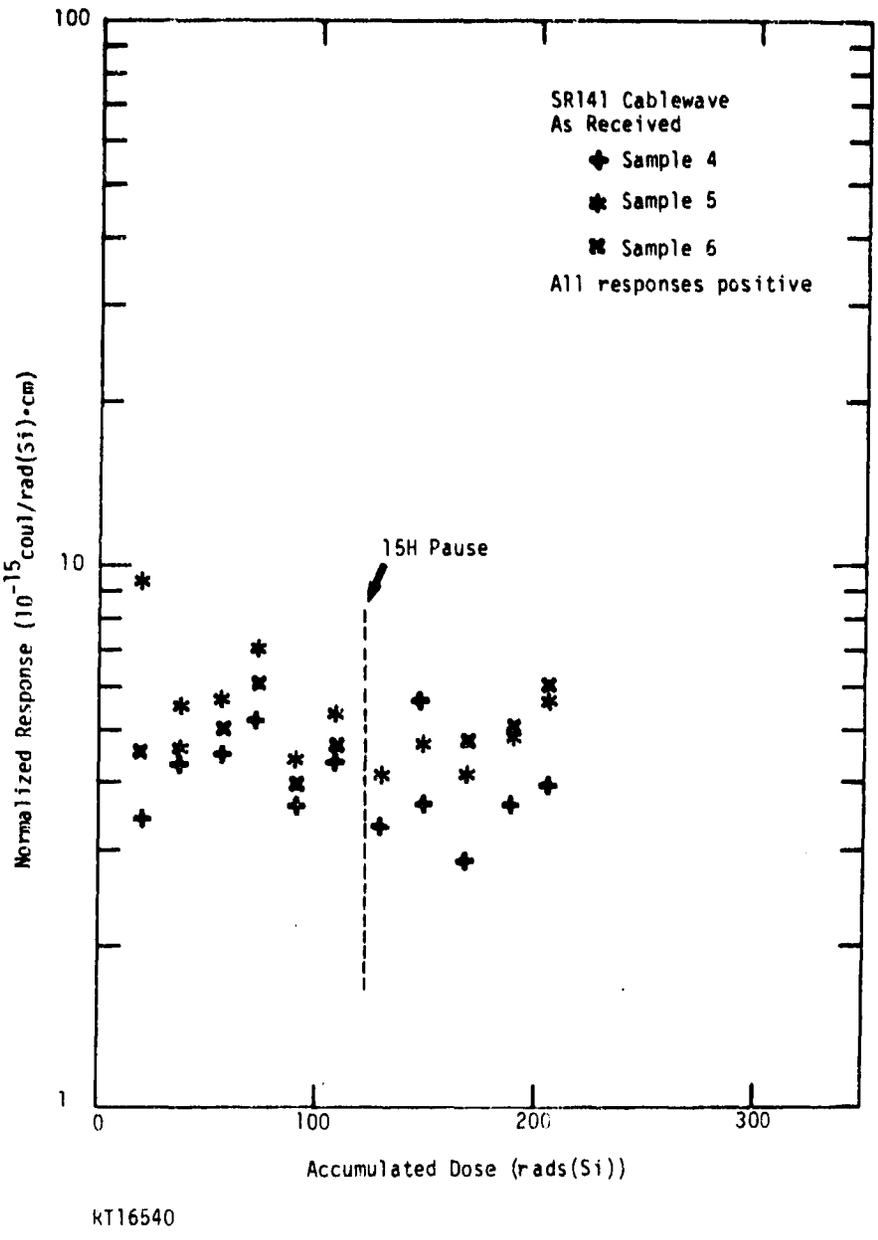

Figure E-18. Shot-to-shot responses of Cablewave SR141 cables as received versus total dose. All responses were positive. The irradiation was stopped after shot 6 and resumed 15 hours later.

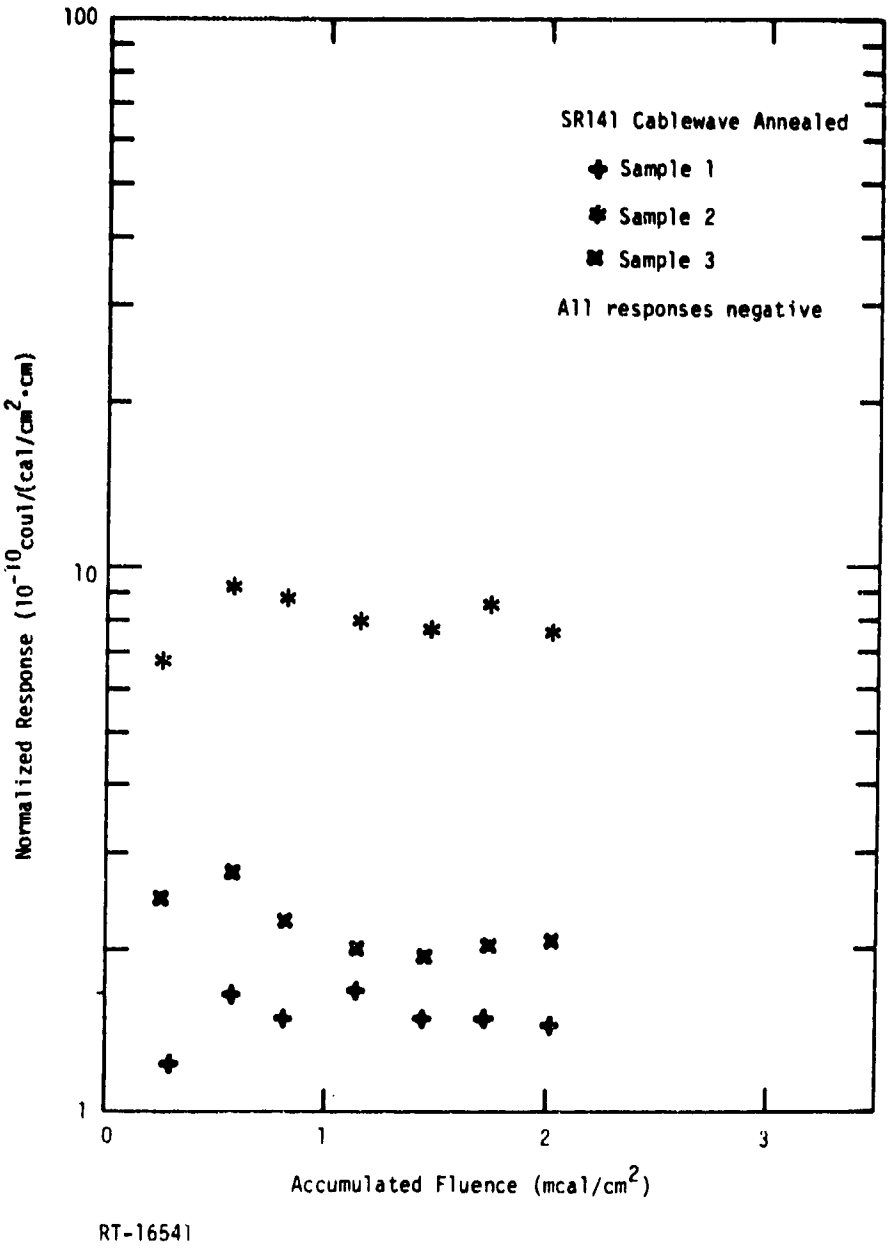

Figure E-19. Shot-to-shot responses of Cablewave SR141 cables after annealing at 150°C for about 12 hours versus total fluence.

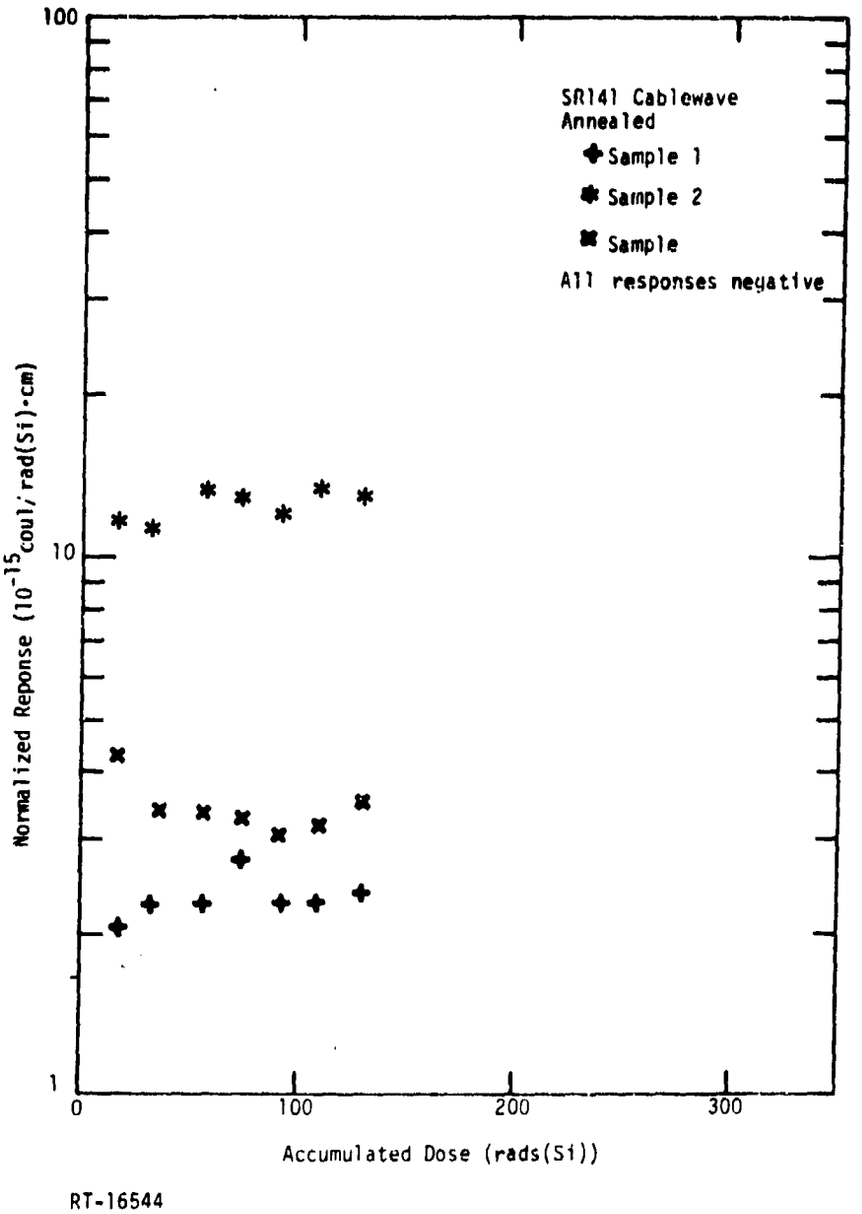

Figure E-20. Shot-to-shot responses of Cablewave SR141 cables after annealing at 150°C for about 12 hours versus total dose.

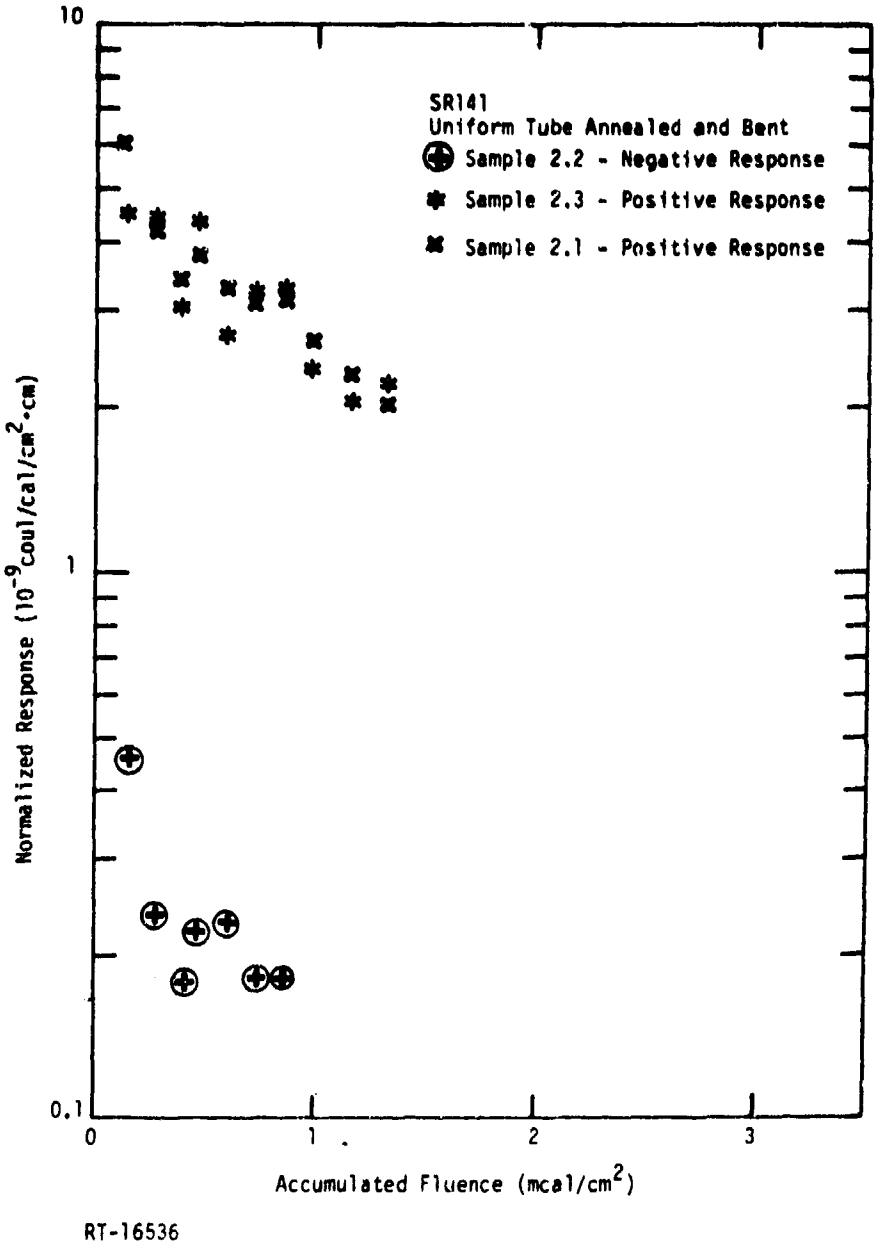

Figure E-21. Shot-to-shot responses of Uniform Tube SR141 cables annealed at 150°C for about 12 hours and then bent into approximately 11 one-inch diameter u-shaped bends versus total fluence. Responses were positive except for the circled points.

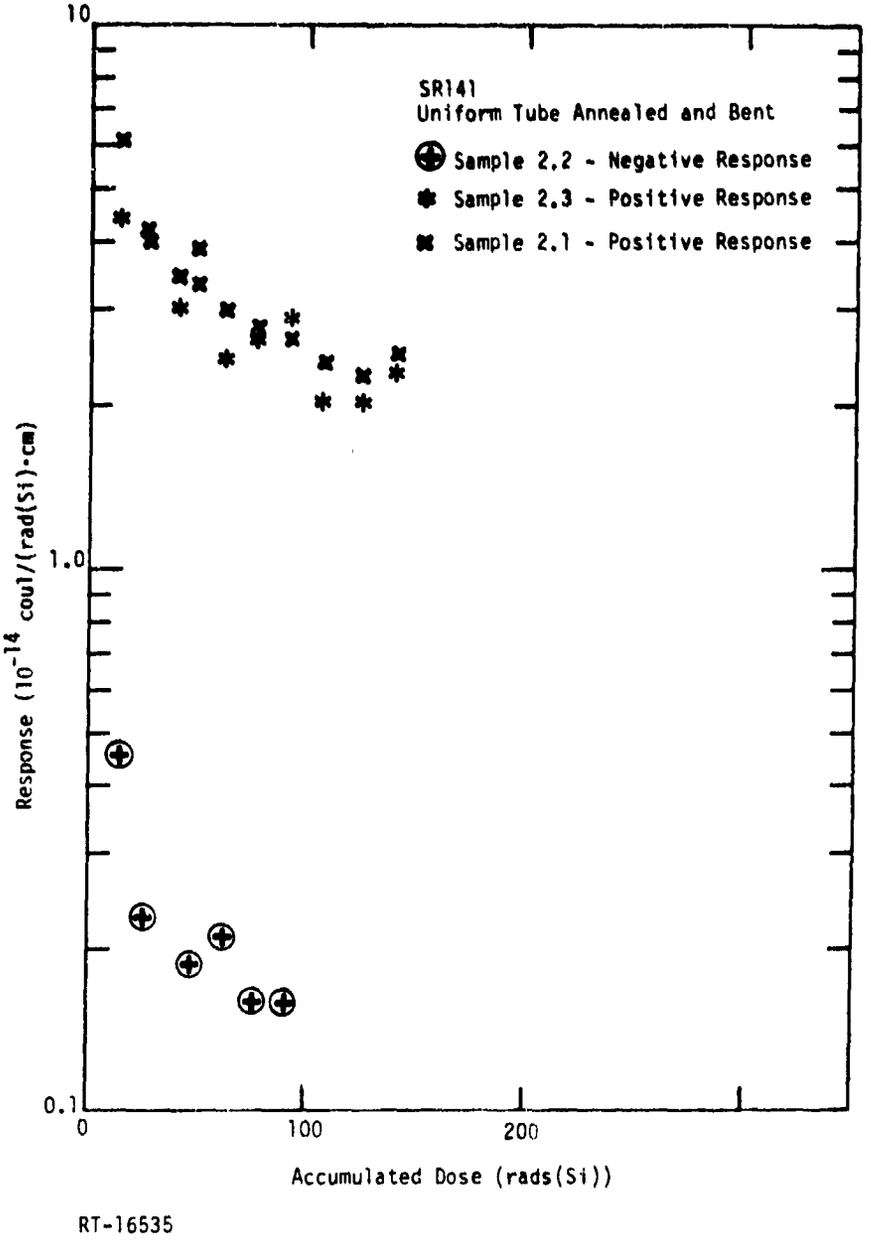

Figure E-22. Shot-to-shot responses of Uniform Tube cables annealed at 150°C for about 12 hours and then bent into approximately 11 one-inch diameter u-shaped bends versus total dose. Responses were positive except for those circled.

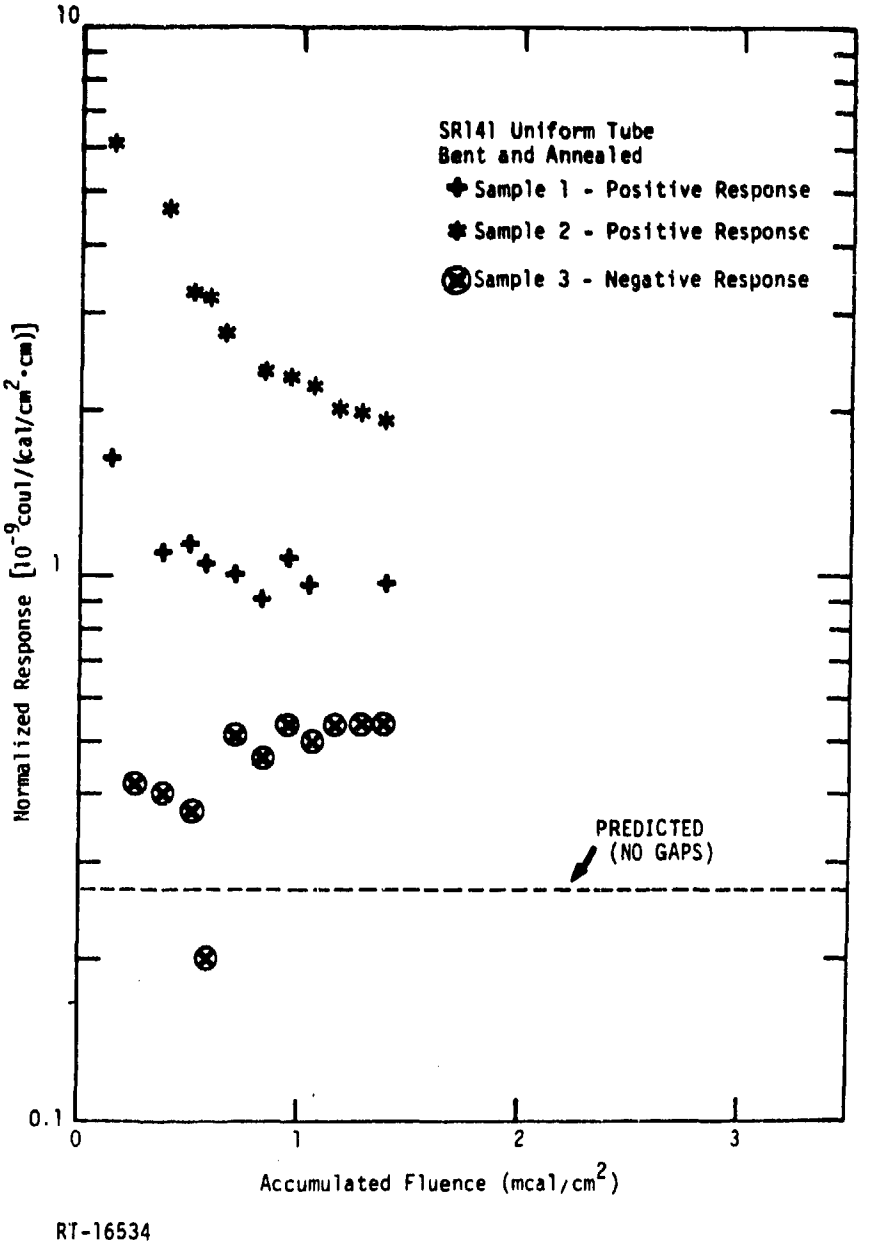

Figure E-23. Shot-to-shot responses of Uniform Tube SR141 cables bent into approximately 11 one-inch diameter u-shapes and then annealed 150°C for about 12 hours versus total fluence. The responses of samples 1 and 2 were positive, and that of 3 negative.

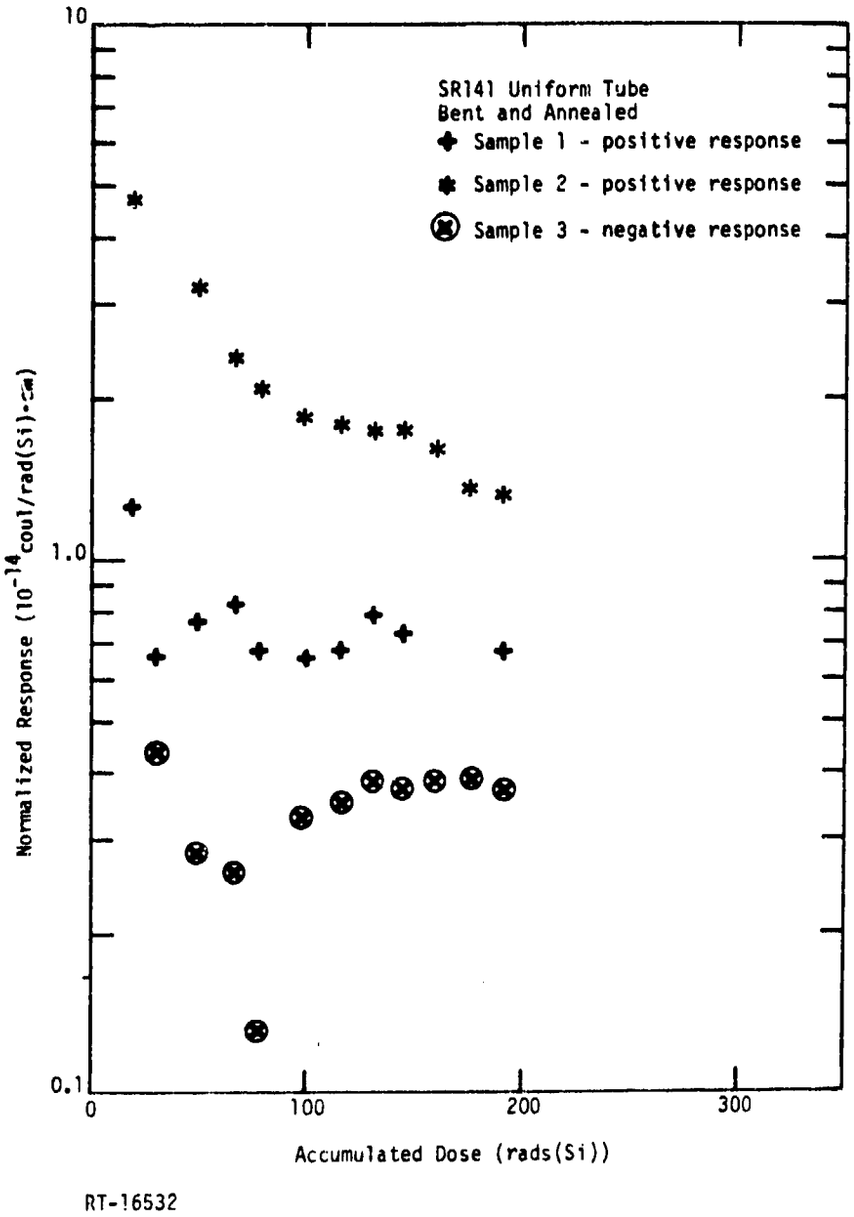

Figure E-24. Shot-to-shot responses of Uniform Tube cables bent into approximately 11 one-inch diameter u-shapes and annealed at 150°C versus total dose. The responses of sample 1 and 2 were positive, that of 3 negative.

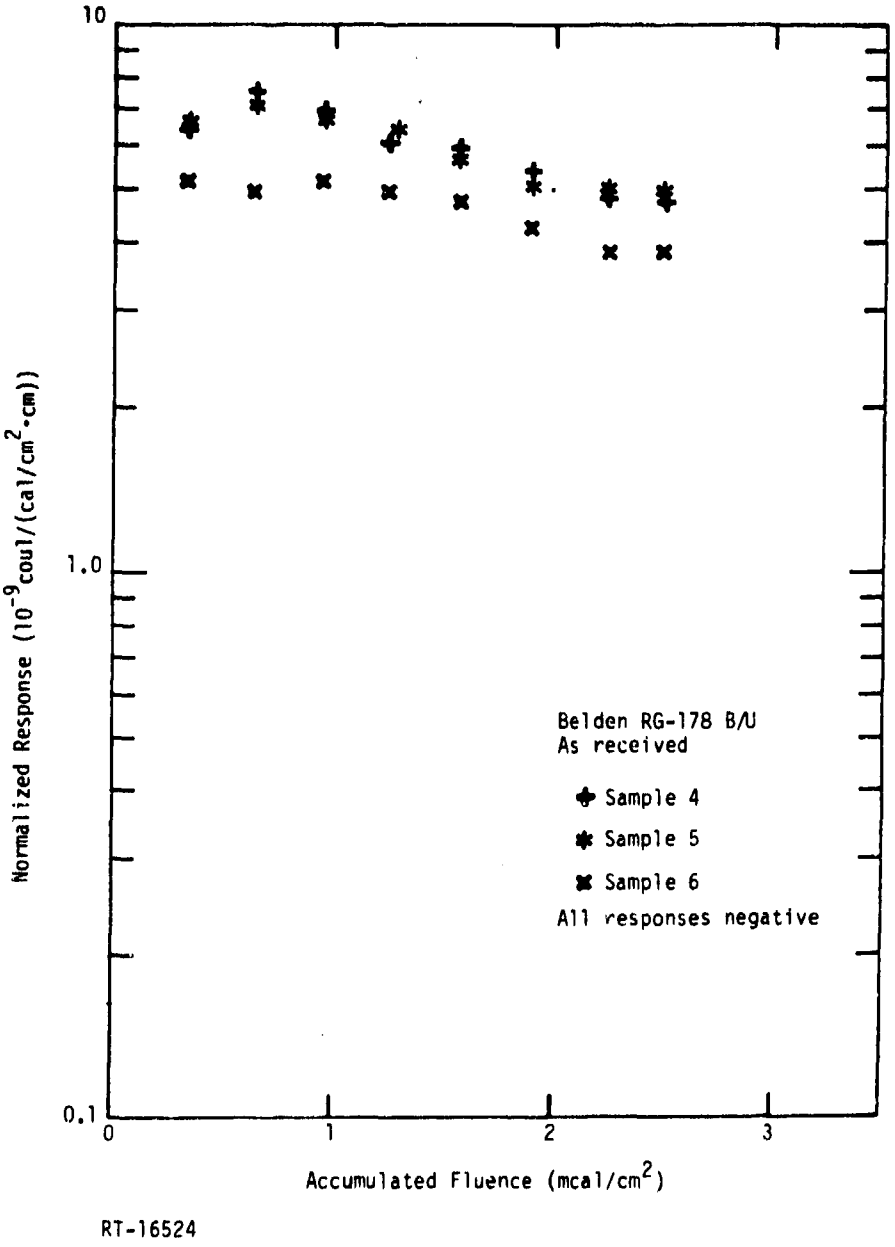

Figure E-25. Shot-to-shot responses of Beldon RG-178B/U cables as received versus total fluence. All responses were negative.

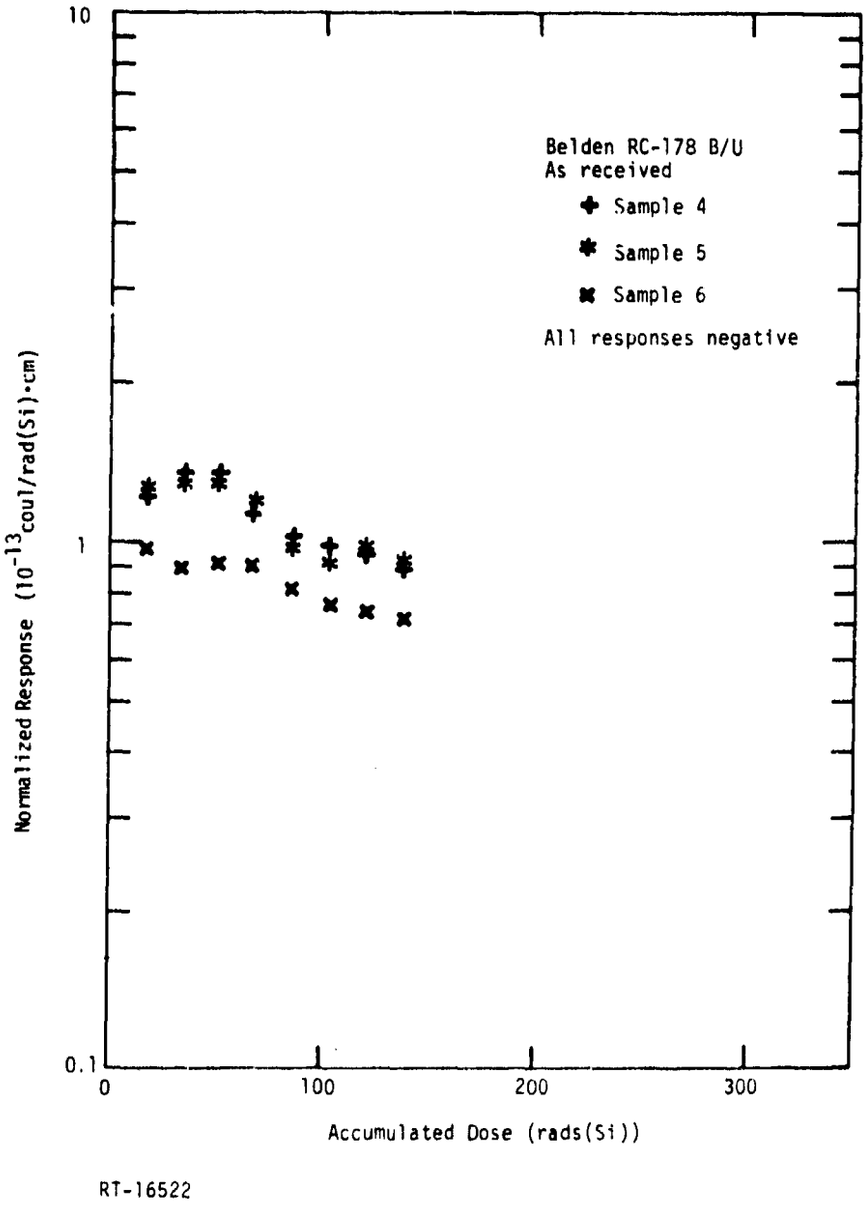

Figure E-26. Shot-to-shot responses of Beldon RG-178B/U cables as received versus total dose. All responses were negative.

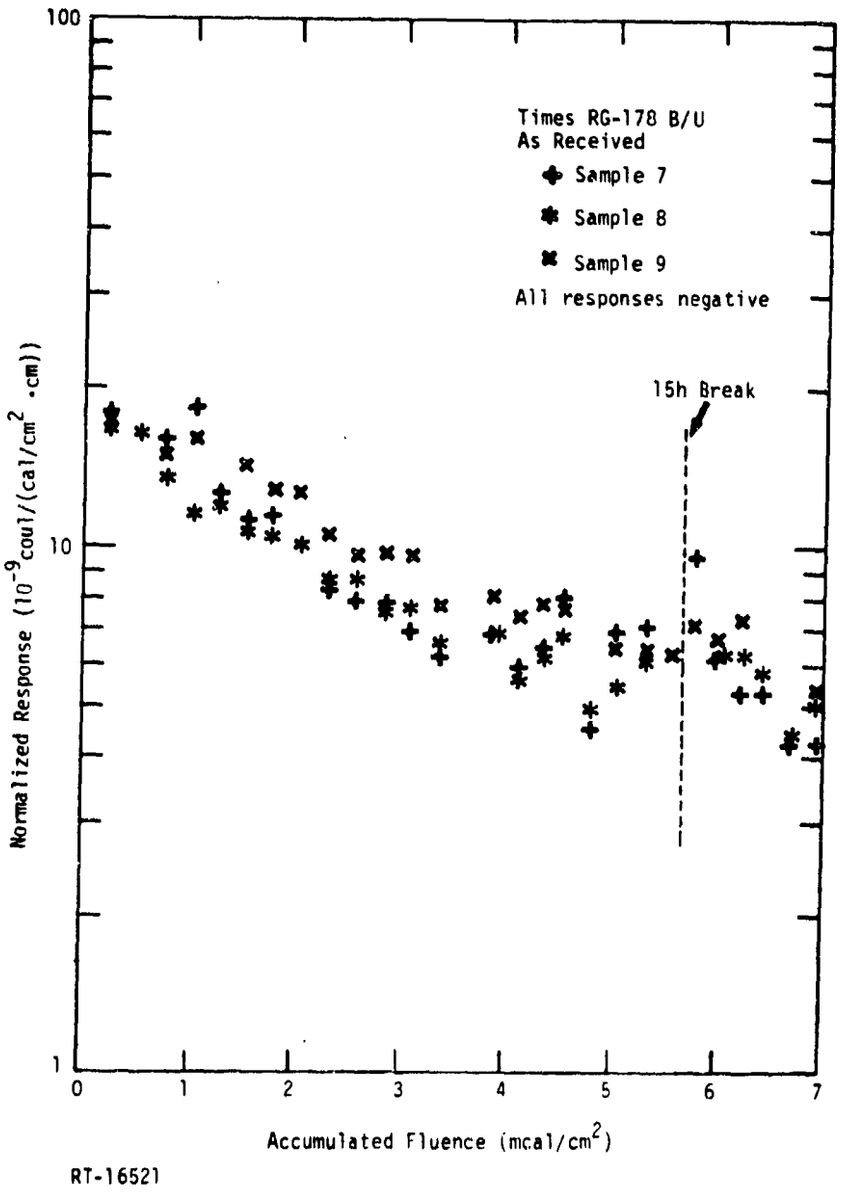

Figure E-27. Shot-to-shot responses of Times RG-178B/U cables as received versus total fluence. The irradiations were interrupted after shot 22 and resumed 15 hours later. All responses were negative.

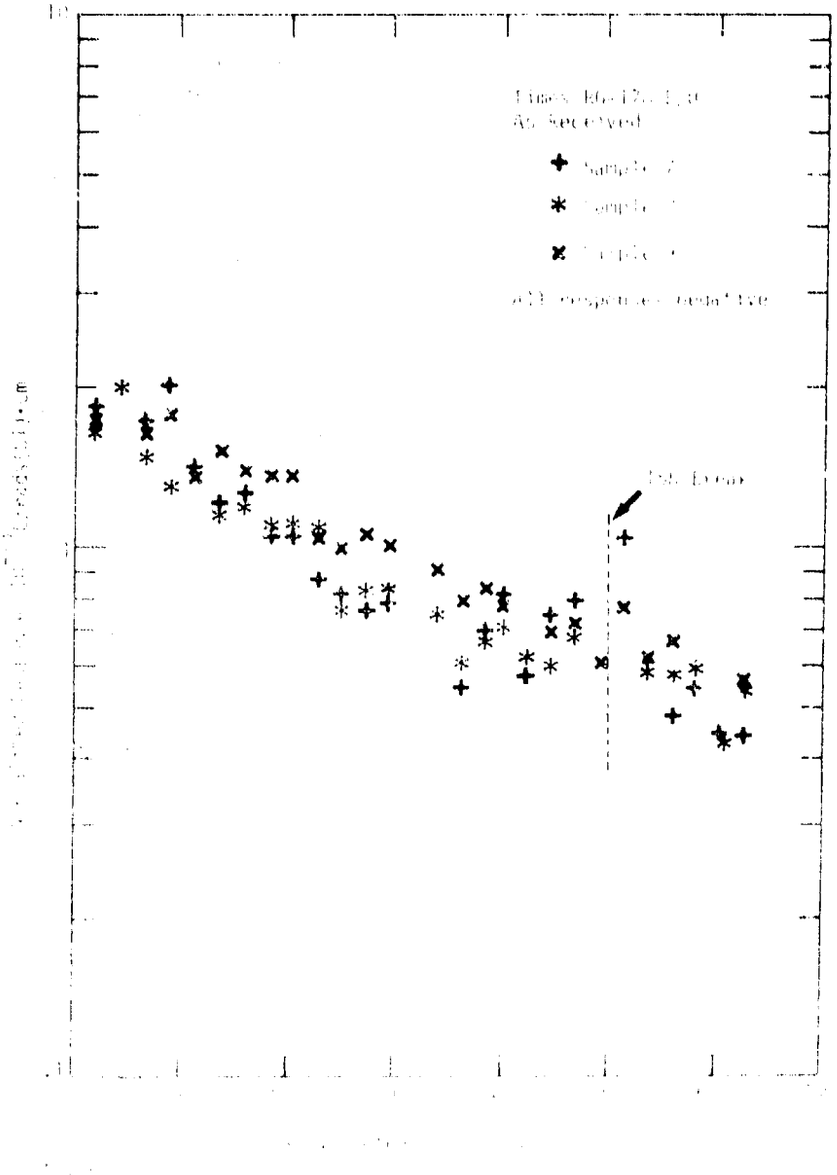

Figure E-28. Shot-to-shot responses of Times RG-178B/U cables as received versus total dose. The irradiations were interrupted after shot 22 and resumed 15 hours later. All responses were negative.

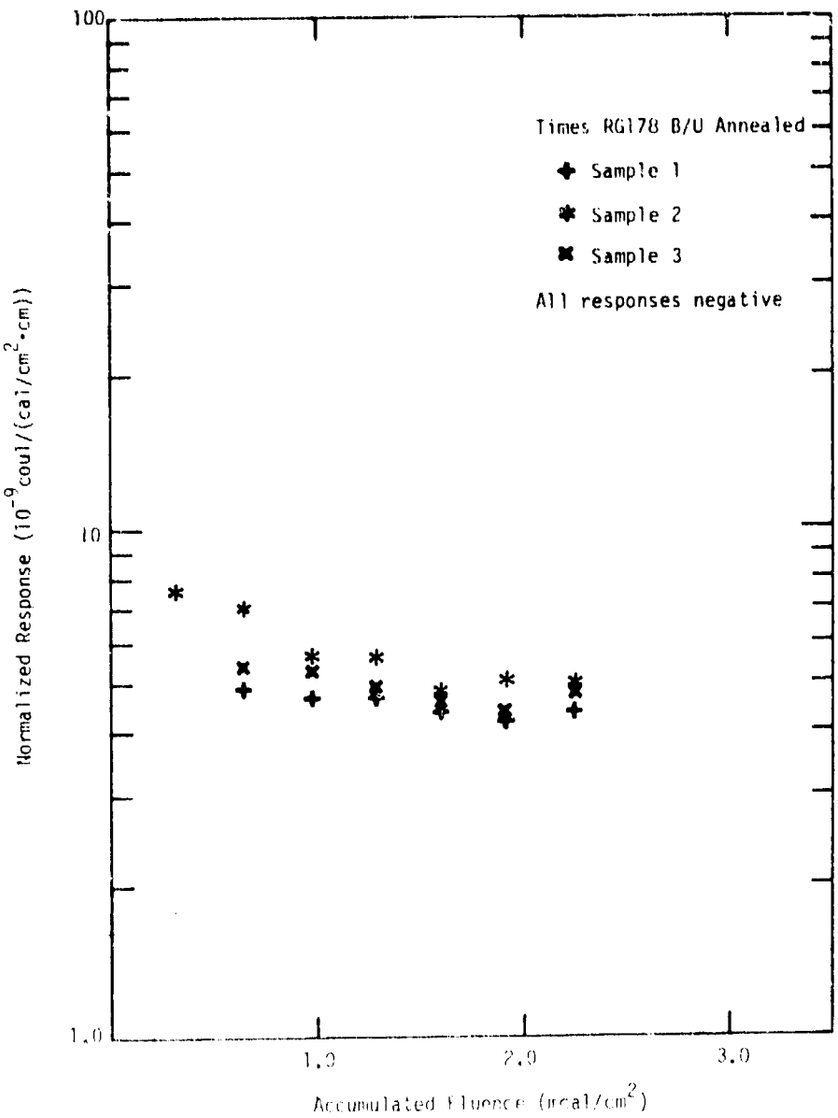

Figure E-29. Shot-to-shot responses of Times RG-178B/U cables annealed at 150°C for 12 hours versus total fluence. All responses were negative.

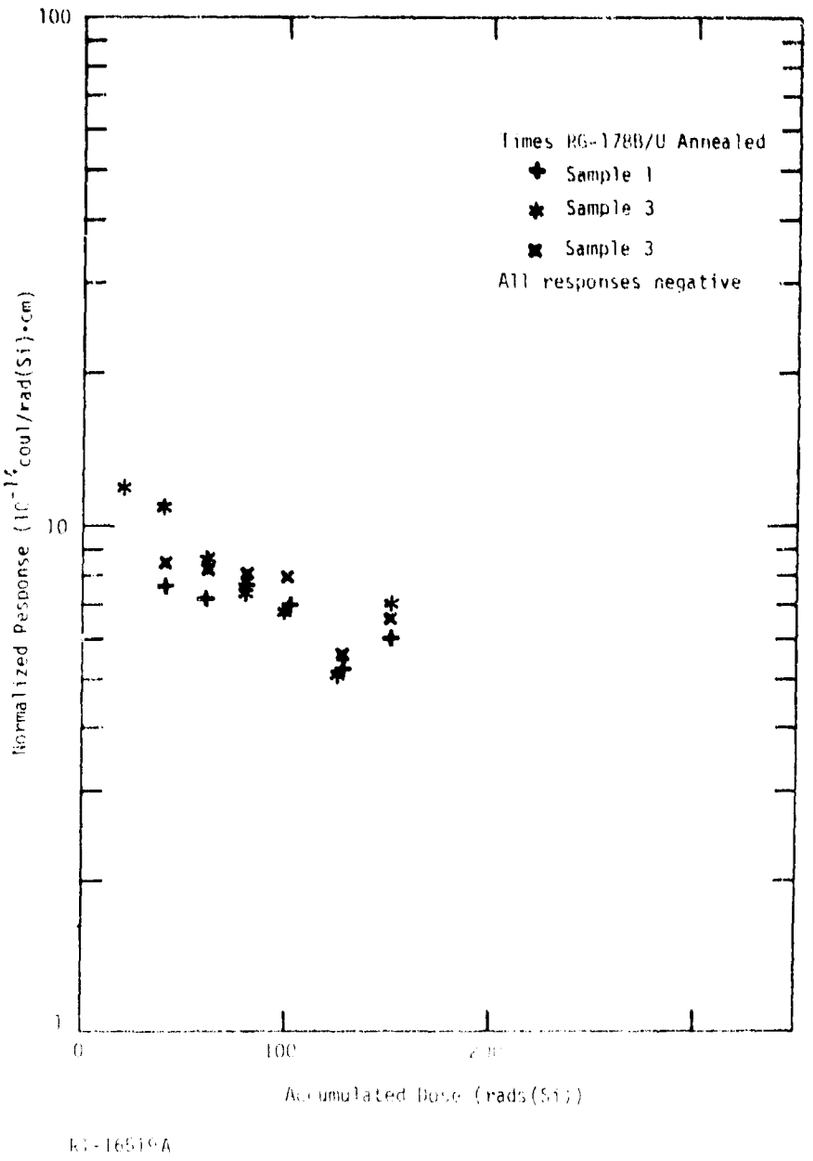

Figure E-30. Shot-to-shot responses of Times RG-178B/U cables annealed at 150°C for 12 hours versus total dose. All responses were negative.

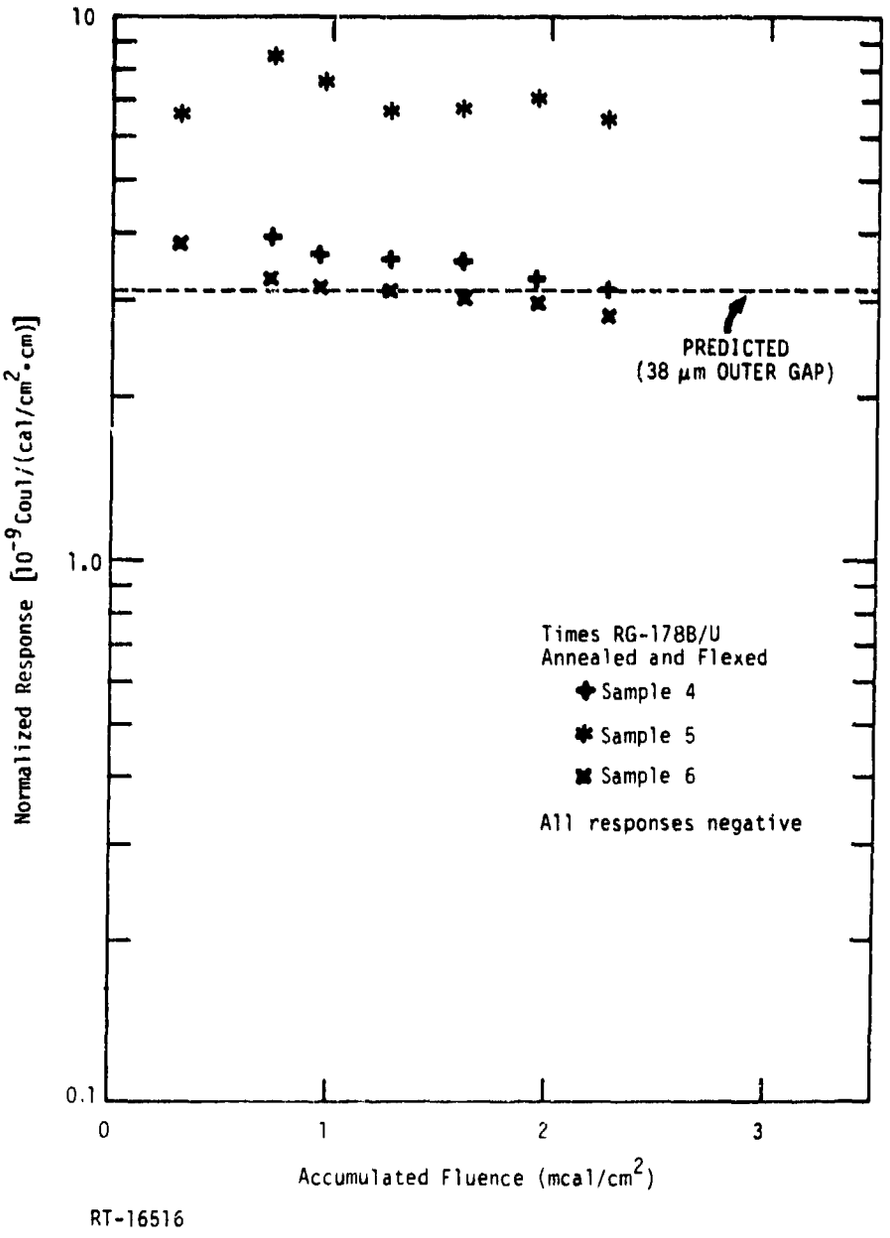

Figure E-31. Shot-to-shot responses of Times RG-178B/U cables annealed at 150°C for 12 hours and then flexed ten times by bending 180° at different points along the cable versus total fluence. All responses were negative.

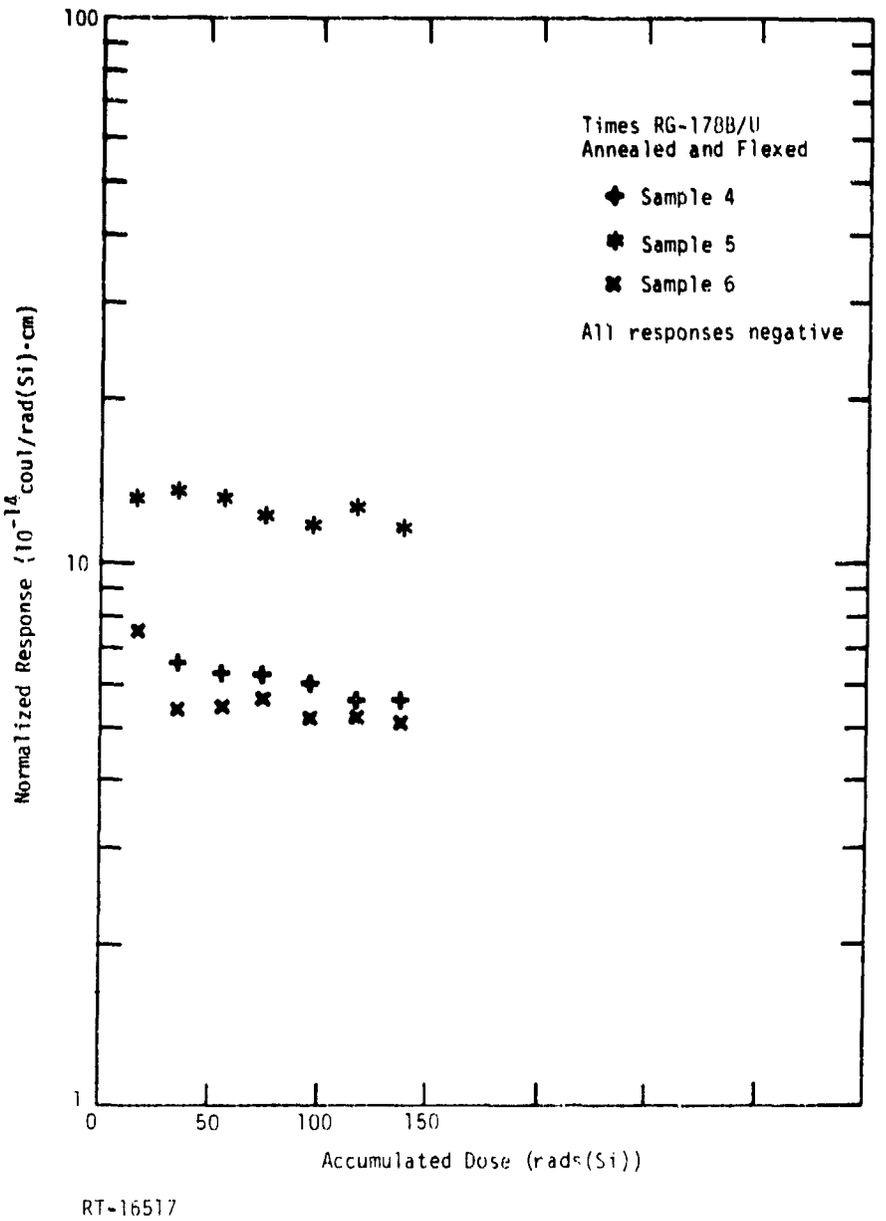

Figure E-32. Shot-to-shot responses of Times RG-178B/U cables annealed at 150°C for 12 hours and then flexed ten times by bending 180° at different points along the cables versus total dose. All responses were negative.

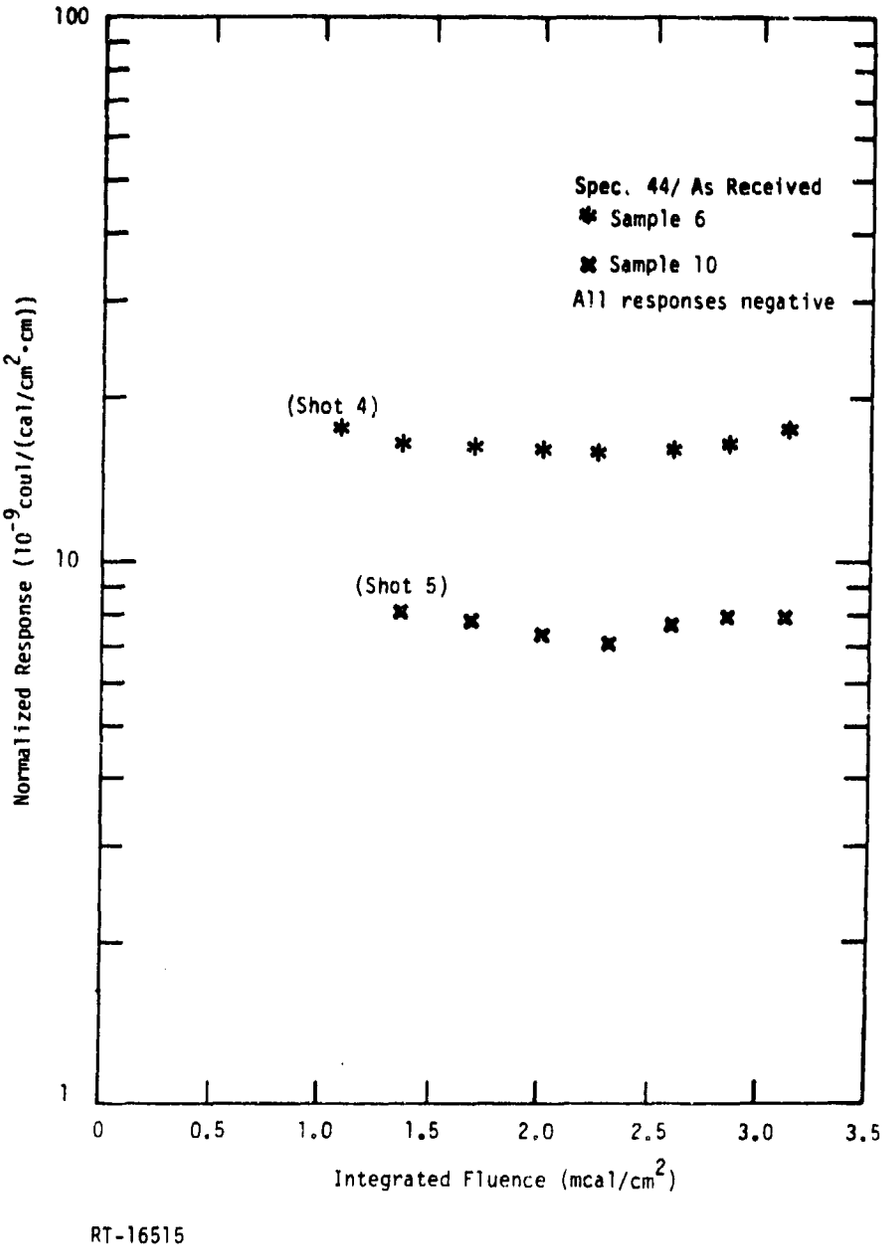

Figure E-33. Shot-to-shot responses of Spec 44/ cables as received versus total fluence. All responses were positive.

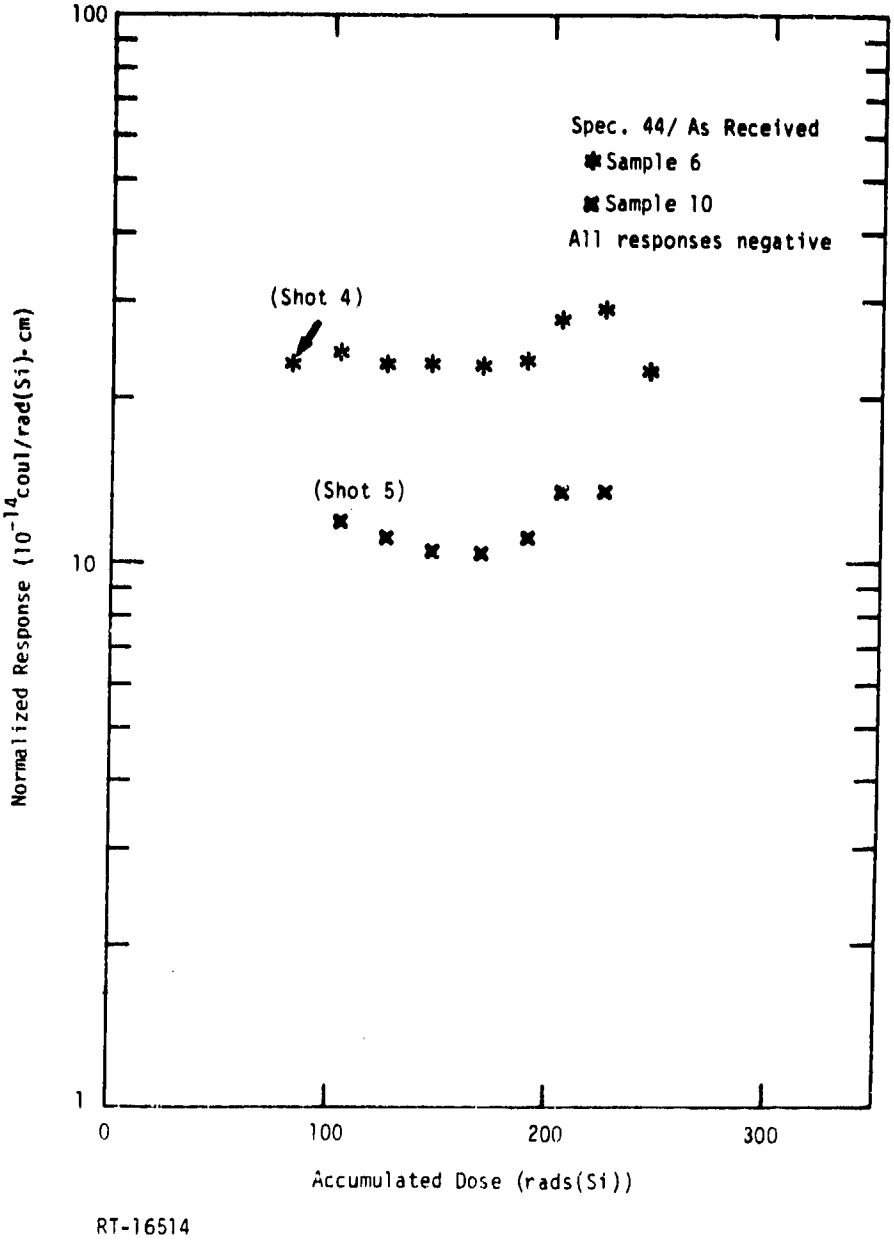

Figure E-34. Shot-to-shot responses of Spec 44/ cables as received versus total dose. All responses were negative.

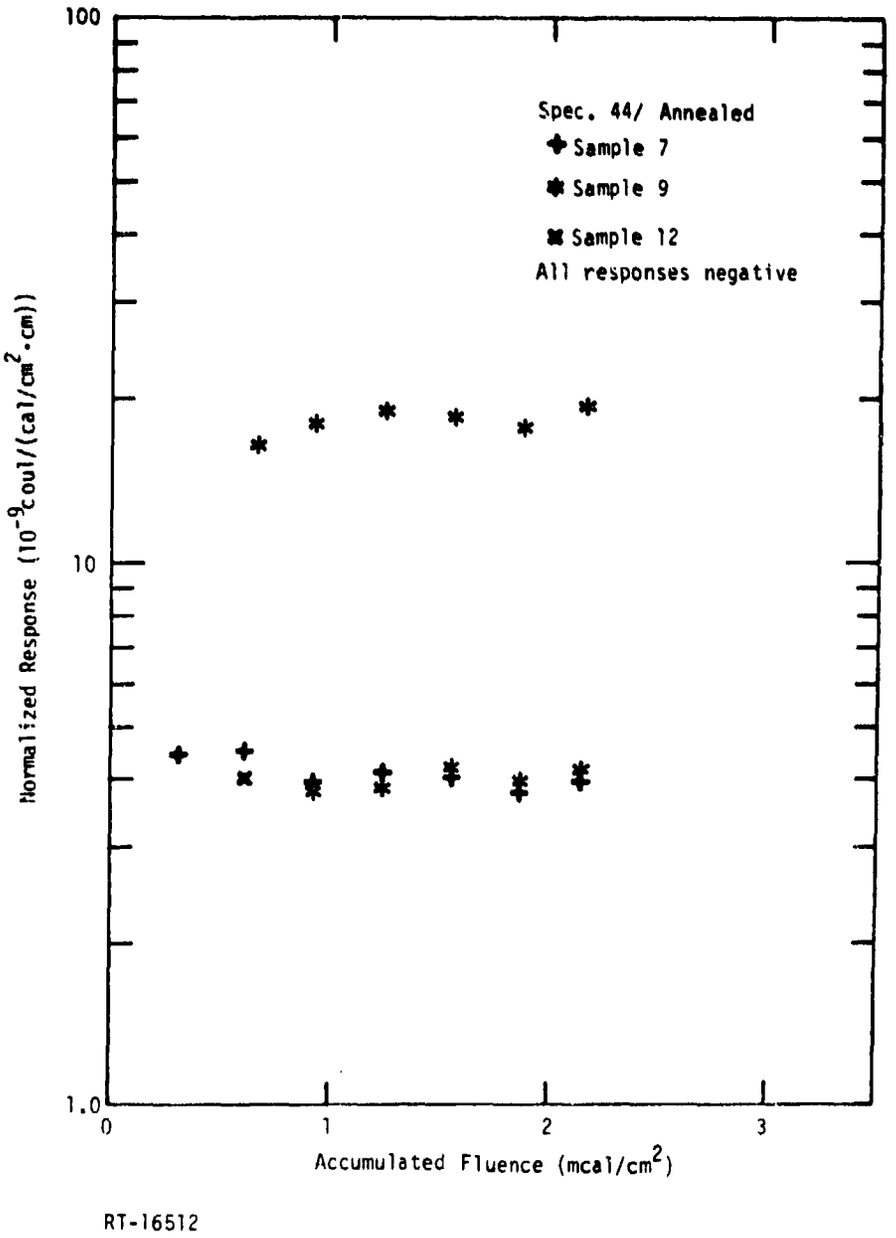

Figure E-35. Shot-to-Shot responses of Spec 44/ cables annealed at 135°C for 12 hours versus total fluence. All responses were negative.

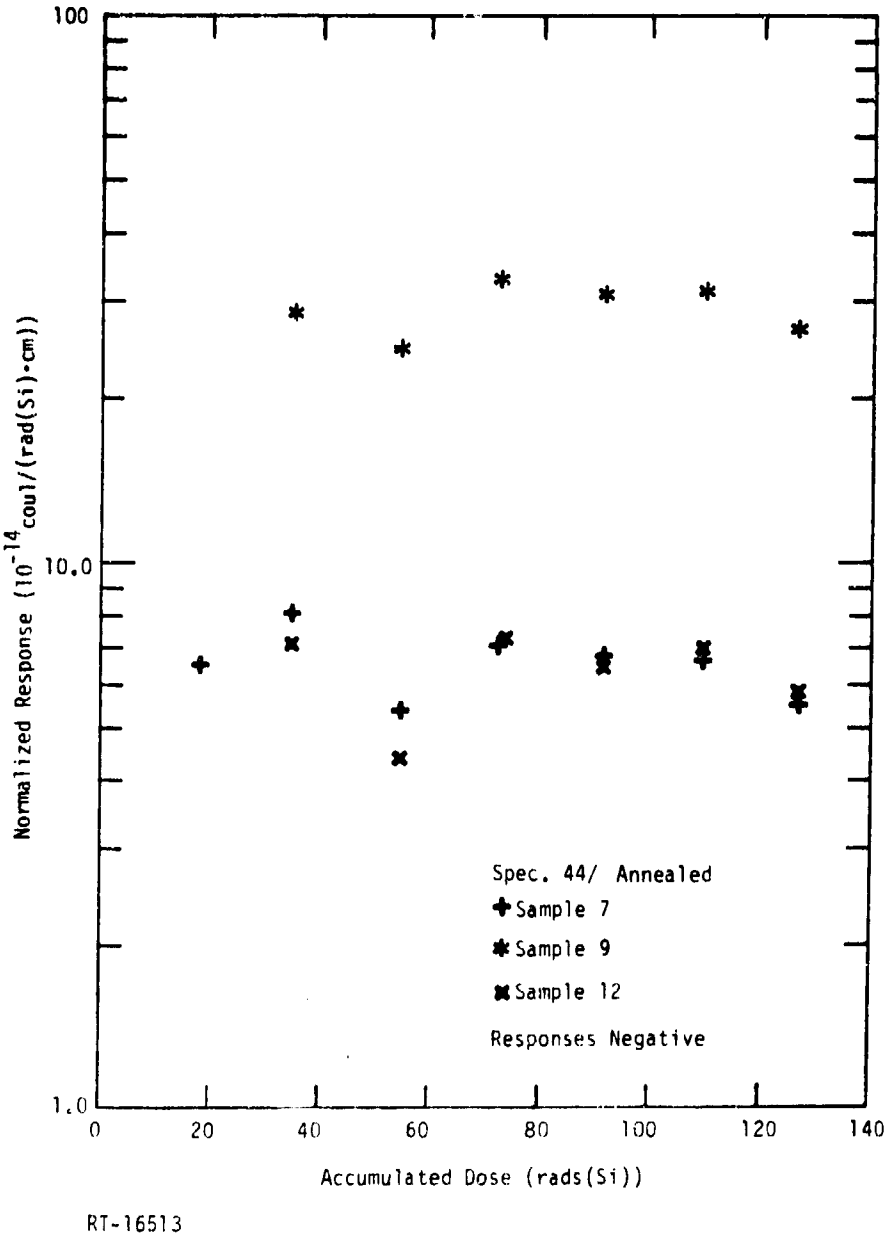

Figure E-36. Shot-to-shot responses of Spec 44/ cables annealed at 135°C for 12 hours versus total dose. All responses were negative.

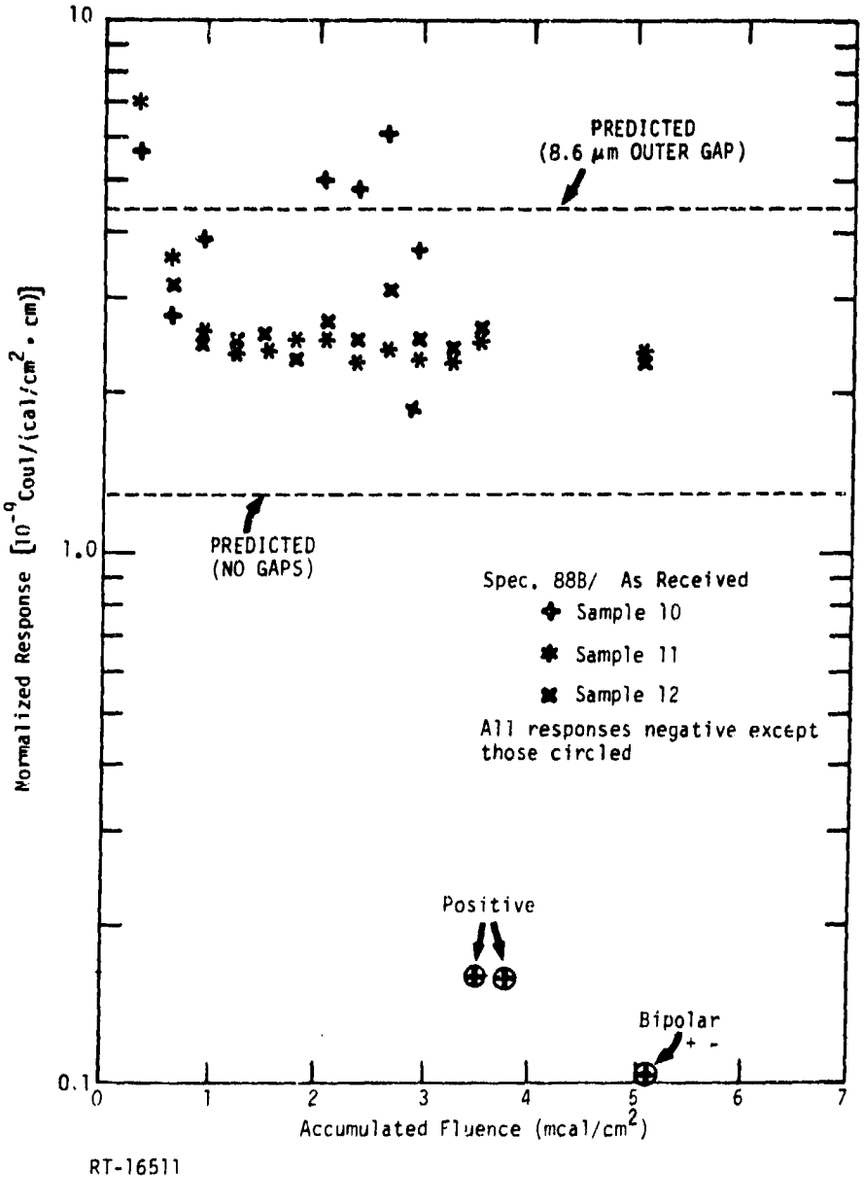

Figure E-37. Shot-to-shot responses of Spec 88/ samples as received versus total fluence.

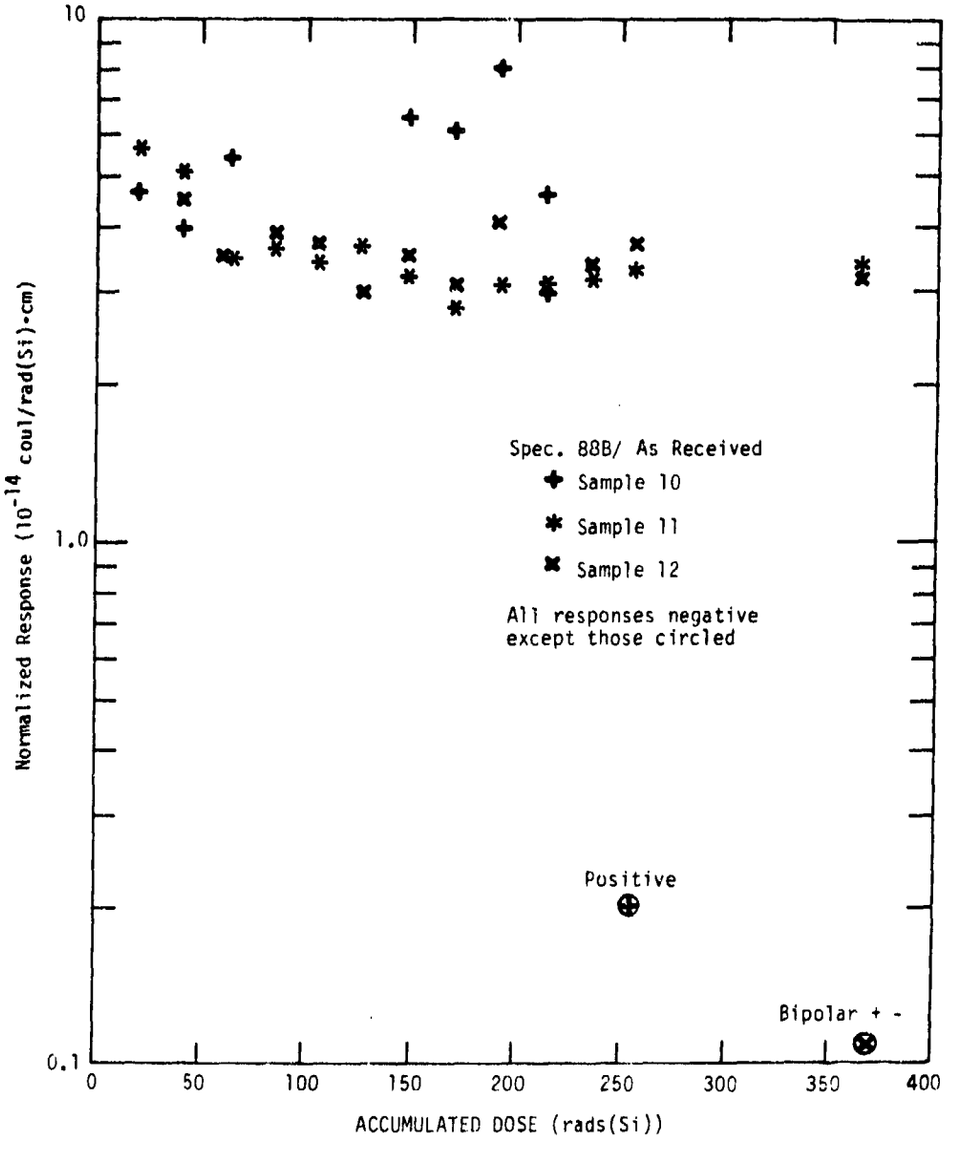

Figure E-38. Shot-to-shot responses of Spec 88/ samples as received versus total dose.

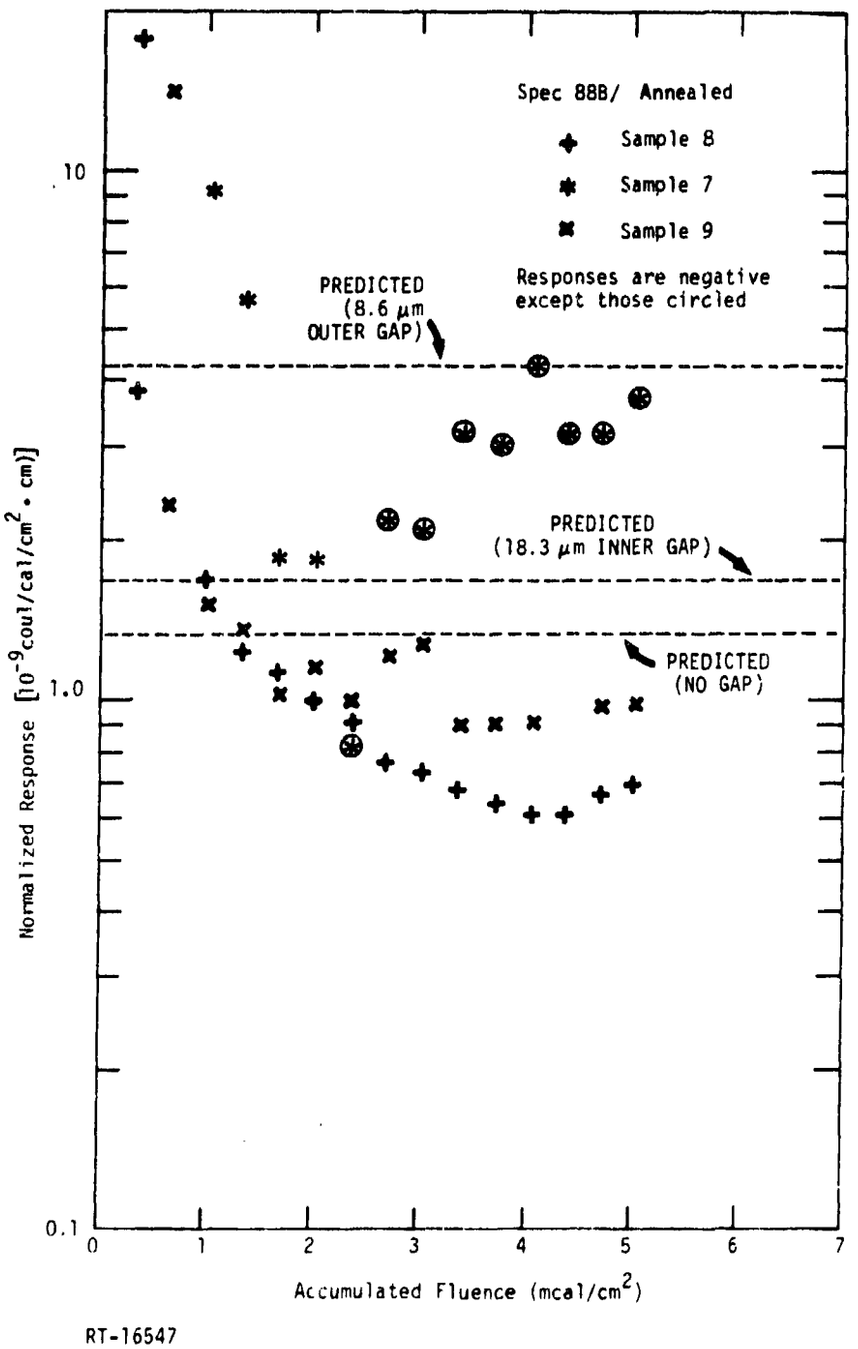

Figure E-39. Shot-to-shot responses of Spec 88B/ samples annealed at 150°C for 12 hours versus total fluence. The response of sample 7 changed sign.

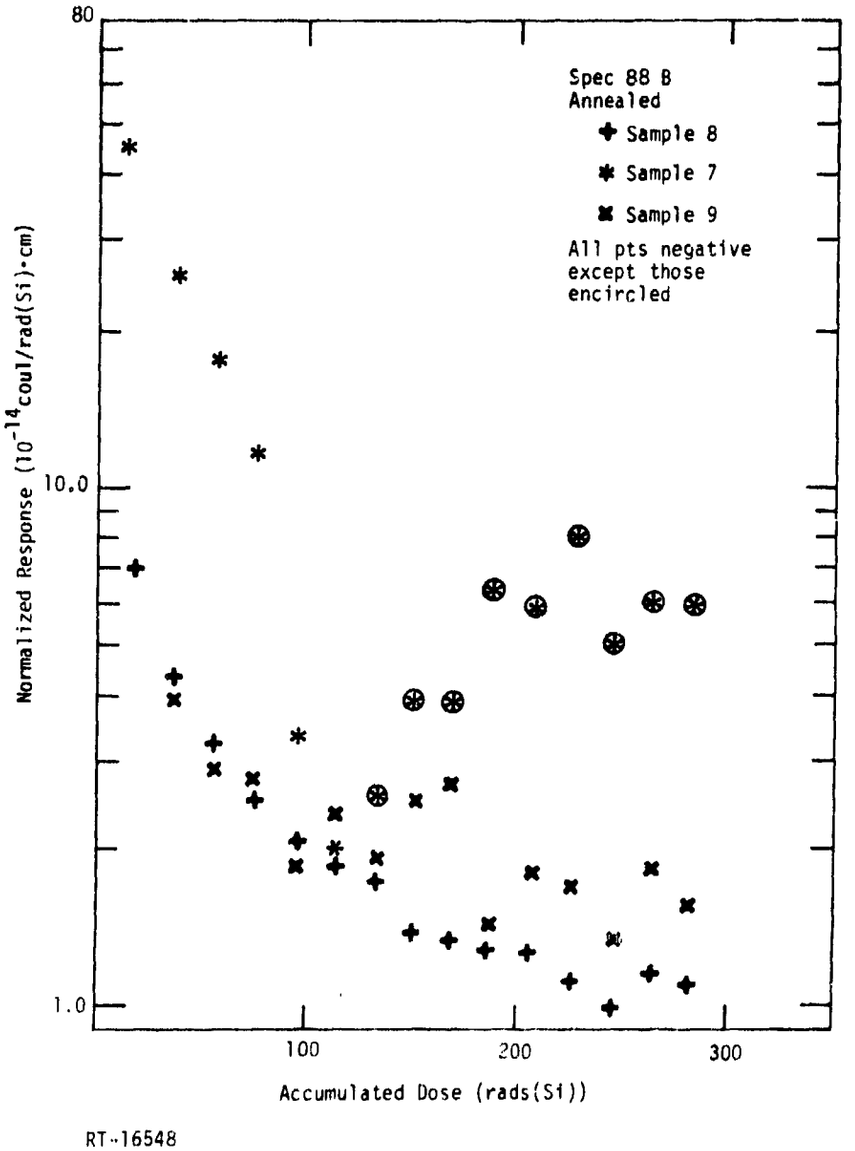

Figure E-40. Shot-to-shot responses of Spec 88B cables annealed at 150°C for 12 hours versus total dose. The response of sample 7 changed sign.

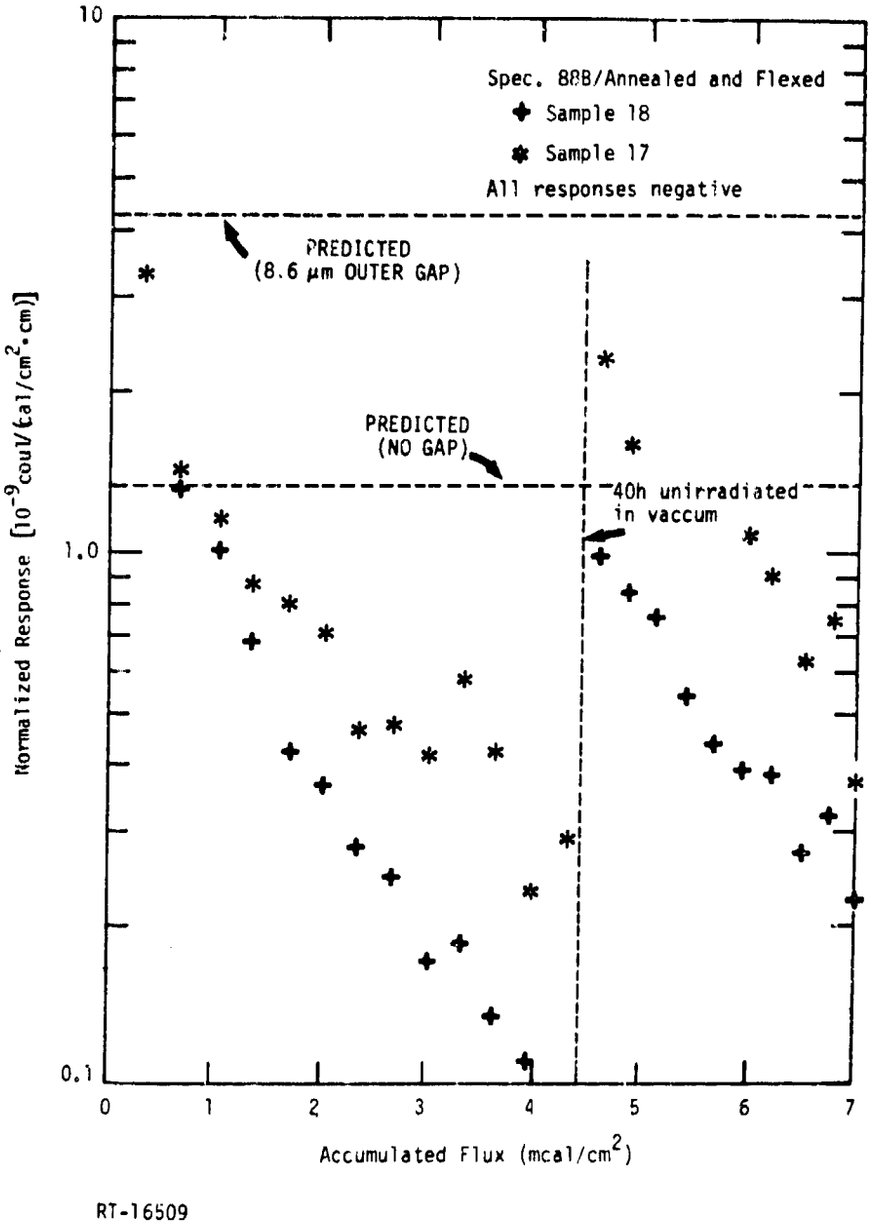

Figure E-41. Shot-to-shot responses of Spec 88B cables annealed at 150°C for 12 hours, then flexed by bending ten times at different points along the cable versus total fluence. All responses were negative. Between shots 13 and 14 there was a 40 hour pause.

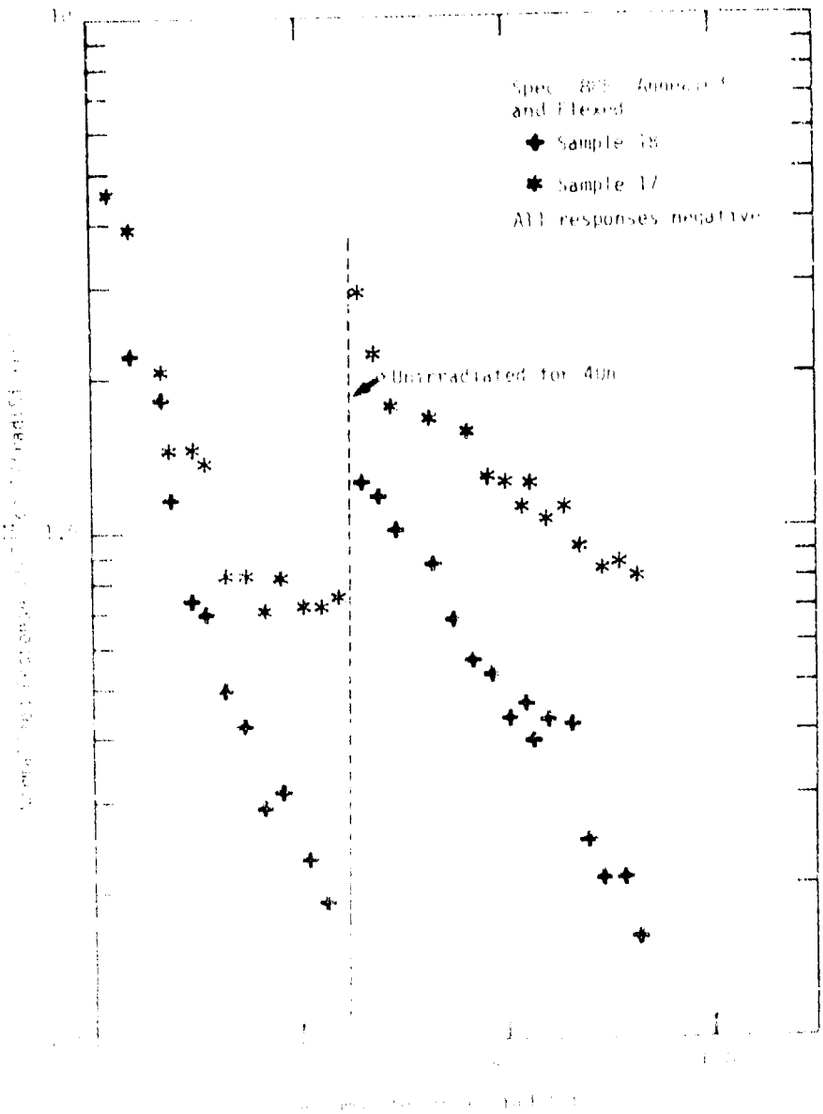

Figure I. 42. Shot to shot responses of Spec 88B cables annealed at 150°C for 12 hours, then flexed by bending ten times at different points along the cable versus total dose. All responses were negative. Between shots 13 and 14 there was a 40 hour pause.

DISTRIBUTION LIST

Department of Defense

1. Assistant to the Secretary of Defense
   Atomic Energy
   Department of Defense
   Washington, DC 20301
   01CY Attn: ATSD (AE)

2. Defense Communication Engineer Center
   1860 Wiehle Avenue
   Reston, VA 22090
   01CY Attn: Code R720 C. Stansberry
   01CY Attn: Code R410

3. Defense Documentation Center
   Cameron Station
   Alexandria, VA 22314
   12CY Attn: TC

4. Commander
   Defense Electronic Supply Center
   1507 Wilmington Pike
   Dayton, OH 45401
   (Thru DSA for CNWDI)
   01CY Attn: DESC-ECS

5. Director
   Defense Intelligence Agency
   Washington, DC 20301
   01CY Attn: DT-1B
   01CY Attn: DB-4C

6. Director
   Defense Nuclear Agency
   Washington, DC 20305
   01CY Attn: STTL
   01CY Attn: TISI
   01CY Attn: DDST
   01CY Attn: RAEV
   01CY Attn: SPSS

7. Commander
   Field Command
   Defense Nuclear Agency
   Kirtland AFB, NM 87115
   01CY Attn: FCPR

8. Joint Chiefs of Staff
Washington, DC 20301
01CY Attn: J-3 WWMCCS Evaluation Office

9. Chief
Livermore Division Fld Command DNA
Lawrence Livermore Laboratory
P.O. Box 808
Livermore, CA 94550
01CY Attn: FCPRL

10. National Communications System
Office of the Manager
Washington, DC 20305
01CY Attn: NCS-TS C. Bodson

11. Director
National Security Agency
Ft. George G. Meade, MD 20755
01CY Attn: Orland O. Van Gunten R-425

12. Under SECY of DEF for RSCH & ENGRG
Department of Defense
Washington, DC 20301
01CY Attn: S&SS (OS)

Department of Army

13. Commander
Aberdeen Proving Ground
Aberdeen Proving Ground, MD 21005
01CY Attn: Steap R. Harrison

14. Director
BMD Advanced Tech Ctr
Huntsville Office
P.O. Box 1500
Huntsville, AL 35807
01CY Attn: F. Hoke

15. Commander
BMD System Command
P.O. Box 1500
Huntsville, AL 35807
01CY Attn: BMDSC-HEN

16. Commander
Fort Huachuca
Fort Huachuca, AZ 85613
01CY Attn: Tech Rev Div

17. Commander
Harry Diamond Laboratories
2800 Powder Mill Road
Adelphi, MD 20783
(CNWDI-Inner Envelope: Attn: DELHD-RBH)
01CY Attn: J. Miletta
01CY Attn: J. Thompkins
01CY Attn: DELHD-RBA J. Rosado
01CY Attn: DELHD-RBG
01CY Attn: DELHD-EM Chief Lab 1000
01CY Attn: DELHD-NP

18. Commander
Redstone Scientific Information Ctr
U.S. Army R&D Command
Redstone Arsenal, AL 35809
01CY Attn: DRDMI-TBD

19. Director
Trasana
White Sands Missile Range, NM 88002
01CY Attn: O. Miller

20. Commander
U.S. Army Armament Research & Development Command
Dover, NJ 07801
01CY Attn: DRDAR-TSI-E A. Grinoch
01CY Attn: DRDAR-LCN-F
01CY Attn: DRDAR-LCN-DP H. Posternak
01CY Attn: DRDAR-TSS No. 59

21. Director
U.S. Army Ballistic Research Labs
Aberdeen Proving Ground, MD 21005
01CY Attn: DRDAR-BLT

22. Chief
U.S. Army Communications Sys Agency
Fort Monmouth, NJ 07703
01CY Attn: CCM-RD-T

23. U.S. Army Electronics Command
Fort Monmouth, NJ 07703
01CY Attn: DRSEL-CT-HDK A. Cohen
01CY Attn: DRSEL-TL-MD Mr. Gaule
01CY Attn: DRSEL-NL-RO R. Brown
01CY Attn: DRSEL-TL-IR E. Hunter

24. Commandant
U.S. Army Engineer School
Ft. Belvoir, VA 22060
01CY Attn: ATSE-CDC

25. Commander
U.S. Army Mat & Mechanics Rsch Ctr
Watertown, MA 02172
(Address CNWDI: Attn: Document Control For:)
01CY Attn: DRXMR-HH J. Dignam

26. Commander
U.S. Army Missile Material Readiness Command
Redstone Arsenal, AL 35809
01CY Attn: Hawk Project Officer DRCPM-HAER

27. Commander
U.S. Army Missile R&D Command
Redstone Arsenal, AL 35809
01CY Attn: DRCPM-PE-EA W. Wagner

28. Commander
U.S. Army Mobility Equip R&D Ctr
Fort Belvoir, VA 22060
(CNWDI to Army Mat Dev & Readiness Command)
01CY Attn: DRDME-E J. Bond Jr.

29. Commander
U.S. Army Night Vision Laboratory
Fort Belvoir, VA 22060
01CY Attn: DRSEL-NV-SD J. Carter
01CY Attn: DRSEL-NV-SD A. Parker

30. Commander
U.S. Army Nuclear & Chemical Agency
7500 Backlick Road
Building 2073
Springfield, VA 22150
01CY Attn: Library

31. Commander
U.S. Army Test and Evaluation Comd
Aberdeen Proving Ground, MD 21005
01CY Attn: DRSTE-EL
01CY Attn: DRSTE-FA

32. Commander
U.S. Army Training and Doctrine Comd
Fort Monroe, VA 23651
01CY Attn: ATORI-OP-SW

33. Project Manager
XM-1 Tank System
28150 Dequindre
Warren, MI 48092
01CY Attn: DRCPM-GCM-SW

Department of Navy

34. Commander
Naval Air Systems Command
Headquarters
Washington, DC 21360
01CY Attn: AIR 5324K
01CY Attn: AIR 350F
01CY Attn: AIR 310

35. Commanding Officer
Naval Avionics Facility
21st and Arlington Avenue
Indianapolis, IN 46218
01CY Attn: Branch 942 D. Repass

36. Commander
Naval Electronic Systems Command
Naval Electronic Systems Cmd Hqs
Washington, DC 20360
01CY Attn: CODE 504510
01CY Attn: PME 117-21
01CY Attn: NAVELEX 51024 C. Watkins

37. Commanding Officer
Naval Intelligence Support Ctr
4301 Suitland Road Bldg. 5
Washington, DC 20390
01CY Attn: NISC Library

38. Commander
Naval Ocean Systems Center
San Diego, CA 92152
01CY Attn: CODE 4471 (Tech Lib)

39. Superintendent (Code 1424)
Naval Postgraduate School
Monterey, CA 93940
01CY Attn: CODE 2124 Tech RPTS Librarian

40. Director
Naval Research Laboratory
Washington, DC 20375
01CY Attn: CODE 6624 J. Ritter
01CY Attn: CODE 6601 E. Wolicki
01CY Attn: CODE 4104
01CY Attn: CODE 5216
01CY Attn: CODE 2627

41. Commander
Naval Sea Systems Command
Department of the Navy
Washington, DC 20362
01CY ATTN: SEA-04531

42. Commander
Naval Ship Engineering Center
Department of the Navy
Washington, DC 20362
(Hyattsville)
01CY Attn: CODE 6174D2

43. Officer-In-Charge
Naval Surface Weapons Center
White Oak, Silver Spring, MD 20910
01CY Attn: CODE WA50, 130-108
01CY Attn: CODE WA501

44. Commanding Officer
Naval Weapons Evaluation Facility
Kirtland Air Force Base
Albuquerque, NM 87117
01CY Attn: CODE AT-6

45. Commanding Officer
Nuclear Weapons TNG Center Pacific
Naval Air Station, North Island
San Diego, CA 92135
01CY Attn: CODE 32

46. Director
Strategic Systems Project Office
Navy Department
Washington, DC 20376
01CY Attn: NSP-2701 J. Pitsenberger
01CY Attn: NSP-27334 B. Hahn

Department of the Air Force

47. AF Aero-Propulsion Laboratory, AFSC
Wright-Patterson AFB, OH 45433
01CY Attn: POE-2 J. Wise

48. AF Materials Laboratory, AFSC
Wright-Patterson AFB, OH 45433
01CY Attn: LTE

49. AF Weapons Laboratory, AFSC
Kirtland AFB, NM 87117
01CY Attn: NT C. Baum
01CY Attn: ELP Tree Section
01CY Attn: SUL
01CY Attn: J. Mullis
01CY Attn: R. Maier

50. AFTAC
Patrick AFB, FL 32925
01CY Attn: TFS Maj. M. Schneider

51. Air Force Avionics Laboratory, AFSC
Wright-Patterson AFB, OH 45433
01CY Attn: DHE-2
01CY Attn: DH LTC McKenzie

52. Headquarters
Air Force Systems Command
Andrews AFB
Washington, DC 20334
01CY Attn: DLCA

53. Commander
ASD
Wright-Patterson AFB, OH 45433
01CY Attn: ASD/ENESS P. Marth
01CY Attn: ENACC R. Fish
01CY Attn: ASD-YH-EX Mr. Sunkes

54. Headquarters
Electronic Systems Division/IN
Hanscom AFB, MA 01731
01CY Attn: INDC/21

55. Headquarters
Electronic Systems Division, (AFSC)
Hanscom AFB, MA 01731
01CY Attn: DRI E. Doherty

56. Commander
Foreign Technology Division, AFSC
Wright-Patterson AFB, OH 45433
01CY Attn: ETDP B. Ballard

57. Commander
Rome Air Development Center, AFSC
Griffiss AFB, NY 13441
01CY Attn: RADC/RBRP C. Lane
01CY Attn: RBRAC I. Krulac

58. Commander
Rome Air Development Center, AFSC
Hanscom AFB, MA 01731
01CY Attn: ESE A. Kahan

59. SAMSO/MN
Norton AFB, CA 92409
01CY Attn: MNNG
01CY Attn: MNNH

60. SAMSO/RS
Post Office Box 92960
Worldway Postal Center
Los Angeles, CA 90009
01CY Attn: RSMG Capt. Collier
01CY Attn: RSMA Lt. D. Higgins

61. SAMSO/SK
Post Office Box 92960
Worldway Postal Center
Los Angeles, CA 90009
01CY Attn: SKF P. Stadler

62. SAMSO/YA
Post Office Box 92960
Worldway Postal Center
Los Angeles, CA 90009
01CY Attn: YAS

63. Commander in Chief
Strategic Air Command
Offutt AFB, NB 68113
01CY Attn: NRI-STINFO Library
01CY Attn: XPFS M. Carra

64. Director (INWS)
3416th Technical Training Squadron (ATC)
Air Training Command
Kirtland AFB, NM 87115
01CY Attn: TTV

Department of Energy

65. Department of Energy
Albuquerque Operations Office
P.O. Box 5400
Albuquerque, NM 87115
01CY Attn: Doc Con for WSSB/OSD R. Shay

66. Division of Military Application
Department of Energy
Washington, DC 20545
01CY Attn: Doc Con for Class Tech Lib

67. University of California
Lawrence Livermore Laboratory
P.O. Box 808
Livermore, CA 94550
01CY Attn: Doc Con for Technical Information Dept. Library
01CY Attn: Doc Con for D. Meeker L-545 (Class L-153)
01CY Attn: Doc Con for R. Ott L-389

68. Los Alamos Scientific Laboratory
P.O. Box 1663
Los Alamos, NM 87545
01CY Attn: Doc Con for Bruce W. Noel

69. Sandia Laboratories
P.O. Box 5800
Albuquerque, NM 87115
01CY Attn: Doc Con for Org 4310 J. Hood
01CY Attn: Doc Con for Org 4213 F. Coppage

Other Government Agencies

70. Central Intelligence Agency
Attn: RD/SI Rm 5G48 HQ Bldg
Washington, DC 20505
01CY Attn: RD/SI Rm 5G48 HQ Bldg

71. Department of Transportation
Federal Aviation Administration
Headquarters Sec Div. ASE-300
800 Independence Avenue, SW
Washington, DC 20591
01CY Attn: ARD-350

Department of Defense Contractors

72. Aerojet Electro-Systems Co.
Div. of Aerojet-General Corp.
P.O. Box 296, 1100 W. Hollyvale Drive
Azusa, CA 91702
01CY Attn: SV/8711/70

73. Aerospace Corp.
P.O. Box 92957
Los Angeles, CA 90009
01CY Attn: S. Bower
01CY Attn: R. Crolius
01CY Attn: J. Reinheimer
01CY Attn: V. Josephson
01CY Attn: W. Willis
01CY Attn: I. Garfunkel

74. Avco Research & Systems Group
201 Lowell Street
Wilmington, MA 01887
01CY Attn: W. Broding

75. Battelle Memorial Institute
505 King Avenue
Columbus, OH 43201
01CY Attn: D. Hamman
01CY Attn: R. Blazek

76. BDM Corp.
P.O. Box 9274
Albuquerque International
Albuquerque, NM 87119
01CY Attn: Marketing
01CY Attn: D. Alexander

77. Bendix Corp.
Communication Division
East Joppa Road
Baltimore, MD 21204
01CY Attn: Document Control

78. Bendix Corp.
Research Laboratories Division
Bendix Center
Southfield, MI 48075
01CY Attn: M. Frank

79. Boeing Co.
P.O. Box 3707
Seattle, WA 98124
01CY Attn: H. Wicklein
01CY Attn: 8k-38
01CY Attn: R. Caldwell

80. Booz-Allen and Hamilton, Inc.
106 Apple Street
Tinton Falls, NJ 07724
01CY Attn: R. Chrisner

81. Brown Engineering Company, Inc.
Cummings Research Park
Huntsville, AL 35807
01CY Attn: J. McSwain

82. Burroughs Corp.
Federal and Special Systems Group
Central Ave and Route 252
P.O. Box 517
Paoli, PA 19301
01CY Attn: Product Eval Lab

83. California Institute of Technology
Jet Propulsion Laboratory
4800 Oak Grove Drive
Pasadena, CA 91103
01CY Attn: J. Bryden
01CY Attn: A. Stanley

84. Charles Stark Draper Laboratory, Inc.
555 Technology Square
Cambridge, MA 02139
01CY Attn: P. Kelly
01CY Attn: R. Maltmaier

85. Computer Sciences Corp.
1400 San Mateo Blvd, SE
Albuquerque, NM 87108
01CY Attn: A. Schiff

86. Cutler-Hammer, Inc.
AIL Division
Comac Road
Deer Park, NY 11729
01CY Attn: Central Tech Files A. Anthony

87. Denver, University of
Colorado Seminary
Denver Research Institute
P.O. Box 10127
Denver, CO 80210
01CY Attn: Sec. Officer for F. Venditti

88. E-Systems, Inc.
ECI Division
P.O. Box 12248
St. Petersburg, FL 33733
01CY Attn: R. French

89. E-Systems, Inc.
Greenville Division
P.O. Box 1056
Greenville, TX 75401
01CY Attn: Division Library
01CY Attn: Library 8-50100

90. Effects Technology, Inc.
5383 Hollister Avenue
Santa Barbara, CA 93111
01CY Attn: E. Steele

91. Ex-Cal. Inc.
Suite 1516, First National Bldg. East
Albuquerque, NM 87108
01CY Attn: R. Dickhaut

92. Fairchild Camera and Instrument Corp.
464 Ellis Street
Mountain View, CA 94040
01CY Attn: Sec Dept for D. Myers

93. Fairchild Industries, Inc.
Sherman Fairchild Technology Center
20301 Century Blvd.
Germantown, MD 20767
01CY Attn: B. Patton

94. Florida, University of
An Institution of Education
Attn: Patricia B. Rambo
P.O. Box 284
Gainesville, FL 32601
01CY Attn: H. Sisler

95. Ford Aerospace & Communications Corp.
Ford & Jamboree Roads
Newport Beach, CA 92663
01CY Attn: E. Poncelet Jr.
01CY Attn: Tech Info Services
01CY Attn: K. Attinger

96. Ford Aerospace & Communications Corp.
3939 Fabian Way
Palo Alto, CA 94303
01CY Attn: E. Hahn MS X22
01CY Attn: Technical Library
01CY Attn: S. Crawford
01CY Attn: D. McMorrow Ms G30

97. Franklin Institute
20th Street and Parkway
Philadelphia, PA 19103
01CY Attn: R. Thompson

98. Garrett Corp.
P.O. Box 92248, 9851 Sepulveda Blvd
Los Angeles, CA 90009
01CY Attn: R. Weir Dept 93-9

99. General Electric Co.
Space Division
Valley Forge Space Center
P.O. Box 8555
Philadelphia, PA 19101
01CY Attn: L. Chasen
01CY Attn: J. Peden VFSC, 4230M
01CY Attn: J. Andrews
01CY Attn: D. Tasca
01CY Attn: L. Sivo
01CY Attn: L. Jeffers
01CY Attn: D. Long

100. General Electric Co.
Re-Entry & Environmental Systems Div.
P.O. Box 7722
3198 Chestnut Street
Philadelphia, PA 19101
01CY Attn: W. Patterson
01CY Attn: J. Palchefsky Jr.
01CY Attn: Tech Lib

101. General Electric Co.
Ordnance Systems
100 Plastics Avenue
Pittsfield, MA 01201
01CY Attn: J. Reidl

102. General Electric Co.
Aircraft Engine Business Group
Evendale Plant, Int Hwy 75 S
Cincinnati, OH 45215
01CY Attn: R. Hellen

103. General Electric Co.
Aerospace Electronics Systems
French Road
Utica, NY 13503
01CY Attn: W. Patterson

104. General Electric Co. - Tempo
Center for Advanced Studies
816 State Street (P.O. Drawer QQ)
Santa Barbara, CA 93102
01CY Attn: M. Espig
01CY Attn: R. Rutherford
01CY Attn: DASIAC
01CY Attn: W. McNamara

105. General Electric Co. - Tempo
Alexandria Office
Huntington Building, Suite 300
2560 Huntington Avenue
Alexandria, VA 22303
01CY Attn: DASIAC

106. General Research Corp.
Santa Barbara Division
P.O. Box 6770
Santa Barbara, CA 93111
01CY Attn: Tech Info Office

107. Georgia Institute of Technology
Office of Contract Administration
Attn: RSCH Security Coordinator
Atlanta, GA 30332
01CY Attn: Res & Sec Coord for H. Denny

108. Goodyear Aerospace Corp.
Arizona Division
Litchfield Park, AZ 85340
01CY Attn: Sec Cont Sta

109. GTE Sylvania, Inc.
Electronics Systems GRP-Eastern Div.
77 A Street
Needham, MA 02194
01CY Attn: C. Thornhill Librarian
01CY Attn: L. Blaisdell

110. GTE Sylvania, Inc.
189 B Street
Needham Heights, MA 02194
01CY Attn: J. Waldron

111. Harris Corp.
Electronics Systems Division
P.O. Box 37
Melbourne, FL 32901
01CY Attn: W. Abare
01CY Attn: C. Davis

112. Harris Corp.
Harris Semiconductor Division
P.O. Box 883
Melbourne, FL 32901
01CY Attn: Mngr Bipolar Digital Eng
01CY Attn: Mngr Linear Eng

113. Hazeltine Corp.
Pulaski Road
Greenlawn, NY 11740
01CY Attn: Tech Info Ctr M. Waite

114. Honeywell, Inc.
Avionics Division
13350 U.S. Highway 19 North
St. Petersburg, FL 33733
01CY Attn: MS 725-5

115. Hughes Aircraft Co.
Centinela and Teale
Culver City, CA 90230
01CY Attn: CTDC 6/E110
01CY Attn: J. Stagletary
01CY Attn: K. Walker
01CY Attn: D. Binder

116. Hughes Aircraft Co.
El Segundo Site
P.O. [illegible]
Los [illegible], CA 90009
01CY Attn: E. Smith M S A620

117. IBM Corp.
Route 17C
Owego, NY 13827
01CY Attn: Electromagnetic Compatability
01CY Attn: Manr Memory Systems

118. Institute for Defense Analyses
400 Army-Navy Drive
Arlington, VA 22202
01CY Attn: Tech Info Services

119. International Tel & Telegraph Corp.
500 Washington Avenue
Nutley, NJ 07110
01CY Attn: Dept 608

120. IRT Corp.
P.O. Box 81087
San Diego, CA 92138
01CY Attn: Physics Division
01CY Attn: Systems Effects Division
01CY Attn: R. Mertz
01CY Attn: MDC

121. Jaycor
205 S. Whiting Street, Suite 500
Alexandria, VA 22304
01CY Attn: R. Sullivan

122. Johns Hopkins University
Applied Physics Laboratory
Johns Hopkins Road
Laurel, MD 20810
01CY Attn: P. Partridge

123. Kaman Sciences Corp.
P.O. Box 7463
Colorado Springs, CO 80933
01CY Attn: J. Lubell
01CY Attn: W. Rich
01CY Attn: President
01CY Attn: W. Ware
01CY Attn: Dir. Science & Technology Div

124. Litton Systems, Inc.
Guidance & Control Systems Division
5500 Canoga Avenue
Woodland Hills, CA 91364
01CY Attn: J. Retzler
01CY Attn: V. Ashby

125. Lockheed Missiles & Space Co., Inc.
P.O. Box 504
Sunnyvale, CA 94088
01CY Attn: L. Rossi
01CY Attn: D. Wolfhard
01CY Attn: E. Smith
01CY Attn: B. Kimura

126. Lockheed Missiles and Space Co., Inc.
3251 Hanover Street
Palo Alto, CA 94304
01CY Attn: Reports Librarian

127. M.I.T. Lincoln Laboratory
P.O. Box 73
Lexington, MA 02173
01CY Attn: Library A-082

128. Martin Marietta Corp.
Orlando Division
P.O. Box 5837
Orlando, FL 32805
01CY Attn: TIC/MP-30

129. Martin Marietta Corp.
Denver Division
P.O. Box 179
Denver, CO 80201
01CY Attn: Rsch Lib 2825
01CY Attn: P. Kase
01CY Attn: Research Lib 6617 J. McKee

130. McDonnell Douglas Corp.
P.O. Box 516
St. Louis, MO 63166
01CY Attn: T. Ender
01CY Attn: Technical Library

131. McDonnell Douglas Corp.
5301 Bolsa Avenue
Huntington Beach, CA 92647
01CY Attn: P. Albrecht

132. Mission Research Corp.
735 State Street
Santa Barbara, CA 93101
01CY Attn: M. Van Blaricum

133. Mission Research Corp.
EM Systems Applications Division
1400 San Mateo Blvd, S.E. Suite A
Albuquerque, NM 87108
01CY Attn: David E. Merewether

134. Mission Research Corp. - San Diego
P.O. Box 1209
La Jolla, CA 92038
01CY Attn: J. Raymond
01CY Attn: V. Van Lint

135. National Academy of Sciences
Attn: Committee on Atmospheric Sciences
2101 Constitution Avenue, NW
Washington, DC 20418
01CY Attn: R. Shane

136. Northrop Corp.
Northrop Research and Technology Ctr
3401 West Broadway
Hawthorne, CA 90250
01CY Attn: J. Srour
01CY Attn: O. Curtis Jr.

137. Northrop Corp.
Electronic Division
2301 West 120th Street
Hawthorne, CA 90250
01CY Attn: D. Strobel

138. Oklahoma, University of
Research Institute
1808 Newton Drive
Norman, OK 73069
01CY Attn: R. Wood

139. Physics International Co.
2700 Merced Street
San Leandro, CA 94577
01CY Attn: Division 6000
01CY Attn: Doc Con for J. Shea

140. Power Conversion Technology, Inc.
11588 Sorrento Valley Road
San Diego, CA 92121
01CY Attn: V. Fargo

141. R&D Associates
P.O. Box 9695
Marina Del Rey, CA 90291
01CY Attn: S. Rogers
01CY Attn: W. Karzas

142. Rand Corp.
1700 Main Street
Santa Monica, CA 90406
01CY Attn: C. Crain

143. Raytheon Co.
Hartwell Road
Bedford, MA 01730
01CY Attn: G. Joshi

144. Raytheon Co.
528 Boston Post Road
Sudbury, MA 01776
01CY Attn: H. Flescher

145. RCA Corp.
Government Systems Division
Astro Electronics
P.O. Box 800, Locust Corner
East Windsor Township
Princeton, NJ 08540
01CY Attn: G. Brucker

146. RCA Corp.
David Sarnoff Research Center
P.O. Box 432
Princeton, NJ 08540
01CY Attn: Office N103

147. Research Triangle Institute
P.O. Box 12194
Research Triangle Park, NC 27709
(all corres Attn: Sec Officer FOR)
01CY Attn: Eng Div Mayrant Simons Jr.

148. Rockwell International Corp.
P.O. Box 3105
Anaheim, CA 92803
01CY Attn: George C. Messenger FB61
01CY Attn: N. J. Rudie FA53
01CY Attn: K. Hull
01CY Attn: James E. Bell HA10

149. Rockwell International Corp.
Space Division
12214 South Lakewood Boulevard
Downey, CA 90241
01CY Attn: D. Stevens
01CY Attn: TIC D/41-092 AJ01

150. Rockwell International Corp.
5701 West Imperial Highway
Los Angeles, CA 90009
01CY Attn: TIC BA08

151. Rockwell International Corp.
Collins Divisions
400 Collins Road NE
Cedar Rapids, IA 52406
01CY Attn: Alan A. Langenfeld
01CY Attn: TIC 106-216

152. Sanders Associates, Inc.
95 Canal Street
Nashua, NH 03060
01CY Attn: L. Brodeur
01CY Attn: M. Aitel

153. Science Applications, Inc.
P.O. Box 2351
La Jolla, CA 92038
01CY Attn: J. Beyster
01CY Attn: L. Scott

154. Science Applications, Inc.
Huntsville Division
2109 W. Clinton Avenue
Suite 700
Huntsville, AL 35805
01CY Attn: N. Byrn

155. Science Applications, Inc.
8400 Westpark Drive
McLean, VA 22101
01CY Attn: W. Chadsey

156. Singer Co. (Data Systems)
150 Totowa Road
Wayne, NJ 07470
01CY Attn: Tech Info Center

157. Sperry Rand Corp.
Sperry Microwave Electronics
P.O. Box 4648
Clearwater, FL 33518
01CY Attn: Engineering Laboratory

158. Sperry Rand Corp.
Sperry Division
Marcus Avenue
Great Neck, NY 11020
01CY Attn: C. Craig EV
01CY Attn: R. Viola
01CY Attn: P. Maraffino

159. Sperry Rand Corp.
Sperry Flight Systems
P.O. Box 21111
Phoenix, AZ 85036
01CY Attn: D. Andrew Schow

160. Spire Corp.
P.O. Box D
Bedford, MA 01730
01CY Roger G. Little

161. SRI International
333 Ravenswood Avenue
Menlo Park, CA 94025
01CY Attn: P. Dolan

162. Sundstrand Corp.
4751 Harrison Avenue
Rockford, IL 61101
01CY Attn: Research Department

163. Tetra Tech, Inc.
1911 Ft. Myer Drive
Arlington, VA 22209
01CY Attn: T. Simpson

164. Texas Instruments, Inc.
P.O. Box 6015
Dallas, TX 75265
(Unclassified to P.O. Box 6015)
01CY Attn: D. Manus

165. TRW Defense & Space Sys Group
One Space Park
Redondo Beach, CA 90278
02CY Attn: O. E. Adams R1-1144
02CY Attn: R. K. Plebuch R1-2078
01CY Attn: Vulnerability & Hardness Laboratory
01CY Attn: R. Webb
01CY Attn: Tech Info Center/S-1930
01CY Attn: A. Narevsky
01CY Attn: H. H. Holloway R1-2036

166. TRW Defense & Space Sys Group
San Bernardino Operations
P.O. Box 1310
San Bernardino, CA 92402
01CY Attn: F. B. Fay
01CY Attn: R. Kitter

167. TRW Systems and Energy
P.O. Box 368
Clearfield, UT 84015
01CY Attn: R. Mathews
01CY Attn: G. Spehar
01CY Attn: D. Millward

168. Vought Corp.
P.O. Box 5907
Dallas, TX 75222
01CY Attn: R. Tomme
01CY Attn: Library

169. Westinghouse Electric Corp.
Defense and Electronic Systems Ctr
P.O. Box 1693
Baltimore-Washington Intl Airport
Baltimore, MD 21203
01CY Attn: Henry P. Kalapaca M S 3525
01CY Attn: MS 3330